THERMAL MANAGEMENT OF ROADWAY-EMBEDDED POWER ELECTRONICS FOR ELECTRIC VEHICLE DYNAMIC WIRELESS CHARGING SYSTEMS

by

Conner R. Sabin

A thesis submitted in partial fulfillment
of the requirements for the degree

of

MASTER OF SCIENCE

in

Electrical Engineering

Approved:

Abhilash Kamineni, Ph.D. Major Professor	Nick Roberts, Ph.D. Committee Member
Hongjie Wang, Ph.D. Committee Member	D. Richard Cutler, Ph.D. Vice Provost of Graduate Studies

UTAH STATE UNIVERSITY
Logan, Utah

2024

ABSTRACT

Thermal Management of Roadway-Embedded Power Electronics for Electric Vehicle Dynamic Wireless Charging Systems

by

Conner R. Sabin, Master of Science

Utah State University, 2024

Major Professor: Abhilash Kamineni, Ph.D.
Department: Electrical and Computer Engineering

Electric vehicle (EV) adoption is increasing, driven by consumer interest and the desire to reduce greenhouse gas emissions. Dynamic wireless power transfer (DWPT) offers a solution to EV charging challenges such as range anxiety and user inconvenience by enabling charging while driving. DWPT systems also distribute power across miles of roadway charging coils rather than relying on centralized charging locations, thus reducing the strain on the power grid.

Current DWPT technologies embed transmitter pads in roadways, with power electronics housed in roadside or underground units. These roadside management units require land easements to install these boxes. Moreover, these management units require long, high-frequency AC cables to be run from the roadside to the wireless charging pad, increasing system losses and system costs.

Embedding power electronics directly in the roadway, alongside transmitter pads, simplifies installation, reduces costs, and minimizes system losses. However, embedding electronics in the roadway raises reliability and maintenance concerns, particularly regarding

thermal management. Embedding electronics in the roadway limits the feasibility of active cooling, necessitating advanced thermal management designs to prevent overheating or excessive thermal cycling, which can significantly reduce component lifespans.

This thesis examines thermal management techniques for roadway-embedded DWPT electronics, considering factors like ambient temperature, roadway material, burial depth, and packaging. Trade-offs between power density, cost, and reliability are investigated through simulations in Ansys Icepak and testing within sand. A design procedure for roadway-embedded electronics is proposed and improvements are suggested for better thermal management and reliability. Through iterative analysis and experimentation, this research aims to optimize the thermal performance of roadway-embedded DWPT systems, ensuring their reliability and longevity.

(145 pages)

PUBLIC ABSTRACT

Thermal Management of Roadway-Embedded Power Electronics for Electric Vehicle Dynamic Wireless Charging Systems

Conner R. Sabin

Electric vehicles (EVs) are gaining popularity worldwide. However, concerns raised by the public about purchasing EVs include the limited availability of charging infrastructure, high costs, and the inconvenience of current charging methods. Dynamic wireless charging systems enable electric vehicles to charge while driving, thereby extending the range of EVs and reducing the necessity for large, expensive batteries. Moreover, these systems can initiate charging automatically without user interaction, enhancing charging convenience.

The ground assembly of existing dynamic wireless charging systems consists of an electromagnetic assembly, power electronics for the transmitter pad, and power electronics for grid connection. Installation of these systems face challenges due to high costs and the requirement for roadside management units to house the electronics. Embedding the power electronics within the roadway alongside with the transmitter pad would enhance installation ease and reduce costs. Placing the electronics closer to the transmitter pad also improves the overall system efficiency.

As power electronics provide charge between the ground and the vehicle, the electronics in the ground heat up due to losses within the system. This thesis seeks to understand techniques for managing the temperature rise of power electronics embedded in the roadway. The presence of electronics within the roadway restricts the use of conventional cooling methods such as fans or liquid cooling. This means that electronics must be cooled without the use of normal cooling methods. This thesis utilizes thermal simulation tools to model roadway-embedded electronics and identify strategies for mitigating temperature rise. Experimental validation of these techniques is then conducted in sand. The results of this

research can help to reduce costs and address installation challenges associated with Dynamic Wireless Power Transfer (DWPT) systems, thereby promoting wider adoption of EV dynamic wireless charging technology.

To my wife and family, for supporting me and listening to my excitement and struggles during this project. You have been so supportive and I appreciate your willingness to listen to my nerdy ranting. Thank you.

ACKNOWLEDGMENTS

Thank you to all the students and faculty that have helped me with this project. A special thank you to my advisor Abhilash Kamineni for teaching me and guiding me during this project as well as to Nick Roberts for your advice and direction during this project. Also, a big thank you to Azmeer Zahid, Abdullah Baig, and Matt Hansen for discussing problems with me and helping me with the design and testing of prototypes.

Conner Sabin

CONTENTS

LIST OF TABLES

LIST OF FIGURES

NOTATION

Symbols

α	Thermal diffusivity
λ	Failure rate
ρ	Density of a body
A	Area of a body
C_{in}	Inverter DC link input capacitance
C_{out}	Rectifier output capacitance
C_{oss}	MOSFET output capacitance
C_p	Specific heat
C_{pp}	LCCL primary side parallel capacitor
C_{ps}	LCCL primary side series capacitor
C_{ps1}	LCCL split compensation primary side series capacitor #1
C_{ps2}	LCCL split compensation primary side series capacitor #2
C_{sp}	LCCL secondary side parallel capacitor
C_{ss}	LCCL secondary side series capacitor
C_{ss1}	LCCL split compensation secondary side series capacitor #1
C_{ss2}	LCCL split compensation secondary side series capacitor #2
D_i	Diode i
d	Distance from the surface of the roadway
f_s	Switching frequency
h	Heat transfer coefficient
I_{DC}	DC input current
k	Thermal conductivity
k_P	Coupling factor between primary and secondary pads
k_L	Coupling factor between split compensation primary side series inductors
L	Characteristic length of a body

L_p	LCCL primary pad
L_{ps}	LCCL primary side series inductor
L_{ps1}	LCCL split compensation primary side series inductor #1
L_{ps2}	LCCL split compensation primary side series inductor #2
L_s	LCCL secondary pad
L_{ss}	LCCL secondary side series inductor
L_{ss1}	LCCL split compensation secondary side series inductor #1
L_{ss2}	LCCL split compensation secondary side series inductor #2
m	Mass of a body
Q	Heat generation rate
$R_{ds(on)}$	On resistance of the MOSFET device
S_i	MOSFET switch i
T_∞	Steady state temperature
ΔT	Change in temperature from ambient
T_A	Ambient temperature
T_i	Initial temperature
T_m	Mean earth surface temperature
t	Time
V	Volume of a body
V_{BAT}	DC output battery voltage
V_{DC}	DC input bus voltage
W	Power loss

ACRONYMS

ASPIRE	Advancing Sustainability through Powered Infrastructure for Roadway Electrification
AC	Alternating current
DC	Direct current
DWPT	Dynamic wireless power transfer
ESR	Equivalent series resistance
EMF	Electromagnetic field
EV	Electric vehicle
FEM	Finite element analysis
FMEA	Failure Mode and Effects Analysis
GA	Ground assembly
HF	High frequency
ICE	Internal combustion engine
MTTF	Mean Time to Failure
PCB	Printed circuit board
PCM	Phase change material
VA	Vehicle assembly
WPT	Wireless power transfer
ZVS	Zero voltage switching

CHAPTER 1

Introduction

1.1 Background

Electric vehicles are increasing in popularity, driven by their potential to offer zero-emission transportation and bolstered by government incentives. According to a 2022 report from the Environmental Protection Agency (EPA), the transportation sector accounted for nearly 29% of greenhouse gas emissions in the U.S. [1]. Transitioning to EVs holds the potential to significantly reduce greenhouse gas emissions originating from the transportation sector.

As of 2022, approximately 59.3% of the U.S. electric power grid relied on fossil fuels, indicating that the electricity used by electric vehicles is not entirely sourced from clean energy [2]. However, as renewable energy sources such as solar, wind, nuclear, or geothermal energy continue to expand, the transition towards electric vehicles will lead to further reductions in emissions. Even considering the current power generation mix, electric vehicles have lower average emissions over their lifetime compared to internal combustion engine (ICE) vehicles [3].

Other factors contributing to increased EV adoption include user experience benefits associated with electric vehicles. Electric vehicles feature regenerative braking, allowing braking energy to recharge the battery while reducing brake wear and tear. EVs are also quieter compared to ICE vehicles. Additionally, EVs offer enhanced handling capabilities due to rapid acceleration and deceleration facilitated by the battery. Overall, EVs are expected to incur lower maintenance costs over their lifespan, as they do not require oil changes and generally contain fewer components compared to ICE vehicles [4].

There are still multiple challenges surrounding the adoption of EV's. Key obstacles include the high cost of batteries, limited range compared to ICE vehicles, lengthy and

inconvenient charging times, and lack of adequate charging infrastructure [5].

Current electric vehicle charging infrastructure predominantly consists of plug-in charging stations. Initially, chargers were designed with lower power outputs, typically 11 kW or 22 kW, allowing for charging of EVs over several hours. However, for long distance journeys and heavy duty vehicles, faster charging times are required.

To address the inconvenience of long charging durations, higher-power chargers known as extreme fast chargers (DC fast chargers) have been developed, reducing charging time from several hours down to 20-30 minutes. Despite this improvement, the charging duration remains lengthy compared to refueling an ICE vehicle. Extreme fast chargers also present usability challenges for vehicle owners because of their bulky and difficult-to-handle charging cables. Additionally, these DC fast chargers have faced issues with vandalism, partly due to the high copper content in their charging cables.

EV wireless charging systems have been proposed as a proven alternative to plug-in charging, offering a more seamless experience for users. These wireless charging systems consist of a ground assembly (GA) and a vehicle assembly (VA). The ground assembly includes power electronics and a transmitter installed on or beneath the roadway. The vehicle assembly includes a receiver and power electronics within the EV to charge the battery. Fig. 1.1 depicts a basic graphic of both the ground and vehicle assembly developed by the EV wireless charging company WiTricity [6].

There are two major types of wireless charging systems: static and dynamic. Static wireless charging involves parking a vehicle on top of a ground assembly. When parked, the vehicle can automatically communicate with the charging infrastructure and initiate charging between ground assembly and vehicle assembly. This approach eliminates the need for user interaction with the charging infrastructure, enhancing convenience.

Despite these benefits, static wireless charging systems do not eliminate the need for large and costly batteries required for extended range. These systems also still face long charging times compared to refueling an ICE vehicle.

Dynamic wireless charging systems allow a vehicle to charge while driving over the

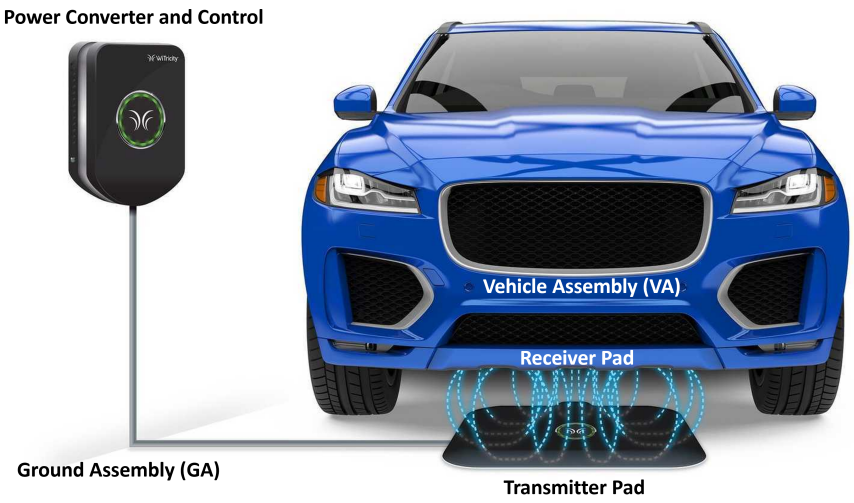

Fig. 1.1: Graphic depicting a basic wireless charging system

top of a ground assembly. The vehicle can communicate with the charging infrastructure and initiate charging while the vehicle is in motion. This approach reduces reliance on large batteries since the vehicle can draw power directly from the roadway. These in-motion charging systems also facilitate opportunity charging, extending the range of EVs and reducing the time required to stop at a charging station. Additionally, dynamic wireless charging takes advantage of electricity during daylight hours when solar energy is most abundant. As solar energy becomes more prevalent on the power grid, charging EVs during daylight hours will alleviate stress on the grid and mitigate issues associated with the "duck curve" [7]. This thesis focuses on the development and improvement of dynamic wireless charging technologies.

1.2 Literature Review

1.2.1 Wireless Power Transfer Technologies

Wireless power transfer has been demonstrated since the time of Nikola Tesla. Since

then, it has found applications in various technologies such as electronic toothbrushes, heating systems, biomedical devices, and more recently, cell phone charging [8].

There are two main types of wireless power transfer technologies: near-field and far-field. Near-field technologies include capacitive and inductive charging. Far-field technologies include power transfer through radiation via microwaves or lasers. For EV charging, near-field technologies are most commonly used due to their higher efficiency and ability to safely operate at high power levels [9].

Among near-field technologies, inductive charging currently shows the most promise for EVs due to its ability to reach high power levels. While less common, capacitive charging is gaining traction with higher power level developments introduced each year.

1.2.2 Electric Vehicle Wireless Power Transfer

The architecture of both near-field wireless charging technologies is similar. Power is sourced from a low voltage or medium voltage grid and converted to DC voltage through rectification. An inverter then takes this DC input and produces a high-frequency AC current which is then passed to the wireless charging transmitter.

In EV wireless charging, the distance between the transmitter and receiver is significant, resulting in a large air gap over which to transfer power. In order to transmit high power over a large air gap, resonant power transfer topologies are utilized.

After power is transferred between the transmitter and receiver, a rectifier on the vehicle converts the high-frequency AC current back to DC to charge the battery. A diagram showing the entire wireless charging architecture is shown in Fig 1.2.

Static wireless charging has been researched at varying power levels, and dynamic wireless charging is emerging at higher power levels. Dynamic wireless power transfer systems utilize the same technology as static wireless charging, but in dynamic systems, charging occurs while the vehicle is in-motion.

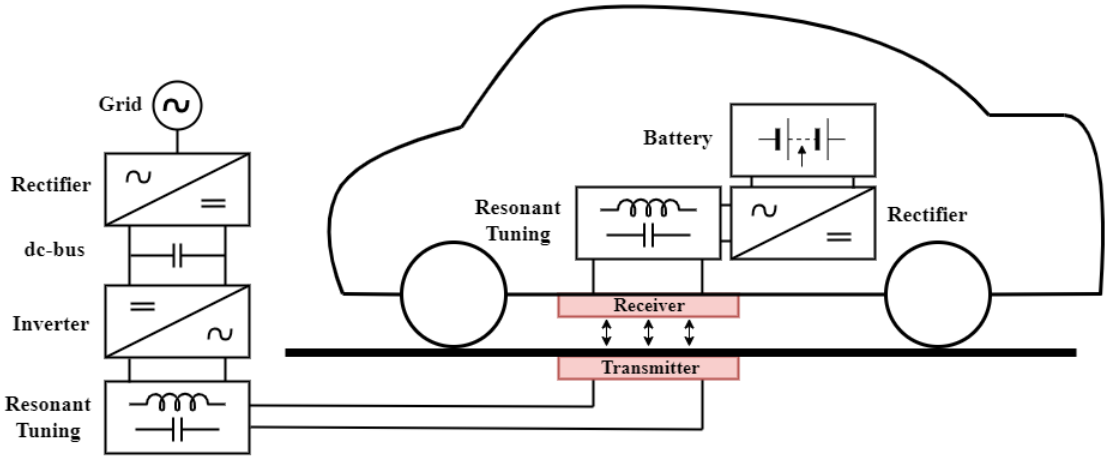

Fig. 1.2: Diagram of common architecture for near-field electric vehicle wireless charging systems

Capacitive Wireless Power Transfer

Capacitive power transfer functions by electric coupling through an electric field. High-frequency AC voltage is created on a metal plate which generates an alternating electric field. When another metal plate is brought within proximity of the electric field, charges are pushed to one side or the other allowing current to flow through the circuit. This power transfer follows Maxwell's equations and can be modeled as capacitors with a large air gap. For capacitive power transfer, MHz frequencies are commonly used.

Various resonant tuning topologies have been investigated for capacitive WPT systems including series compensation, LC compensation, LCL compensation, LCLC compensation, and CLLC compensation circuit. A diagram of these different system topologies is shown in Fig. 1.3 [10].

Inductive Wireless Power Transfer

Inductive power transfer functions by magnetic coupling through a magnetic field. High-frequency AC current flows through coils which generates an alternating magnetic field. When another coil is brought within proximity of the magnetic field, voltage is induced

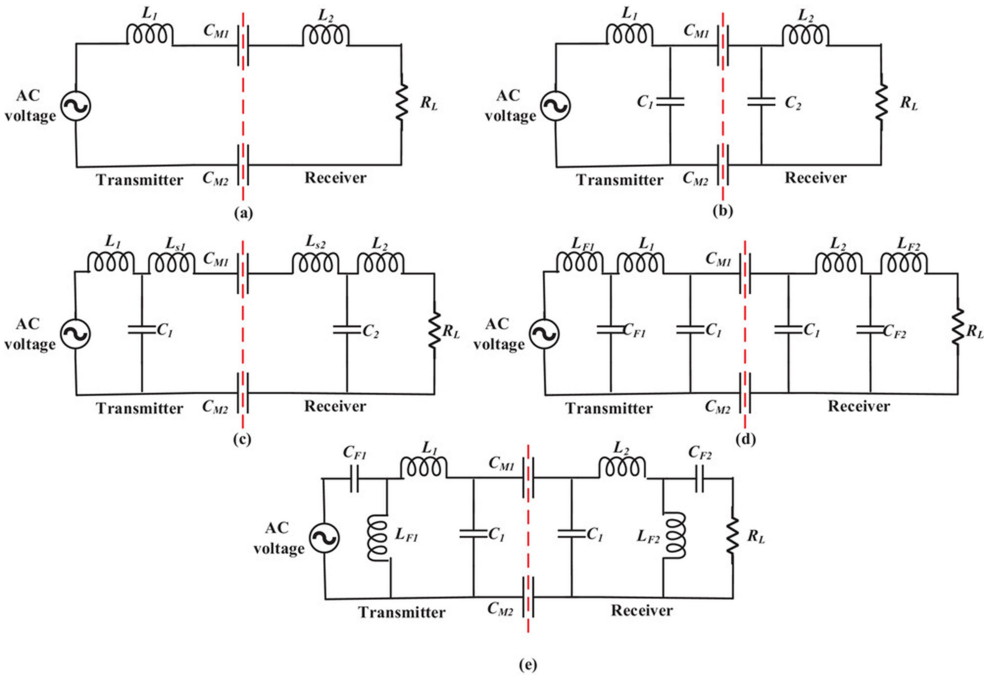

Fig. 1.3: Different compensation characteristics relevant in capacitive DWPT. (a) L compensation circuit, (b) LC compensation circuit, (c) LCL compensation circuit, (d) LCLC compensation circuit, and (e) CLLC compensation circuit.

across the wires and current flows through the circuit. This power transfer follows Maxwell's equations as can be modeled as loosely coupled coils. For inductive power transfer, 85kHz is a commonly used frequency since that has been chosen as the J2954 standard.

Various configurations have been proposed for inductive WPT systems including both 3-phase and single-phase topologies. Various resonant tuning topologies have also been investigated, including series tuning, parallel turning, series-parallel, LCCL-series, LCCL-parallel, and LCCL-LCCL [11]. A diagram of these different system topologies is shown in Fig. 1.4. Among inductive resonant topologies, the double-sided LCCL design has shown promise for providing load independent power control, low electromagnetic interference (EMI) compared to other topologies, and flexibility under varying misalignment conditions. [12]

Figure 1.5 depicts a typical schematic of the inductive LCCL EV wireless charging system, which is the standard topology examined in this thesis. While the principles discussed in this thesis are applicable to nearly all near-field resonant topologies, the simulation and

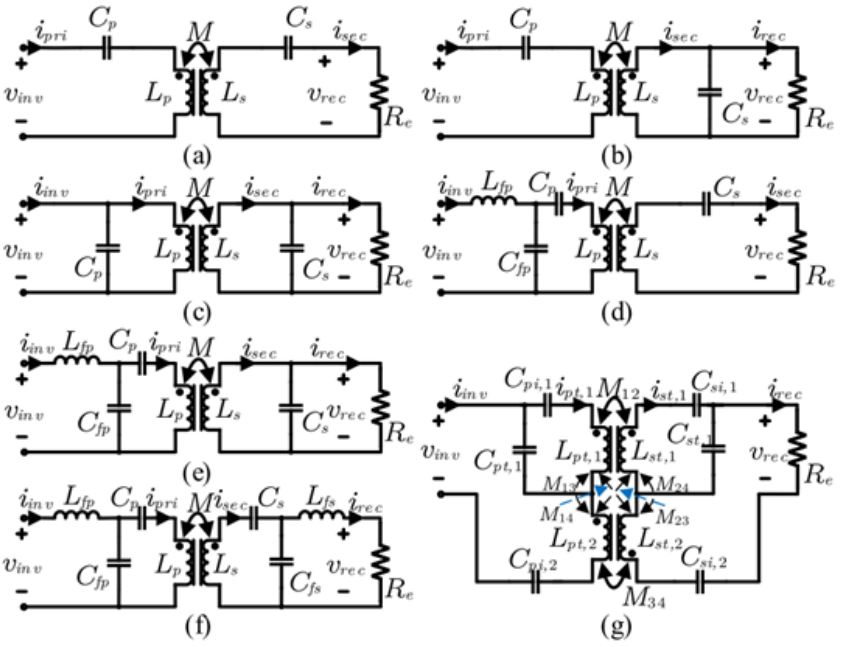

Fig. 1.4: Different compensation characteristics relevant in inductive DWPT. (a) SS. (b) SP. (d) LCCL-series (LCCL-S). (e) LCCL-parallel (LCCL-P). (f) LCCL-LCCL. (g) Series hybrid

hardware results presented in this thesis focus on an LCCL ground assembly for simplicity and consistency.

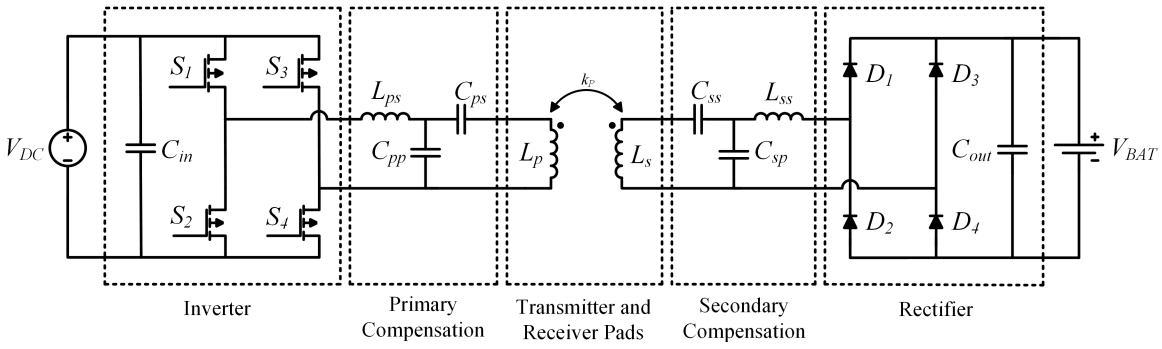

Fig. 1.5: Inductive LCCL WPT circuit schematic

1.2.3 Dynamic Wireless Power Transfer Implementation

In static wireless charging, the transmitter pad can be positioned slightly above the ground, such as in a parking stall shown in Fig. 1.6 [13]. However, this configuration is not feasible for dynamic systems, such as those used on interstate roadways. Dynamic wireless power transfer (DWPT) transmitters need to be installed beneath the roadway surface to avoid obstructing vehicles traveling on the road.

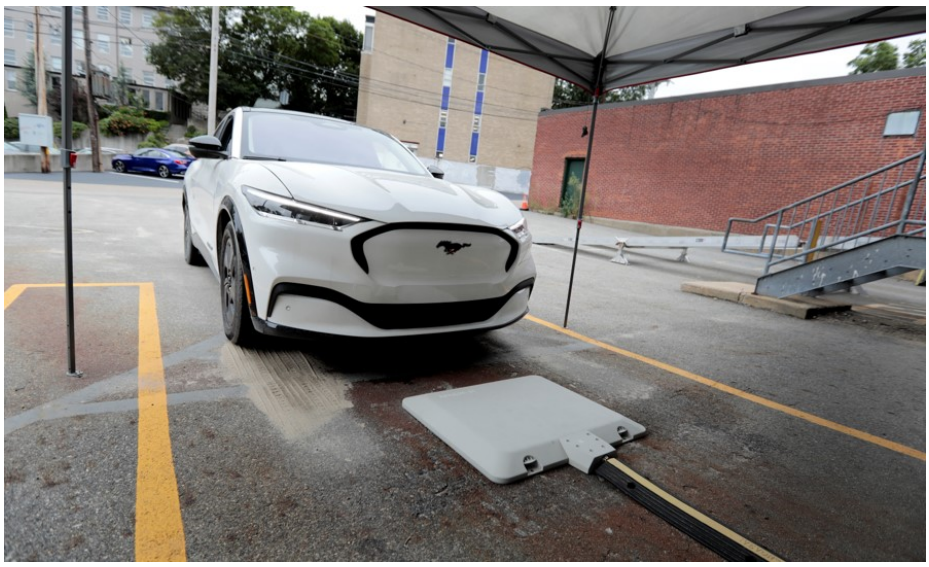

Fig. 1.6: Witricity static wireless charging system.

Multiple researchers have explored and are exploring effective ways to embed inductive wireless charging pads in the roadway [14–16]. These wireless charging pads generally come with a full electromagnetic assembly (Including the transmitter coil, ferrite, aluminum plate, and potting material). Some designs have removed the ferrite and aluminum in order to reduce costs, but this can negatively impact system performance. Researchers have found effective ways to embed systems in the roadway with and without ferrite and aluminum while minimizing the temperature of the coils [17–21].

Regardless of the near-field technology and resonant tuning topology chosen, every wireless charging system requires a power electronic inverter, tuning capacitors or inductors, and a transmitter pad. The high-frequency inverter and resonant tuning network connect

in between the power grid and the transmitter pad, and in previous studies, these have been housed in a roadside cabinet or in a trench alongside the roadway [22]. Electreon, an industry leader in these systems, places their power electronic management units at the roadside, as depicted in Fig. 1.7.

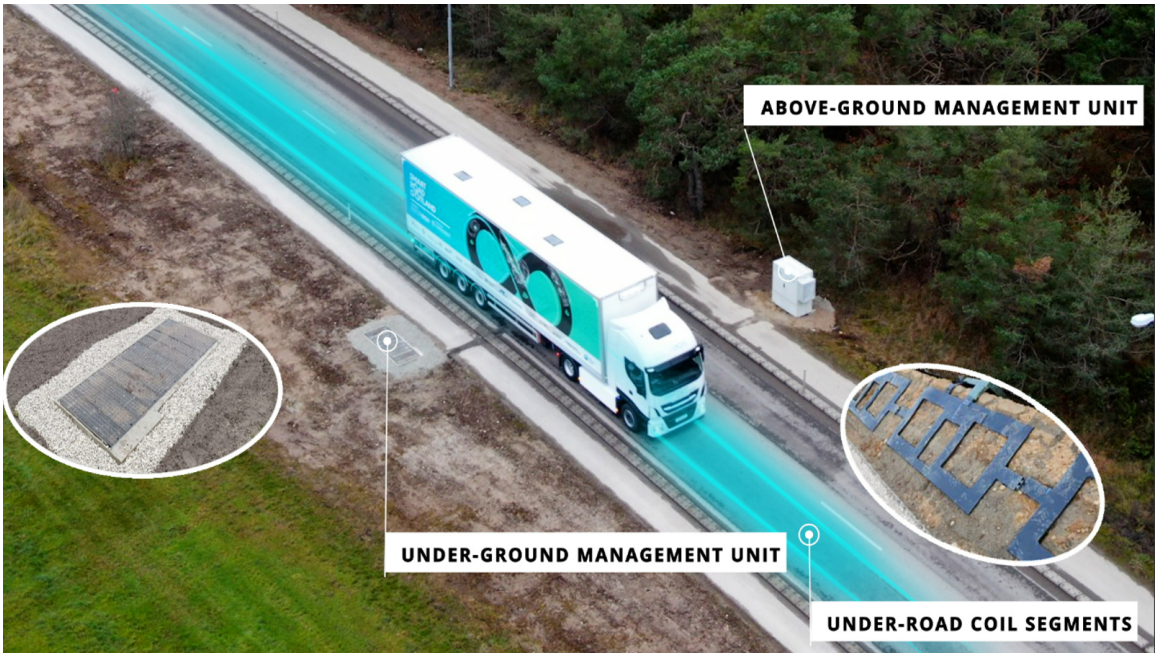

Fig. 1.7: Electreon system with roadside management units

Positioning management units at the roadside requires the installation company to obtain easements and right-of-way for the designated area where these cabinets will be constructed. This permitting procedure adds complexity and cost to the system. The number of roadway management units varies based on the chosen topology, but in the case of Electreon, roadside management units are needed approximately every 100 meters [23]. For the Indiana pilot project being developed by Purdue University, roadside management units are required every 7-8 meters.

In these state of the art designs, high-frequency, high-power cables such are required to connect the cabinets at the roadside to the transmitter pads under the road. These high-frequency cables increase eddy current losses in the system, and their long length

introduces additional inductance. Integrating this additional inductance into the tuning network poses a challenge, particularly because the positioning of each roadside management unit is tailored to the specific project requirements, meaning the lengths of wire between roadside management units and transmitter pads can vary with each installation. The AC cables connecting the management units to the charging coils typically consist of expensive Litz wire, further elevating the overall system cost.

Embedding the power electronics, including the inverter and tuning network, directly within the concrete or asphalt roadway alongside the transmitter pad can lead to increased system efficiency, simplified installation, and reduced costs. By integrating the power electronics close to the transmitter pad, only a DC cable is necessary to connect the ground assembly to a DC distribution line. This DC distribution line then connects to smaller and less frequent roadside management units which would only convert high-voltage AC power from the power grid to a DC bus. Consequently, the DC cables running from these management units can be standard copper cables instead of expensive Litz wire cables, thus reducing the system costs. A diagram of the traditional DWPT system compared to a fully-embedded DWPT system is shown in Fig. 1.8.

1.2.4 Roadway-Embedded Power Electronics

When embedding power electronics in the roadway, concerns surface regarding the long-term reliability of these systems. A Failure Modes and Effects Analysis (FMEA) of a double-sided LCCL WPT system conducted by Oak Ridge National Laboratory (ORNL) highlighted thermal management and thermal failures as primary reliability concerns [24]. Similarly, industries like aerospace have identified temperature-related failures as the leading cause of electronics failures, accounting for up to 55% of incidents [25]. The FMEA analysis conducted by ORNL was adapted for this thesis to include roadway-embedded power electronics and indicated that besides the electromagnetic assembly, the inverter and tuning capacitors are the power electronic components at the highest risk of failure (see Appendix). Other reliability considerations include failures due to environmental factors such as water damage, humidity, and vibrations. Additionally, long-term concerns include

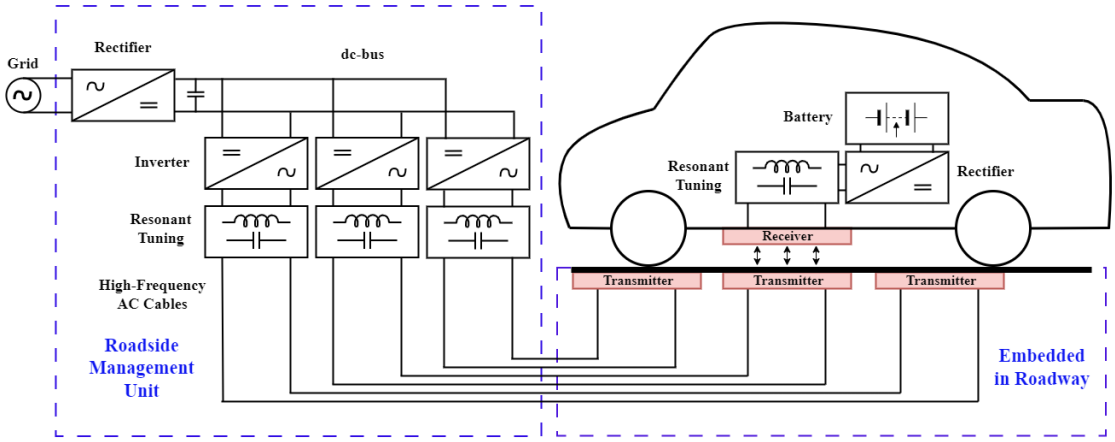

(a) Traditional DWPT system with non-embedded power electronics

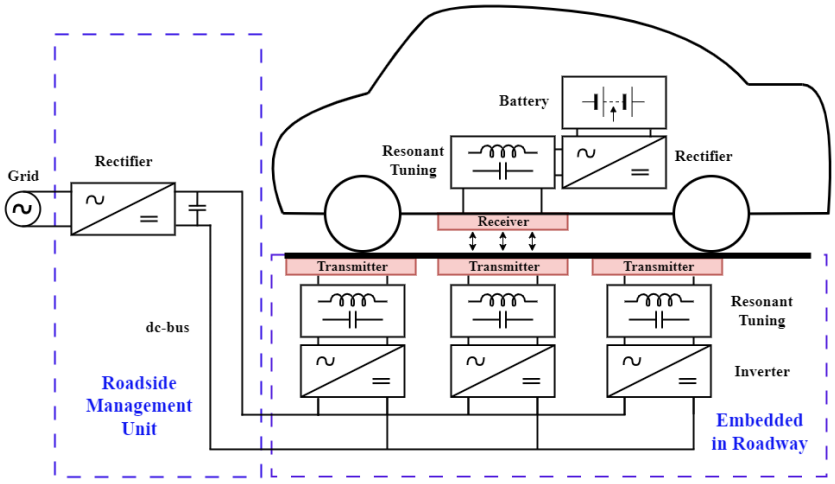

(b) Proposed DWPT system with roadway-embedded power electronics

Fig. 1.8: Different roadway-embedded DWPT system configurations

the serviceability of these systems as they reach the end of their lifespan or in the event of a failure.

Research on the thermal management of roadway-embedded power electronics is currently limited. One paper has explored the thermal management of ground assembly power electronics, placing components such as the inverter and tuning network beneath the roadway [26]. However, this paper lacks hardware validation of its simulation results, and focuses on an underground management unit beneath the electromagnetic assembly, rather than addressing a fully roadway-embedded scenario. The configuration proposed in [26], and illustrated in Fig. 1.9, may be suitable for static wireless charging, but would be expensive and time-consuming to implement for dynamic wireless charging systems and could negatively impact the structural integrity of the roadway.

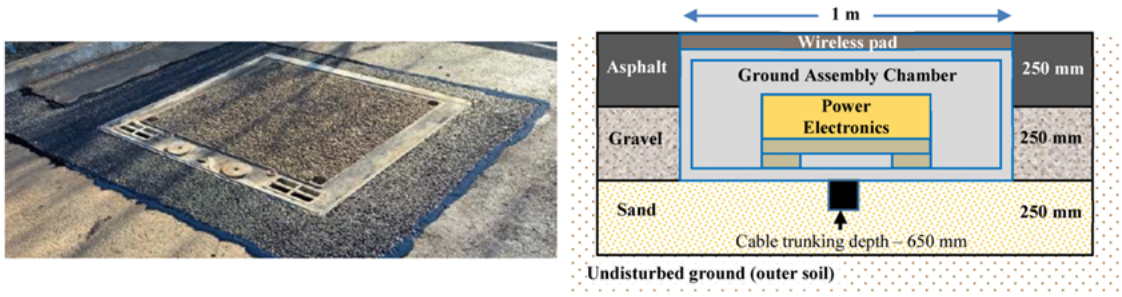

Fig. 1.9: Warwick University underground WPT design

In standard roadside cabinets, the thermal management of high-power electronics is well-researched, utilizing both active and passive cooling methods. Typically, fans or natural air convection are employed. In scenarios where fans are not practical or for higher power levels, such as with DC fast chargers, liquid cooling with chill plates is often used to reduce component temperature [27].

When cooling electronics embedded in interstate highways, forced air cooling is impractical, and while liquid cooling of embedded DWPT systems has been attempted, it is costly and raises significant reliability concerns [28]. Furthermore, the space required for liquid cooling storage and management units poses an additional challenge, requiring easements

for roadside installation. Therefore, passive cooling methods are preferred for the thermal management of roadway-embedded electronics to achieve benefits in terms of cost, space efficiency, and ease of installation.

1.2.5 Thermal Management Considerations for Roadway-Embedded Electronics

When designing thermal management systems for roadway-embedded electronics, many factors must be considered including component losses, ambient roadway temperature, power electronics packaging, and roadway construction materials.

In passive thermal management scenarios such as the encapsulation of power supplies, inductors, transformers, and coils, thermally conductive potting material such as epoxy has been used [29]. This material provides a path for heat to transfer out of a component before dissipating into the air. This potting material also provides a protective coating from environmental elements such as water and humidity.

Another passive management technique uses heat sinks integrated with a phase change material (PCM) or two-phase material [30]. When these heat sinks reach the temperature at which the PCM (such as paraffin wax) melts, a phase change begins to occur due to the latent heat required to change phases. The material is able to continue absorbing heat energy without the temperature of the material increasing. This is a passive way of limiting the temperature in the case of pulse mode operations by storing the heat during the "on" cycle and dissipating the heat (as the PCM refreezes) during the "off" cycle [31].

Recent roadway-embedded DWPT systems have utilized passive cooling materials such as thermally conductive epoxies and PCM in their designs [14, 21, 32]. Current research in this field has predominantly focused on the electromagnetic assembly, but similar principles could be extended to passive cooling of the power electronics.

Previous research has extensively focused on improving efficiency and reducing losses in wireless charging systems. This thesis aims to explore methods for dissipating heat from roadway-embedded power electronics, assuming power loss has already been minimized. While this thesis does not focus on reducing losses, it is still essential to understand loss

generation and the typical failure temperature ranges of components to improve modeling and prediction of temperature rise.

Inverter Losses

For the power electronic inverter, MOSFET devices have been commonly used for their ability to operate at high frequencies, handle high voltage levels, and withstand elevated temperatures.

Losses from the MOSFET are generated within the junction of the device. These losses are primarily due to switching loss and conduction loss. If soft switching is achieved within the DWPT system, then losses are primarily due to conduction loss and can be calculated using the $R_{ds(on)}$ of the MOSFET switch as shown in equation (1.1)

$$P_{L(switch)} = I_{rms}^2 R_{ds(on)} \,. \tag{1.1}$$

Other losses within the inverter include power loss from the gate driver circuitry, auxiliary power supplies, and DC link capacitors.

The thermal management of MOSFETs and power inverters has been extensively studied [33–35]. Common techniques include using thermal interface materials such as thermal grease or thermal paste to connect a heat sink to the MOSFET modules. The heat sink is then cooled with air from a fan or by natural convection. The increased surface area of the heat sink enhances heat transfer from the high thermal conductivity material, typically aluminum, to the surrounding air. In passive thermal management, the heat sink can be combined with phase change material (PCM) to cool the inverter [36]. In a roadway-embedded environment, heat dissipation involves transferring heat from the heat sink, PCM, and PCB to the surrounding roadway material.

MOSFET junctions are typically rated for maximum temperatures between 125 - 175°C. For continuous, reliable operation, MOSFETs should be maintained below these temperature limits. Furthermore, at higher power levels, the recommended maximum temperature indicated in the datasheet might be lower.

Resonant Capacitor Losses

In previous DWPT systems, a variety of capacitors have been used in the resonant tuning network. Film capacitors have been the most popular choice due to their low ESR, high-frequency capabilities, and self-healing abilities. Ceramic capacitors with constant DC voltage ratings have also been widely used for DWPT tuning networks due to their low cost, compact size, and high-temperature ratings. For roadway-embedded applications, it is important to select an appropriate capacitor type that will minimize temperature rise and enhance reliability.

Losses from the resonant capacitors and DC link capacitors are generated within the internal structure of the capacitor. These losses are primarily due to the metal losses and dielectric losses within the material. These losses are are given in capacitor datasheet either in terms of the capacitor dissipation factor or ESR of the capacitor as shown in equation (1.2) and equation (1.3).

$$P_{L(cap)} = I_{rms}^2 ESR_{(cap)} \,. \tag{1.2}$$

$$P_{L(cap)} = V_{rms} I_{rms} tan(\delta) \,. \tag{1.3}$$

Where $ESR_{(cap)} = \frac{tan(\delta)}{\omega C}$ and tan(δ) is the dissipation factor (DF), ω is the frequency in radians, and C is the capacitance of the capacitor.

The thermal management of roadway-embedded capacitors can be achieved using thermally conductive potting material, PCM, and electronics packaging designed to reduce the thermal resistance path to the roadway.

Both film and ceramic capacitors are typically rated for maximum temperatures between 100 - 125°C. For continuous and reliable use, it is recommended that these capacitors operate below their maximum temperature, which is often derated at higher current and voltage levels. Resonant capacitors in the ground assembly have the lowest allowable operating temperature among WPT components. Therefore, roadway-embedded capacitors

must be carefully designed to prevent reduced lifespan and potential failure.

Resonant Inductor Losses

In previous DWPT systems, tuning inductors have generally been designed with Litz wire and ferrite cores.

Losses from the tuning inductor are generated within the copper and ferrite used in their designs. The copper losses primarily result from eddy current loss at high frequencies and conduction loss through copper. Eddy current loss in large Litz wire is difficult to calculate analytically and is typically evaluated through simulations or experiments [37]. Ferrite losses are primary due to core loss caused by high-frequency magnetic flux through the ferrite. Conduction loss is calculated based on the ESR of the wire material and the current through the coils as shown in equation (1.4).

$$P_{L(inductor)} = I_{rms}^2 ESR_{(wire)} \,. \tag{1.4}$$

For passive thermal management of inductors, thermally conductive epoxy has been used to provide insulation and transfer heat to the ambient. This method can also be utilized in roadway-embedded scenarios.

Litz wire and ferrite core can survive temperatures as high as 200°C before failure. In practical operation, the temperature of tuning inductors are generally kept below 150°C.

Electromagnetic assembly losses

Losses in wireless charging coils closely resemble losses in tuning inductors, as they stem from the copper and ferrite materials. Additional losses in the electromagnetic assembly may arise from eddy current loss in potential aluminum shielding.

The losses attributed to the electromagnetic assembly have been studied in previous research and continue to be researched by other groups [38–40]. This thesis primarily addresses thermal management due to loss within the power electronics, but it is crucial to also consider the losses from the electromagnetic assembly, especially if those losses are in

close proximity to the power electronic components. The heat generated from power loss within the entire DWPT system must be dissipated away from the electronics to ensure that the thermal design is successful.

Temperature and Reliability

Reliability is an important consideration for roadway-embedded DWPT systems due to the challenges associated with their repair and replacement. Reducing operating temperature and minimizing thermal cycling of components has been shown to enhance reliability. High-temperature operation can cause reduced Mean Time To Failure (MTTF) due to increased electromigration [41], while increased temperature cycling can lead to stress or fatigue failures due to thermal expansion [42].

In power electronic components, there is an inherent trade-off between cost, power density, and reliability. As power density increases, components generally experience higher power loss per unit area, leading to greater temperature gradients. Although more expensive components often offer better thermal performance, their higher costs can make large-scale implementation impractical. Optimizing this trade-off is essential to maximizing the effectiveness of DWPT systems.

Ambient Roadway Conditions

Asphalt and concrete roadways can experience temperatures ranging from -25°C to 70°C due to weather conditions and solar radiation [26]. These high temperatures can increase the overall DWPT system temperature, making their consideration essential for thermal design.

The temperature of roadway-embedded electronics increases with higher ambient temperatures, leading to higher steady-state temperatures for the components. The temperature rise from ambient needs to be small enough to prevent temperature failure, particularly during extreme temperature conditions such as an unshaded roadways in the summer heat. Heat from a single DWPT component can also elevate the temperature of the roadway leading to a higher ambient temperature for nearby components, thus making it important

to consider all sources of heat in a roadway-embedded system design. In severe temperature scenarios, the system might need to be temporarily turned off to avoid thermal failure.

Roadway Construction Materials

The temperature of the roadway depends the type of pavement used and the thermal properties of the surrounding roadway materials. Common pavement types include rigid pavements like concrete, flexible pavements like asphalt, and composite pavements with both concrete and asphalt layers. Typical road construction consists of a sub-grade layer, a sub-base or base course layer for support, and a surface layer of concrete or asphalt, as shown in Fig. 1.10. The thickness of these layers can vary based on factors such as location, usage, and age of the roadway.

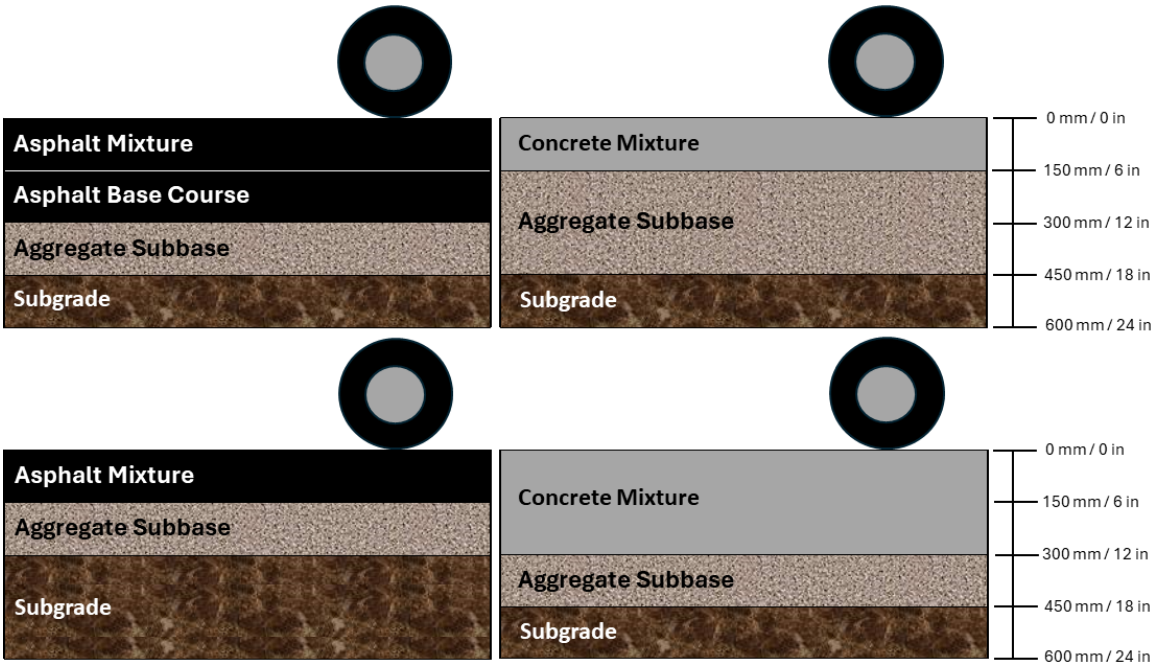

Fig. 1.10: Different roadway layer stackups with flexible and rigid pavement

In DWPT systems, the materials surrounding the power electronics will depend on the roadway's thickness and the feasibility of various installation depths. Previous research has demonstrated that the transmitter pad can be installed in either the asphalt layer or the

sub-base layer depending on the specific application, as shown in Fig. 1.11 [38]. Similarly, power electronics could be embedded in the asphalt or concrete layers, or buried in the sub-base or sub-grade layers.

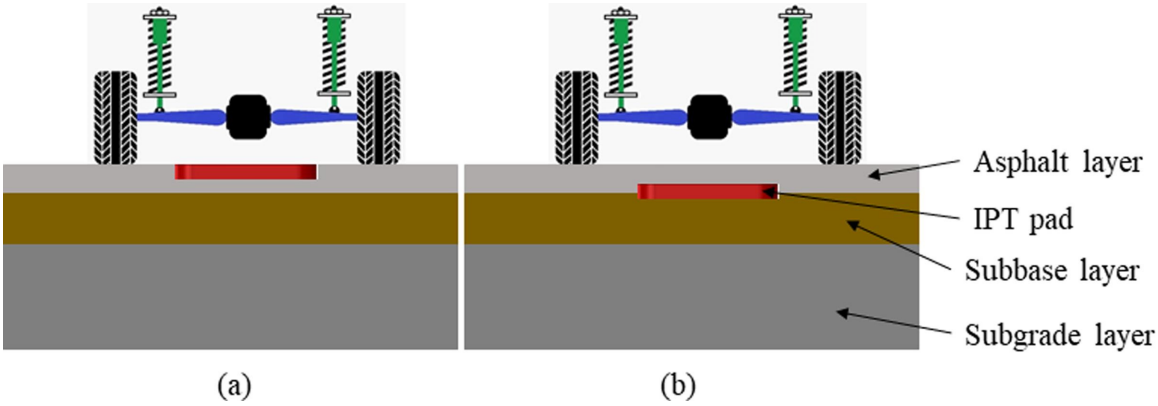

Fig. 1.11: Graphic illustration of the 2D cross-sectional view of an inductive power transfer (IPT) pad. (a) Transmitter pad in the asphalt pavement layer, and (b) buried between the asphalt and sub-base layer.

Ideally, a universal ground assembly design would accommodate any roadway type. However, since roadway construction varies, it is likely that the design and construction of electronics will need to be adapted for different roadways. Therefore, it is important to consider the thermal properties of common roadway materials and determine where the power electronics can feasibly be embedded within the roadway structure.

The thermal conductivity of concrete has been measured in various studies and changes depending on cement type, mixture ratios, and aggregate varieties [21]. The thermal conductivity of concrete can range from 0.1 $\frac{W}{mK}$ to 3.3 $\frac{W}{mK}$, with the average value around 1.8 $\frac{W}{mK}$. This broad range suggests that the effectiveness of heat transfer is heavily influenced by the source and composition of the concrete. Asphalt roadways face similar challenges with inconsistent thermal conductivity, though their thermal conductivity is even lower than concrete, ranging from 0.7 $\frac{W}{mK}$ to 1.7 $\frac{W}{mK}$.

Common materials used in base-course and sub-base road construction include Granite, Limestone, Quartzite, Sandstone, Syenite, Dolostone, and Gabbro. These materials have

thermal conductivities ranging from 0.2 $\frac{W}{mK}$ to 1.2 $\frac{W}{mK}$ when dry and up to 5 $\frac{W}{mK}$ with high water content [43].

Roadway-embedded electronics will likely be encapsulated in a thermally conductive epoxy first and then surrounded by roadway material. Modern epoxies have thermal conductivities above 2 $\frac{W}{mK}$, which surpasses the average thermal conductivity of concrete and asphalt [44]. This higher thermal conductivity suggests that epoxy can help transfer heat away from the electronics better than most roadway materials. In addition to enhancing thermal management, epoxy can help protect the electronics during the installation and construction process, shielding them from the high temperatures of freshly poured asphalt and the pressure from heavy rock aggregates in new concrete.

Encapsulating electronics in epoxy and embedding them in concrete or asphalt significantly increases the thermal mass. Consequently, the electronics will exhibit a much longer RC time constant compared to natural convection or active cooling methods. In a roadway-embedded scenario, the roadway serves as a thermal sink, facilitating heat dissipation and prolonging the transient temperature rise. As a result, it is important to consider systems that may never reach thermal equilibrium. Due to variations in roadway materials across different locations, both transient and steady-state temperature rises will differ, even with similar power losses.

1.2.6 Dynamic Wireless Power Transfer Utilization Patterns

Current DWPT systems are used by a limited number of vehicles for the brief periods of time when a vehicle drives over the system. With current EV adoption rates, the system may only be active for a few seconds and then inactive for minutes to hours. In such cases, the high thermal mass of the roadway keeps temperatures low and the systems have time to fully cool down between charging sessions.

As electric vehicle adoption increases, DWPT systems are likely to experience higher utilization rates. In worst-case scenarios, prolonged stop-and-go traffic from electric vehicles may resemble static charging patterns. This increased utilization will result in higher temperature rises, bringing systems closer to thermal equilibrium. Therefore, DWPT systems

should be designed considering various utilization profiles and anticipated ambient roadway temperatures. If the utilization of these systems exceeds design specifications and temperatures rise beyond safe limits, the system can be temporarily deactivated until temperatures returns to acceptable levels.

1.3 Proposed Work

1.3.1 Research Objectives

This thesis seeks to develop a generic design procedure for roadway-embedded power electronics which takes into account power electronics design, losses, power level, electronics packaging, ambient conditions, roadway construction, and lifetime requirements. This thesis also seeks to analyze multiple past and current DWPT systems and propose modifications and practical design changes that will improve the systems ability to include roadway-embedded power electronics.

1.3.2 Thesis Organization

This thesis will be organized as follows: Chapter 2 discusses the successes and failures of a formerly-embedded DWPT system. Chapter 3 discusses a proposed design procedure for roadway-embedded electronics. Chapter 4 discusses a current DWPT system, what it would take to embed this current system in the roadway, and proposed modifications to the inverter and capacitor bank that would improve the ease of embedding the system with passive thermal management. Chapter 5 discusses a proposed new capacitor bank, outlines simulation and experiment results for this component, and discusses a full DWPT roadway-embedded design example. Chapter 6 offers a conclusion, outlines the contributions of this work, and discusses future work.

CHAPTER 2

Previous 50 kW Concrete-Embedded Power Electronics

2.1 Overview of Utah State University Concrete-Embedded DWPT Project

At Utah State University, a 2021 research project explored embedding various DWPT systems in concrete, focusing on how the electronics affected the structural integrity the concrete and how the concrete impacted the temperature rise of the electronics. The project involved three different concrete blocks: one with only the transmitter pad embedded, another with the transmitter pad and tuning network embedded, and a third with the transmitter pad, tuning network, and inverter embedded in the concrete. These concrete blocks are illustrated in Fig. 2.1, as discussed in [17, 21, 32]. This chapter investigates the third block, which includes the entire ground assembly embedded in concrete.

Fig. 2.1: Previous concrete-embedded DWPT systems

Very little testing of these power electronics was conducted within concrete before the system experienced failure. As part of this thesis, the two-year-old concrete-embedded power electronics were removed, the cause of failure identified, and an analysis conducted to evaluate how well the packaging, thermal, and electrical designs of the power electronics functioned within the concrete. The topology of this formerly-embedded DWPT system was a double-sided LCCL split compensation tuning topology as shown in Fig. 2.2.

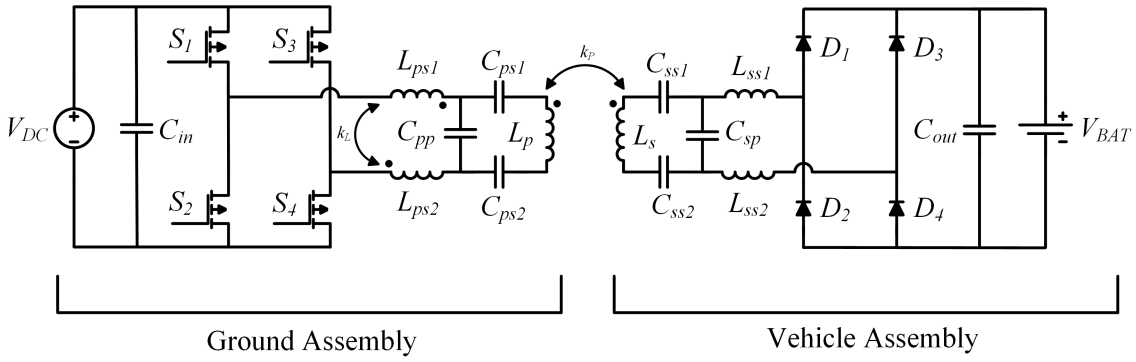

Fig. 2.2: Formerly-embedded electronics circuit diagram

The hardware component values for the ground assembly are shown in Table. 2.1. Various types of vehicle assemblies can be designed to utilize the same ground assembly, resulting in vehicle assembly component values that vary depending on the automotive company's design. Consequently, the component values for the vehicle assembly have not been specified.

Table 2.1: Hardware component values for formerly-embedded ground assembly

Component	Hardware Value
V_{DC}	600 V
f_s	85 kHz
C_{in}	104 uF
L_{ps1}	3.51 uH
L_{ps2}	2.3 uH
k_L	0.3
C_{ps1}&C_{ps2}	425.8 nF
C_{pp}	440 nF
L_p	24.2 uH

When this system was designed, the power electronic components were first encapsulated in epoxy and later embedded in concrete. Over the course of two years, the concrete block containing these encapsulated electronics was exposed to various natural elements including rain, snow, humidity, and extreme temperatures. During these two years, the electronics were operated intermittently at differing duty cycles. Thermal sensors and strain sensors were included within the concrete block to monitor temperatures during and after operation of these electronics. Electrical values were also measured via a USB connection to the inverter FPGA within the concrete block. For convenience, some tests were conducted in a $k_p = 0$ no-load condition with only the ground assembly. During one of these no-load tests, the measured power through the system halved, and the system was never able to return to full power operation. After this failure occurred, no further useful data could be extracted, so the concrete block was dismantled to retrieve the electronics. Fig. 2.3 shows an image of these epoxy-potted power electronic components captured during their removal from the concrete block.

Fig. 2.3: Power electronics components, including an inverter (left), inductors (middle), and capacitor bank (right), extracted from concrete after being embedded and exposed to environmental conditions for two years

2.2 Failure Analysis

After removing these power electronics from concrete, each of the three components were independently inspected, tested, and measured to evaluate functionality and identify the component responsible for the system failure. Visual examination revealed no visible water or stress damage on any of the components. The electrical safety limits were tested thoroughly before embedding the inverter, and since the failure occurred during steady-state operation without triggering any faults, it is presumed that electrical over-voltage or over-current was not the cause of failure. Both the tuning inductor and tuning capacitor retained their original component values and operated as expected. The inverter, however, failed to generate the correct square wave voltage waveform on its output. The output voltage waveform from the inverter was measured when connected to an inductive and resistive load as shown in Fig. 2.4. The component values for this test are listed in Table. 2.2. The gate drivers were given a 50% duty cycle waveform with a 450 ns dead-time and the output voltage waveform was measured between node V_a and V_b. A screenshot of the oscilloscope inverter output voltage measurement is shown in Fig. 2.5.

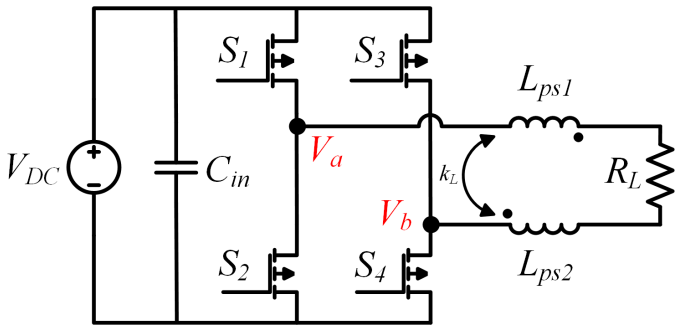

Fig. 2.4: Inverter testing circuit with inverter connected to an inductive/resistive load

The inverter switches appear to operate correctly, as evidenced by their ability to generate both high and low voltages, but the positive side of the waveform does non sustain the high voltage for the entire duration. This observed behavior indicates a malfunction in one of the MOSFET gate drivers. When the high side gate driver is disconnected or the signal to the gate driver is insufficient to drive it high, the MOSFET switch is unable to

Table 2.2: Hardware component values for inverter testing circuit

Component	Hardware Value
V_{DC}	0.3 V
f_s	85 kHz
C_{in}	104 uH
L_{ps1}	3.51 uH
L_{ps2}	2.3 uH
k_L	0.3
R_L	2.5 Ω

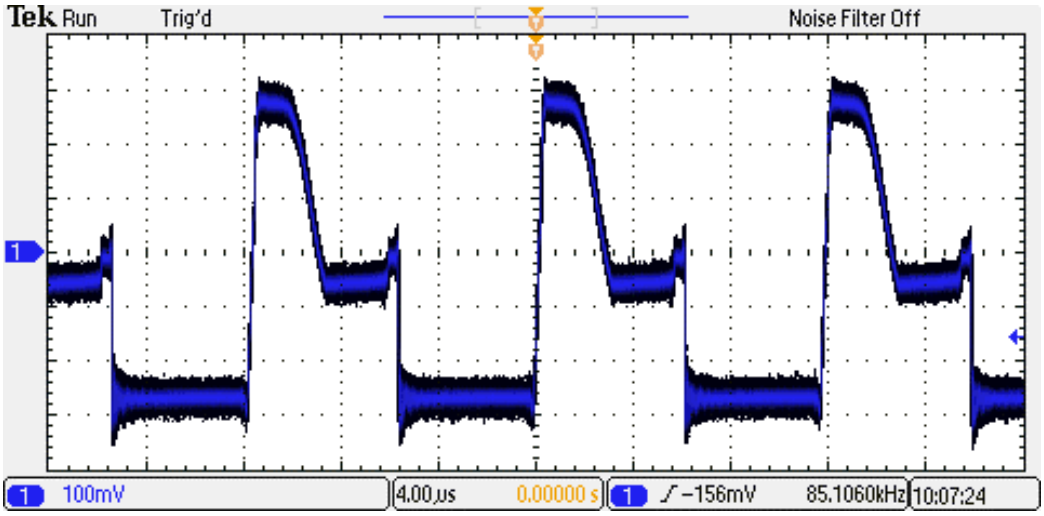

Fig. 2.5: Inverter output voltage waveform as measured by oscilloscope

stay on and the voltage drops. This is confirmed by LTspice simulation results shown in Fig. 2.4 which closely resembles the measured output voltage waveform from the inverter.

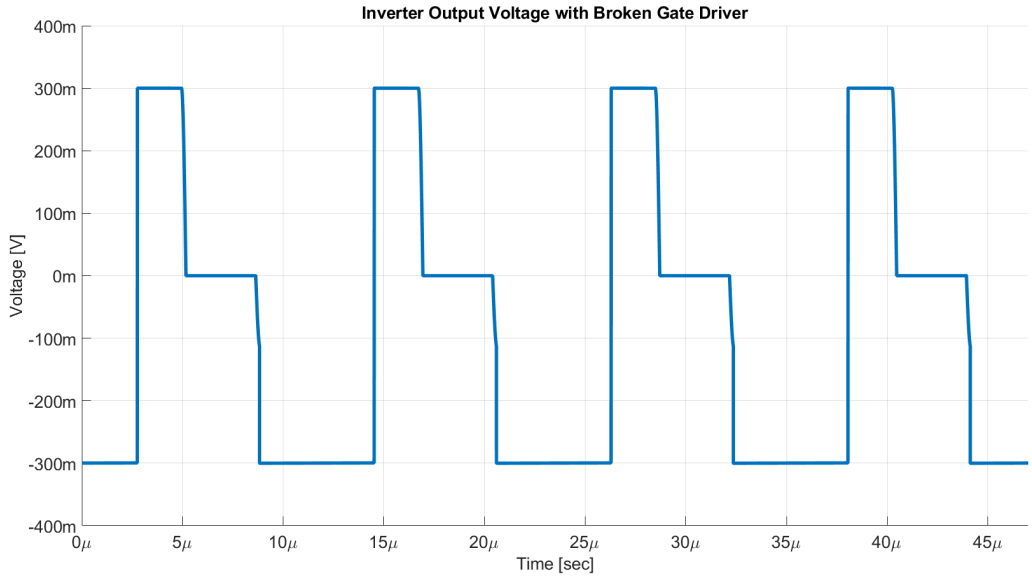

Fig. 2.6: Inverter output voltage waveform from LTspice when high side gate driver is disconnected

Upon closer examination of a duplicate inverter that was neither encapsulated in epoxy nor embedded in concrete, it was found that under certain operating conditions, the gate drive board reached steady-state temperatures as high as 90°C with natural convection. Fig. 2.7 displays a FLIR thermal image depicting this high-temperature operation, alongside T-type thermocouple measurements of the Wolfspeed CGD15HB62LP gate drive board. The hottest points on these gate drive boards are concentrated at the output gate resistors.

The high temperature of the gate drive boards occurred when the inverter was functioning in a no-load condition as shown in Fig. 2.8. In this scenario, most of the power flowing through the circuit is reactive and the resulting current flowing through inverter is low. It appears that in this no-load condition, the current required to discharge the switch C_{oss} capacitance is insufficient at the standard dead time to achieve soft switching. When the inverter is hard switching, more gate current is required to switch the MOSFET resulting in increased power dissipation across the gate resistor and subsequent temperature rise.

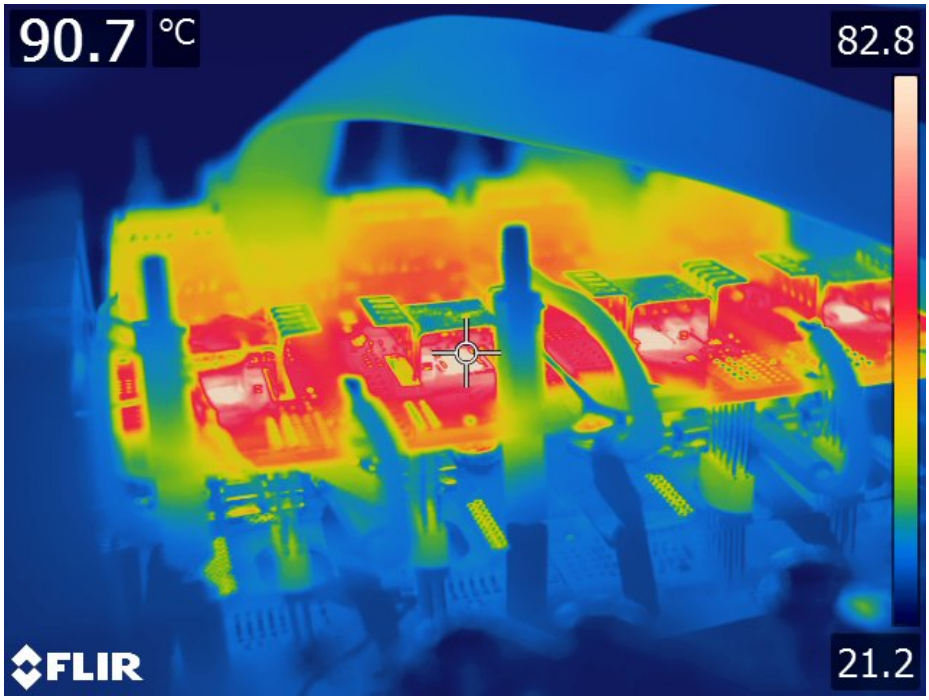

(a) FLIR thermal camera image of gate driver

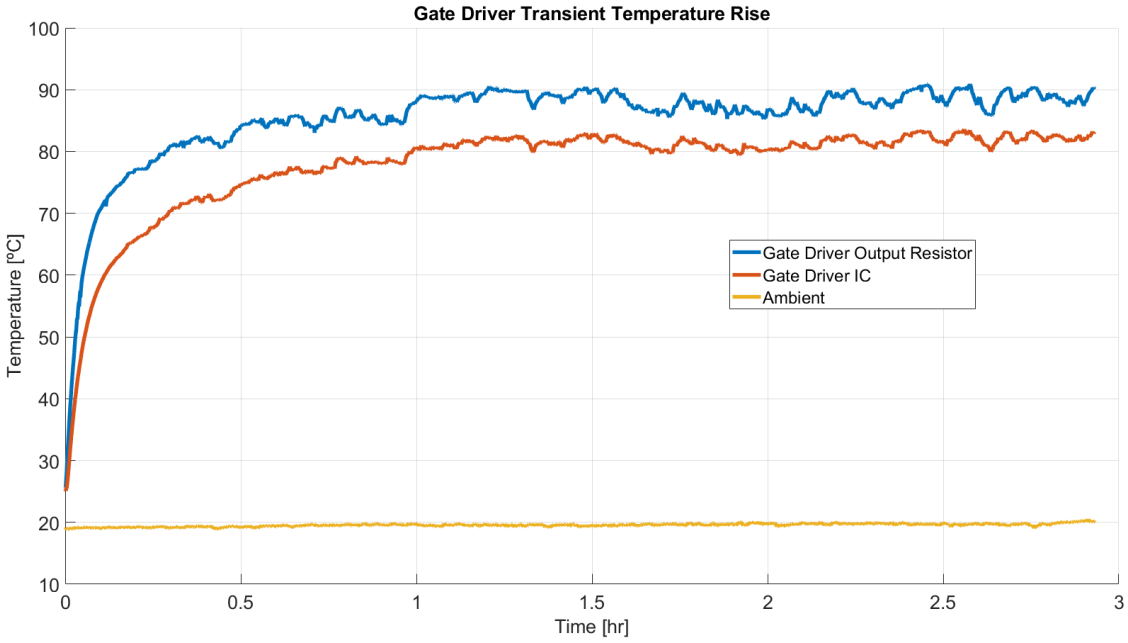

(b) T-Type Thermocouple Measurements of Gate Driver

Fig. 2.7: Temperature measurements of Wolfspeed CGD15HB62LP gate driver board

The cooling of the gate driver was not initially considered a significant concern when this system was first designed, and this high-temperature operation went unnoticed prior to encapsulating and embedding the inverter. It is likely that while conducting prolonged thermal no-load tests within the concrete, the temperature of an output gate resistor and corresponding gate drive board increased above their maximum rated temperature, resulting in internal component failure or causing surrounding components to fail.

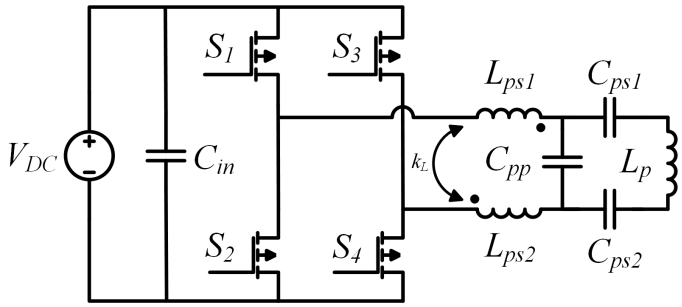

Fig. 2.8: LCCL tuning network no-load condition

In future designs, the dead time of the inverter should be increased during low-load conditions, allowing more time for the MOSFET C_{oss} capacitance to dissipate, thereby ensuring soft-switching across all operating conditions.

2.3 Inverter Analysis

The formerly-embedded inverter utilized two CREE CAS325M12HM2 MOSFET modules along with the corresponding CREE CGD15HB62LP gate drive boards. The inverter also included an FPGA control board with sensing and protection functionalities. The MOSFET modules were attached to a PCM heat sink which utilized RT82 Rubitherm PCM. The inverter board, control board, and PCM heat sink were all encapsulated in Epoxies 50-2151 FR polyurethane potting material. The inverter after being removed from concrete is shown in Fig. 2.9.

In an attempt to access the gate driver boards, the epoxy encasing the inverter was chipped away. Only a hard epoxy was used to pot the inverter, and since this epoxy bonded

Fig. 2.9: Inverter encapsulated in epoxy after being removed from the concrete block

very well to the PCBs, the attempt to remove epoxy from the inverter was ineffective. Ultimately, these attempts resulted in further damage to the inverter, rendering it impossible to access the gate driver board for repair or verification of the failure.

Instead, the inverter epoxy block was cut directly in half so the packaging, potting, and PCM could be analyzed. The PCM was originally added to the heat sink with the fins oriented downward. When embedded in concrete, the inverter was positioned in the opposite direction with the fins facing upward. The upward positioning of the fins was done deliberately so when the heat sink reached a temperature sufficient to melt the PCM, the PCM would flow downward to the heat sink's base where the hottest spots of the inverter heat sink were located. The hot, melted PCM would then rise and be replaced with colder PCM causing eddy current heat flow within the heat sink. When the inverter was cut in half, as shown in Fig. 2.10, there was a visible gap between the PCM and the heat sink's base. This gap suggests that the heat sink never reached a temperature high enough to fully liquefy the PCM. If the PCM, which melts between 77°C and 82°C, remained solid, it suggests that the inverter switches, which have a maximum temperature of 175°C, never got hot enough to encounter thermal failure.

Fig. 2.10: Cross section of formerly-embedded inverter PCM heat sink

For future roadway-embedded inverters, additional testing and design of the gate driver is needed to ensure that the temperature in maintained below acceptable limits across all operating points. Moreover, further testing and validation of the PCM heat sink design is needed to determine its effectiveness for roadway-embedded applications.

2.4 Capacitor Bank Analysis

The formerly-embedded capacitor bank utilized high power film capacitors interconnected with copper bus bars. These power capacitors are rated for internal operating temperatures up to 85°C. The full capacitor bank was first surrounded by PureTemp 68 PCM and then encapsulated in Epoxies 50-2151 FR polyurethane thermally conductive potting material as shown in Fig. 2.11. The capacitor bank after being removed from concrete is shown in Fig. 2.12.

The effectiveness of the PCM used in the capacitor bank was not documented prior to embedding it in concrete. It was deemed necessary to conduct thermal testing on the formerly-embedded capacitor bank to evaluate the cooling effectiveness of the packaging and PCM. To facilitate this, small holes were cut in the epoxy block and thermocouples were inserted into the block and attached to the copper bus bars of the capacitor bank. These thermocouples were positioned at the locations indicated by the yellow stars in Fig. 2.13.

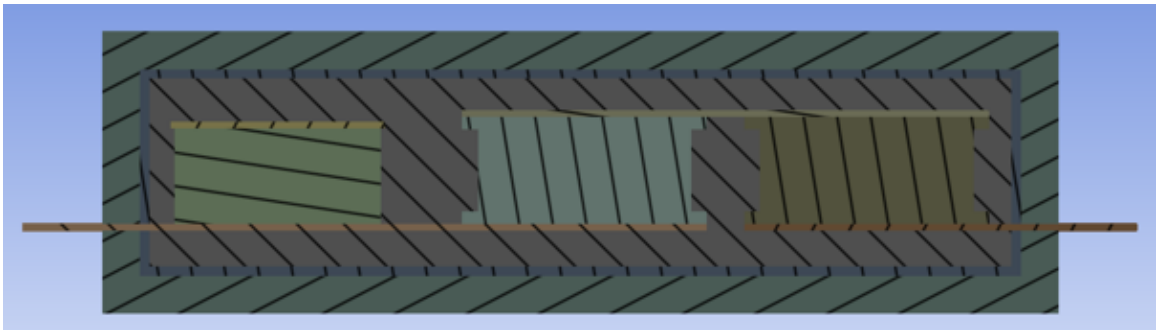

Fig. 2.11: Cross-sectional side view of formerly-embedded capacitor bank in box filled with PCM (red) and coated in epoxy (green)

Fig. 2.12: Top view of formerly-embedded capacitor bank with epoxy potting

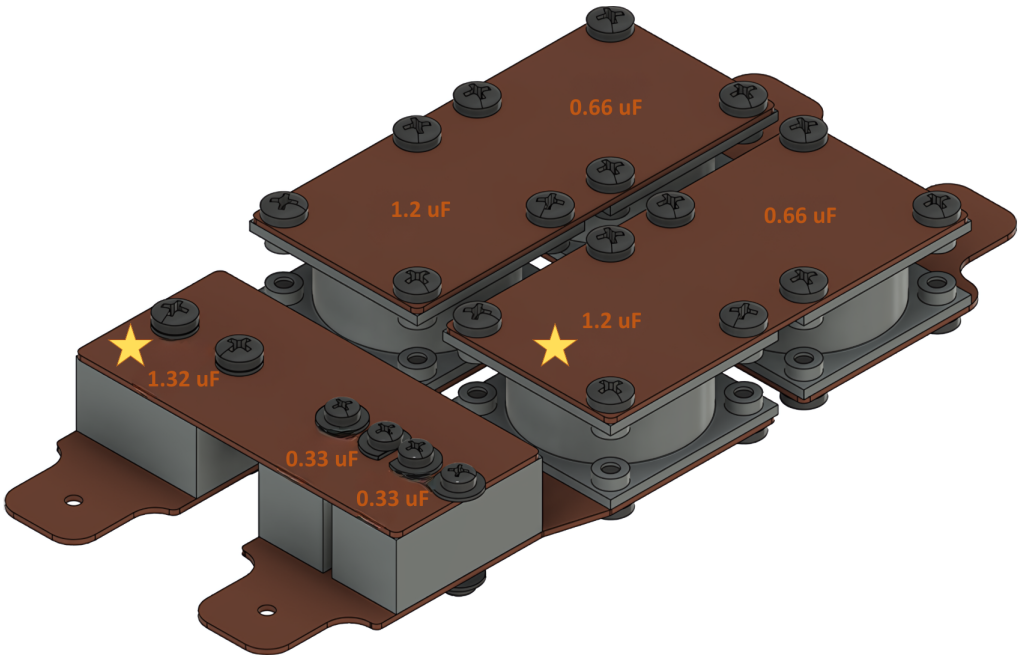

Fig. 2.13: Diagram of formerly-embedded capacitor bank before being surrounded by PCM and encapsulated in epoxy. Yellow stars represent where thermocouples were attached on copper bus bars to measure the temperature of the capacitor bank

The capacitor bank, surrounded by PCM and encapsulated in epoxy, was tested under conditions similar to a no-load LCCL tuning network. The original tuning inductors extracted from concrete were used as the series tuning inductors. A duplicate version of the inverter was used in place of the broken inverter. Since the coil was not removed from the concrete block, a duplicate version of the coil with the same inductance was created. The component values for the LCCL no-load capacitor bank test are listed in Table. 2.3.

The capacitor bank was tested at a 500 V DC input to the inverter which corresponds to 85% of the full power operation. The inverter generated an 85 kHz, 50% duty cycle square wave which was passed through the tuning inductors, capacitor bank, and substitute coil designed for this test. A picture of the test setup is shown in Fig. 2.14.

The capacitor bank was run continuously for 7 hours to fully melt the PCM, determine the time required for the system to reach steady state, and evaluate the impact of the PCM on the capacitor bank's performance. It can be seen in the results from Fig. 2.15 that the PCM did successfully slow down the transient thermal response. Between hours 1 and 3,

Table 2.3: Hardware component values for formerly-embedded capacitor bank test setup

Component	Hardware Value
V_{DC}	500 V
f_s	85 kHz
C_{in}	104 uF
L_{ps1}	3.51 uH
L_{ps2}	2.3 uH
k_L	0.3
C_{ps1}&C_{ps2}	425.8 nF
C_{pp}	440 nF
L_p	25 uH

Fig. 2.14: Formerly-embedded capacitor bank no-load LCCL test setup for thermal testing

the transient curve starts to level off. After 4 hours, the PCM, which has a melting point of 68°C, has melted and the temperature continues to increase normally without any effect from the PCM.

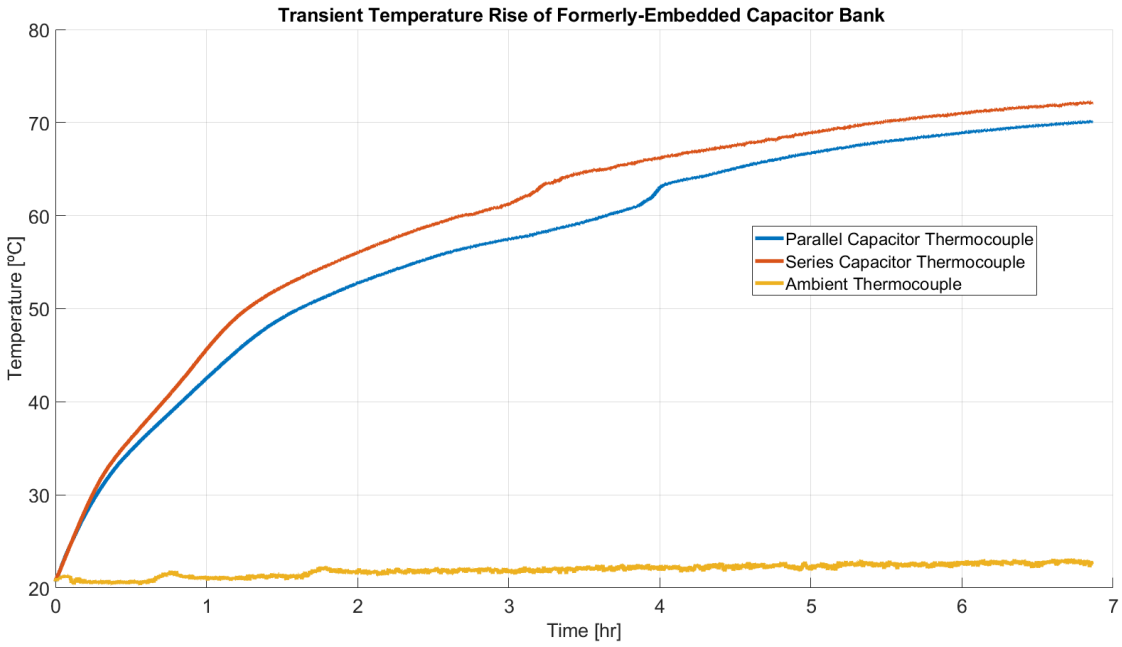

Fig. 2.15: Transient temperature rise of formerly-embedded capacitor bank after 7 hours of continuous power testing

The encapsulated capacitor bank's bus bars reached a temperature of approximately 72°C after 7 hours of operation. It appears that the steady-state temperature would reach approximately 75°C once the temperature stabilizes. In concrete, where there's a greater thermal resistance to ambient, the capacitor bank is expected to reach an even higher steady-state temperature than measured in this 7-hour experiment. Additionally, concrete's higher thermal mass suggests a longer time constant for transient temperature stabilization.

Overall, these results indicate that the PCM and epoxy encapsulation effectively dissipate heat from the capacitor bank. Under low DWPT utilization and moderate ambient temperatures, the heat generated from the capacitor bank appears manageable. However, for high utilization or extreme ambient temperatures, more comprehensive thermal management design may be necessary to prevent thermal failure in the capacitor bank.

2.5 Conclusions from Previous Concrete-Embedded Project

Several lessons were learned from removing and testing the formerly-embedded DWPT power electronics. A summary of these findings is mentioned below:

1. Soft epoxy can be used in the future potting designs to allow easier access for repair.

2. For future embedded designs, the thermal management of the gate driver and control board components need to be considered. Although the MOSFETs have the highest predicted loss, they are not the only component likely to fail due to poor thermal management.

3. The inverter MOSFET switches never got hot enough to test the effectiveness of the PCM material and additional PCM heat sinks should be developed to more fully validate their effectiveness.

4. Testing of the capacitor bank showed that PCM material can successfully delay the transient temperature rise.

CHAPTER 3

Roadway-Embedded Power Electronics Design

3.1 Roadway-Embedded Power Electronics Design Tools

The design of roadway-embedded DWPT power electronics vary significantly based on topology and power level. Additionally, the design and implementation are influenced by factors such as location, roadway material, ambient temperature, burial depth, desired lifetime, and expected utilization. Prototyping these systems is challenging due to construction timelines and high costs involved. Therefore, it is beneficial to utilize alternative tools to predict the expected temperature rise of roadway-embedded power electronics prior to roadway installation, helping to save both time and expense. This thesis will utilize tools such as analytical heat transfer equations, ANSYS FEM simulations, and sand-embedded experiments to achieve these predictions.

3.1.1 Analytical Heat Transfer Equations

Heat is transferred through conduction, convection, and radiation. In embedded electronics, conduction is the primary mode of heat transfer, describing how heat moves between components, their packaging, and the roadway. Convection and radiation are also important to consider at the roadway's surface, where wind and solar radiation affect heat transfer.

Generic heat transfer equations describe how heat moves across space and time. These equations incorporate factors such as heat generation, thermal properties, and material geometries. To solve heat transfer equations, certain assumptions are made to simplify the equations into more manageable forms or approximations. In this design procedure, lumped system approximations are used for analytical heat transfer equations, assuming a uniform temperature distribution within the heat-generating component.

Analytical equations are often much quicker to use than setting up simulations or

running experiments, making them useful for rapidly assessing the feasibility of a design. However, because the analytical equations in this thesis involve many assumptions, they should not be relied upon for detailed thermal behavior analysis.

3.1.2 ANSYS FEM Simulations

Finite Element Method (FEM) simulations enable 3D modeling of electric components, which can be solved for various parameters such as power loss and temperature rise. Ansys Icepak, an FEM simulator integrated into the Ansys Electronics Desktop, is utilized for estimating temperature rise based on power loss. Ansys Icepak is favored for thermal modeling in this design procedure due to its simplicity and user-friendliness for electrical engineers, as well as its ability for coupled electro-thermal models with other Ansys products.

Ansys Icepak can be coupled with Maxwell or HFSS or operate as a standalone product, with power loss inputs derived from analytical calculations and manually inserted into the model. In this design procedure, the latter approach has been chosen, utilizing analytical power loss calculations for the models. Consequently, the accuracy of the Ansys models depends on the precision of the inputted power loss calculations. Additionally, the 3D models are simplified to reduce simulation time and eliminate unnecessary meshing complexity, making the simulation results accurate only within the context of the simplified model.

Since power losses and material properties can vary in a real system, Ansys simulations can be refined and adjusted based on experimental results to enhance accuracy. For all simulations conducted in this thesis, power loss calculations were updated using measured voltages and currents. Material properties in the simulation were selected based on a combination of data-sheet information and measured values. Additionally, ambient temperatures were chosen based on actual measurements or expected temperature conditions.

When simulation results align with simplified experimental outcomes, the simulations can be adjusted to extrapolate results for a full roadway-embedded scenario. For example, power losses or thermal material properties can be modified to reflect differing design scenarios. Ambient conditions can also be modified to reflect varying environmental conditions.

Ansys Icepak simulations can help evaluate whether an existing power electronic design can be embedded in concrete, and if so, determine the necessary packaging and limitations. Moreover, these simulation results can guide decisions during the initial design phase, aiding in the selection of components and packaging for roadway-embedded electronics.

3.1.3 Sand-Embedded Experiments

Given the challenges of prototyping electronics within roadway materials, a temporary solution allowing for easy removal, modification, and retesting is desired. Sand has similar thermal conductivity, density, and specific heat compared with other materials used in roadway construction, indicating its use as a replacement material for thermal experiments. Assessing electronics' performance in sand can serve as a valuable indicator for the behavior in concrete or asphalt roadways.

Electronics can undergo testing in sand either before or after packaging. Since epoxy potting materials exhibit higher thermal conductivity than sand or other roadway material, the use of epoxy encapsulation is expected to enhance the system's thermal management. Therefore, testing electronics in sand before packaging will be a worst-case thermal management scenario. Conducting thermal tests without packaging can establish a baseline for evaluating the effectiveness of PCM and epoxy encapsulation in enhancing the thermal management of these embedded components.

Results from sand experiments combined with simulation results can provide quicker insights into embedded thermal management design with less cost and time than directly embedding these electronics in roadway materials. Once simulations have been calibrated to match the sand experimental results, the sand material can be substituted with various roadway materials to predict how the system will perform in a real roadway-embedded environment. These predictions can accelerate the prototyping process, providing system designers with greater confidence in their designs when these electronics are eventually embedded within roadways.

3.2 Roadway-Embedded Electronics Design Procedure

Passive thermal management of roadway-embedded power electronics is a unique situation that requires interdisciplinary design principles. The design of these electronics includes multiple environmental and use case considerations outlined throughout this design procedure.

The discussed design procedure utilizes a mix of various analytical, simulation, and experimental methods mentioned previously. This procedure is not strictly linear, allowing certain steps can be conducted independently of each other.

3.2.1 Identify DWPT power level, topology, and power losses

Each DWPT deployment is tailored to a specific use case, targeting different vehicle classes. The intended use case dictates the required power levels. For example, as the trend towards electrification extends toward heavy-duty vehicles, higher power levels are becoming essential to charge these vehicles and sustain their operations. Recent DWPT research is shifting towards power levels of 100 kW - 300 kW to accommodate these wider range of vehicle classes [45, 46]. With increased power levels comes greater power loss and consequently higher potential temperatures in the DWPT power electronics.

Current DWPT systems are also trending towards using a ground assembly featuring an LCCL tuning topology. This tuning configuration offers increased interoperability with various receiver coils and tuning methods as well as reduced EMI within the system. Additionally, studies have demonstrated that this tuning topology exhibits improved performance when the tuning compensation is divided [47]. An illustration of this split LCCL primary tuning network is depicted in Fig. 3.1.

Determining the expected power loss in each component of the DWPT system is a crucial early step in designing the thermal management of embedded electronics. These losses can be calculated using the fundamental analytical equations mentioned previously. For an LCCL primary tuning topology, losses must be estimated in the high-frequency inverter, the tuning capacitors, and the tuning inductors.

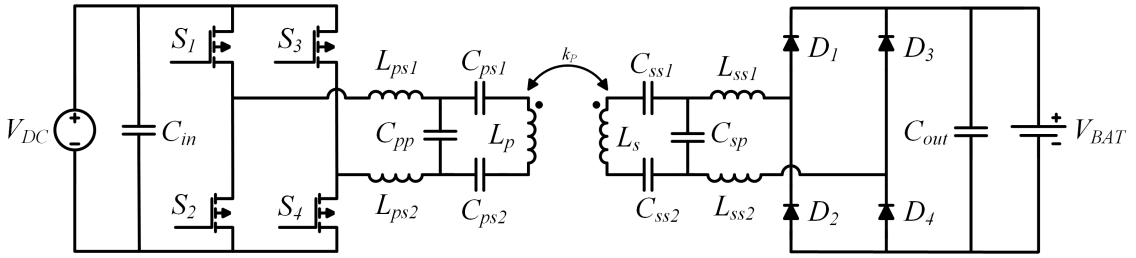

Fig. 3.1: Split LCCL tuning network for ground assembly

3.2.2 Identify roadway requirements and temperature characteristics

Each DWPT deployment location will have different year-round ambient temperatures, varying roadway layers and thicknesses, and differing roadway construction techniques, necessitating different burial depths. Each of these factors will influence the overall ambient temperature of the roadway surrounding the embedded power electronics.

The ambient temperature of the roadway experiences daily and seasonal temperature variations. For a specific burial depth, roadway material, and mean earth temperature at a given location, the underground temperature underground over a certain time period can be estimated using equation (3.1) [48, 49].

$$T(0,t) = T_m + A_0 e^{d\gamma} cos[\frac{2\pi}{P}(t - t_0) - d\gamma] \tag{3.1}$$

Where T_m is the mean surface temperature of a specific location, A_0 is the amplitude of the temperature variation of the soil surface over time period P (This considers solar radiation and wind), d is the distance from the surface of the road, t_0 is the time offset from the coldest measured temperature during time period P, and γ is the inverse of the damping depth of the roadway material given by equation (3.2)

$$\gamma = \sqrt{\frac{\pi}{\alpha P}} \tag{3.2}$$

Where α is the thermal diffusivity of the roadway material and P is the period of time of a full temperature cycle.

For example, in Logan Utah, the mean earth temperature is approximately $15°C$, and

the approximate amplitude of the temperature variation of the roadway throughout the year is approximately $30°C$. If we simplify and say that the entire roadway stack is concrete, we can calculate the thermal diffusivity of the roadway material based on equation (3.3).

$$\alpha = \frac{k}{\rho C_p} \tag{3.3}$$

where k is the thermal conductivity of the concrete, ρ is the density of concrete, and C_p is the specific heat of concrete. When we plug all of those variables into equation (3.1), we get Fig. 3.2 as a function of time, temperature, and burial depth.

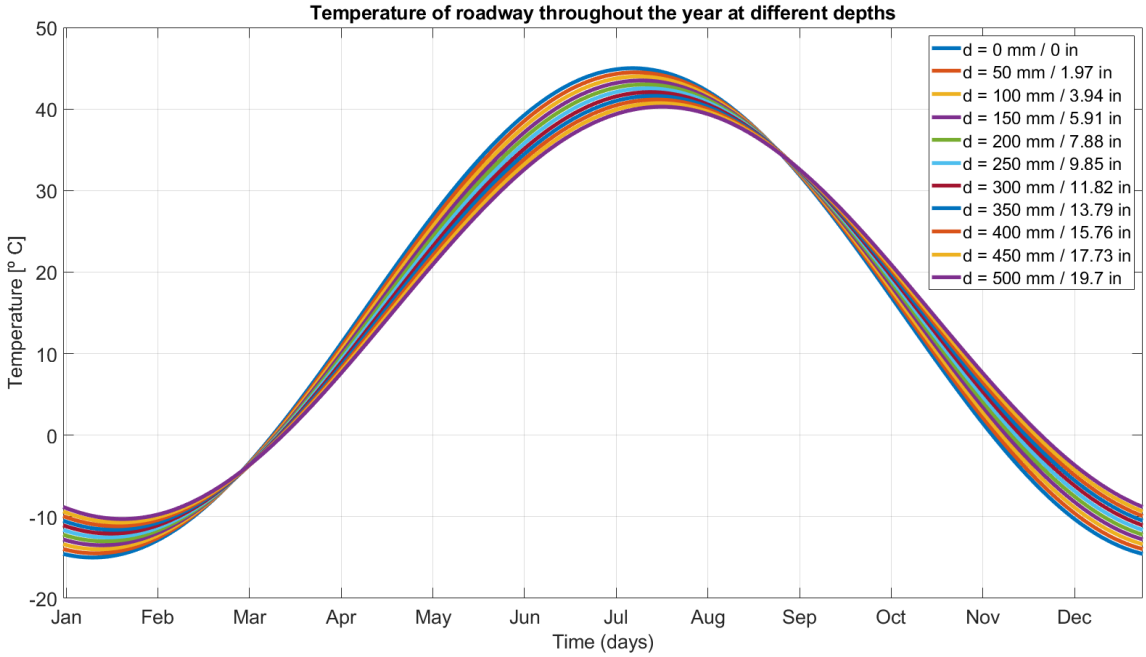

Fig. 3.2: Temperature of the roadway at different burial depths within concrete for the entire year

This equation allows us estimate the maximum worst-case ambient temperature that roadway-embedded electronics will experience at a certain burial depth throughout the year. The electronics can then be designed to withstand this worst-case temperature, or the system can be designed for slightly lower maximum temperature limits based on utilization and transient temperature characteristics.

3.2.3 Determine maximum operating temperatures based on component temperature limits and desired component lifespan

The system's maximum operating temperature can be determined using datasheet specifications for maximum operating temperatures and reliability engineering analysis that considers both temperature and voltage.

As an example, the TDK metallized film capacitors often used in current EV WPT systems are rated to a max operating temperature of $125°C$. According to the datasheet, their failure rate is specified as $\lambda = 1$ fit, or 1×10^{-9} failures per hour, at half the rated DC voltage and an operating temperature of $40°C$ [50]. Failures are considered to be randomized, but the distribution of failures follows an exponential approximation described by equation (3.4).

$$F(t) = 1 - e^{-\lambda t} \tag{3.4}$$

A graph of this failure probability distribution is shown in Fig. 3.3. The x-axis represents time in amount of hours and the y-axis is the percentage of components that have failed or are failing at a given time.

Since interpreting failures per hour can be challenging, failure rates are often expressed in terms of the Mean Time to Failure (MTTF), calculated as $1/\lambda$. In this example, the MTTF equates to 1,000,000,000 hours. As shown graphically in Fig. 3.3, this implies that in an application where numerous film capacitors are used, approximately 63% of these film capacitor components will have failed after 1 billion hours. For higher operating temperatures or higher voltage utilization, the failure rate varies based on equation (3.5) given in the IEC61709:2017 standard, with correction factors π_v and π_t as indicated in Fig. 3.4 [51].

$$\lambda = \lambda_{ref} \pi_v \pi_t \tag{3.5}$$

With a 100% voltage utilization and an $85°C$ operating temperature, the failure rate becomes $\lambda = 1 \times 10^{-9} \times 6.09 \times 12 = 73.08 \times 10^{-9}$ resulting in a MTTF of 13,683,634 hours.

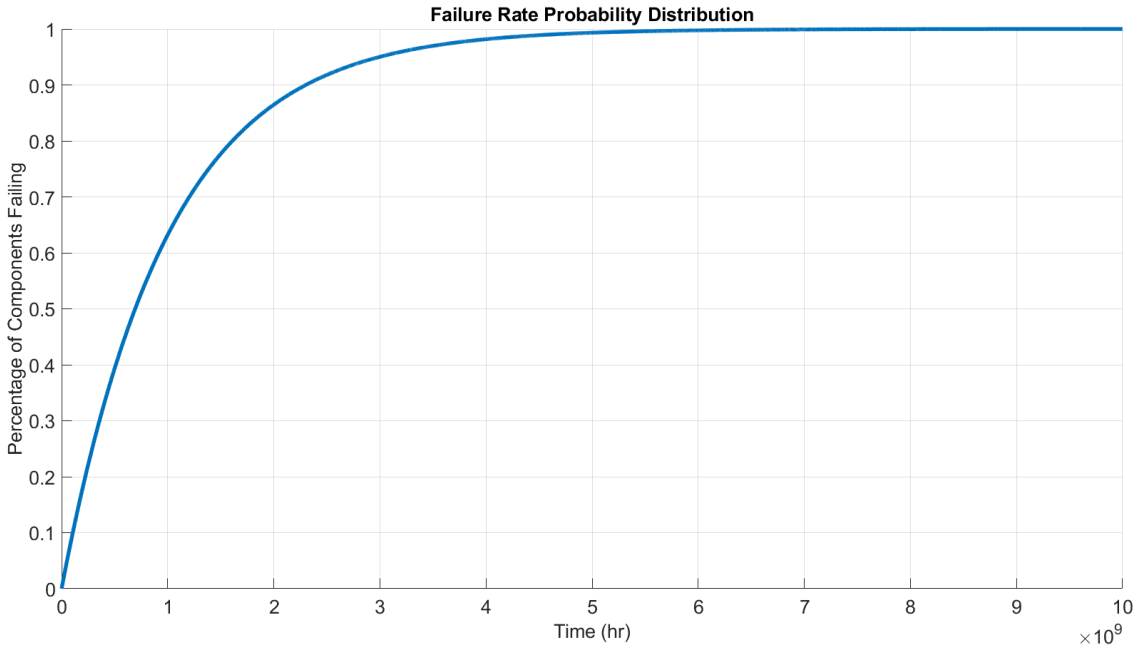

Fig. 3.3: Failure rate cumulative probability distribution. Hours on the x-axis, percentage of failed components on the y-axis

T (°C)	π_T
≤40	1.0
50	1.8
55	2.3
60	3.1
70	5.2
80	9.0
85	12
90	16
100	33
105	50
110	77
120	206
125	346

V/V_R	π_V
10%	0.26
25%	0.42
50%	1.00
60%	1.42
70%	2.04
80%	2.93
90%	4.22
100%	6.09
110%	9.00
120%	13.00

Fig. 3.4: Correction tables for updating the failure rate at different operating conditions

This implies that approximately 63% of components will have failed by 13 million hours. Since our system is unusable long before a 63% failure, we can establish a service life using a probability confidence interval. For instance, if we aim for a service life where only 2% of the components have failed, then using a 98% confidence interval as given in Fig. 3.5 [51], we obtain the service life of our product using equation (3.6).

confidence level (%)	p
37	0.716
63	0.333
75	0.207
90	0.076
95	0.037
98	0.015

Fig. 3.5: Service life p values for varying confidence levels

$$t_{SL} = \frac{p}{\lambda} \tag{3.6}$$

Given $\lambda = 73.08 \times 10^{-9}$, we have a service life of $0.015/73.08 \times 10^{-9} = 205,254.5$ hours. Or in other words, assuming a very large sample size, we would expect 2% of the components to have failed after approximately 23 years.

Since roadways have an expected lifespan of 20-25 years, roadway-embedded DWPT systems should last at least that long to reduce costs and align DWPT repairs with roadway maintenance schedules. To maximize component lifetimes, the trade-off between voltage derating, temperature derating, and lifetime should be optimized. These trade-offs can be displayed using service life calculations as shown in Fig. 3.6.

The graph illustrates that the lifespan of the capacitor bank diminishes exponentially as the operating temperature increases. The graph also shows that a 10% reduction in voltage from the maximum rated voltage can yield a similar increase in lifespan as a 5-7°C decrease in temperature.

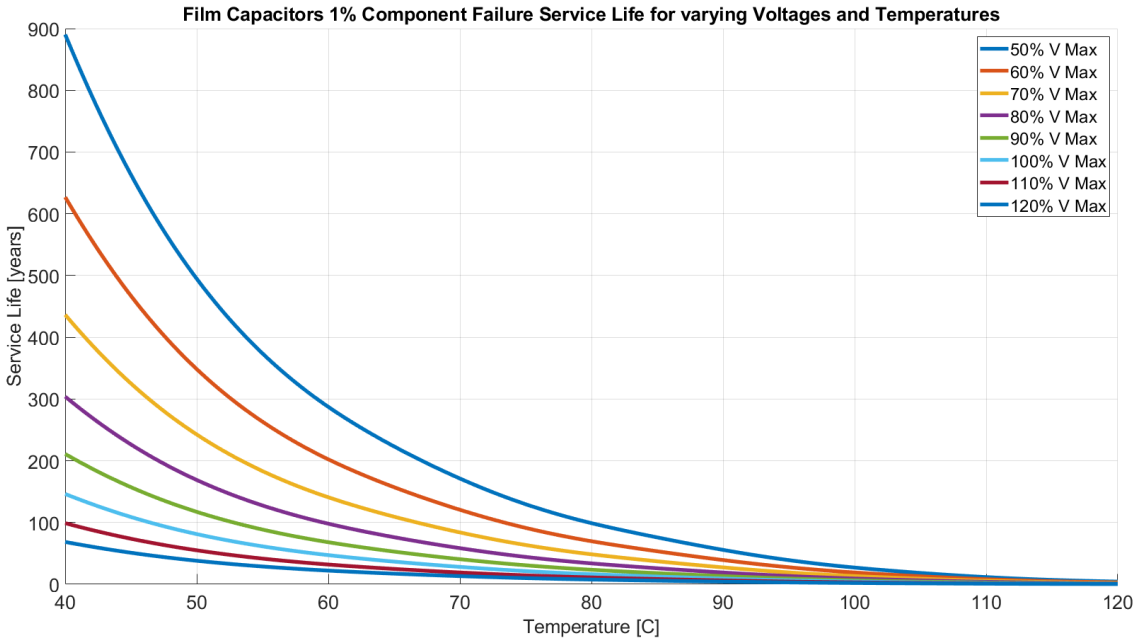

Fig. 3.6: Graph of service life of capacitor bank based on 1% of total film capacitors having failed. Voltage vs Temperature trade-off

3.2.4 Determine the maximum allowable power density within the roadway for passively cooled electronics under steady-state conditions

Using the power electronic losses, ambient temperature, and roadway material properties, we can estimate the maximum achievable power density possible within the roadway at steady-state operating conditions. The steady-state temperature rise of a solid body, considering material properties and conduction heat transfer via a lumped system analysis, is shown in equation (3.7).

$$T_\infty = T_A + \frac{QL}{kA} \tag{3.7}$$

Where T_∞ is the steady-state temperature, T_A is the ambient temperature, Q is the heat generation rate in watts (W), L is the characteristic length of the body, A is the surface area of the body in contact with the environment, and k is the thermal conductivity of the surrounding material. This equation shows that as the surface area of the body in contact with the environment increases, the steady-state temperature decreases. Conversely, as

the losses increase or the thickness of the body increases (reflected by L), the steady-state temperature will increase.

This equation assumes a uniform temperature across the body, which is an oversimplification as real-world temperatures will vary. Additionally, it assumes that heat transfer occurs solely through conduction until reaching ambient temperature, which is another simplification. In reality, once heat reaches the surface of the roadway, convection from the air and radiation from the sun will contribute to the overall heat transfer.

Considering the simplifications inherent in these analytical equations, simulation can provide further insight into determining the theoretical maximum allowable power densities achievable in the roadway. For example, in Ansys Icepak, we can create a generic block representing a component with varying sizes and power losses. We can then surround this block with concrete representing a roadway-embedded scenario and simulate the steady-state temperature rise. A screenshot of the Ansys simulation is shown in Fig. 3.7. For the Ansys Icepak simulation, the bottom and side boundaries of the concrete were modeled with a constant ambient temperature wall condition, and the top and side boundaries of the air above the concrete were modeled as a constant ambient temperature opening condition. The concrete block was designed with large dimensions to ensure that the heat flux at the boundaries are small, allowing us to approximate these boundaries as having a constant ambient temperature. This assumption may fail for larger block sizes or greater power losses.

The power density trade-offs were simulated in Ansys Icepak and the results are shown in Fig. 3.8. These results provide insight into the concrete roadway's ability to passively dissipate heat. The red line on this graph is at $85°C$ which represents a common suggested operating temperature for capacitors given the desire for a long lifespan. These simulation results can be modified to any roadway layer stack-up and any ambient temperature to determine the maximum power density a component can achieve in a passive-cooled, roadway-embedded scenario based on the fixed component power losses.

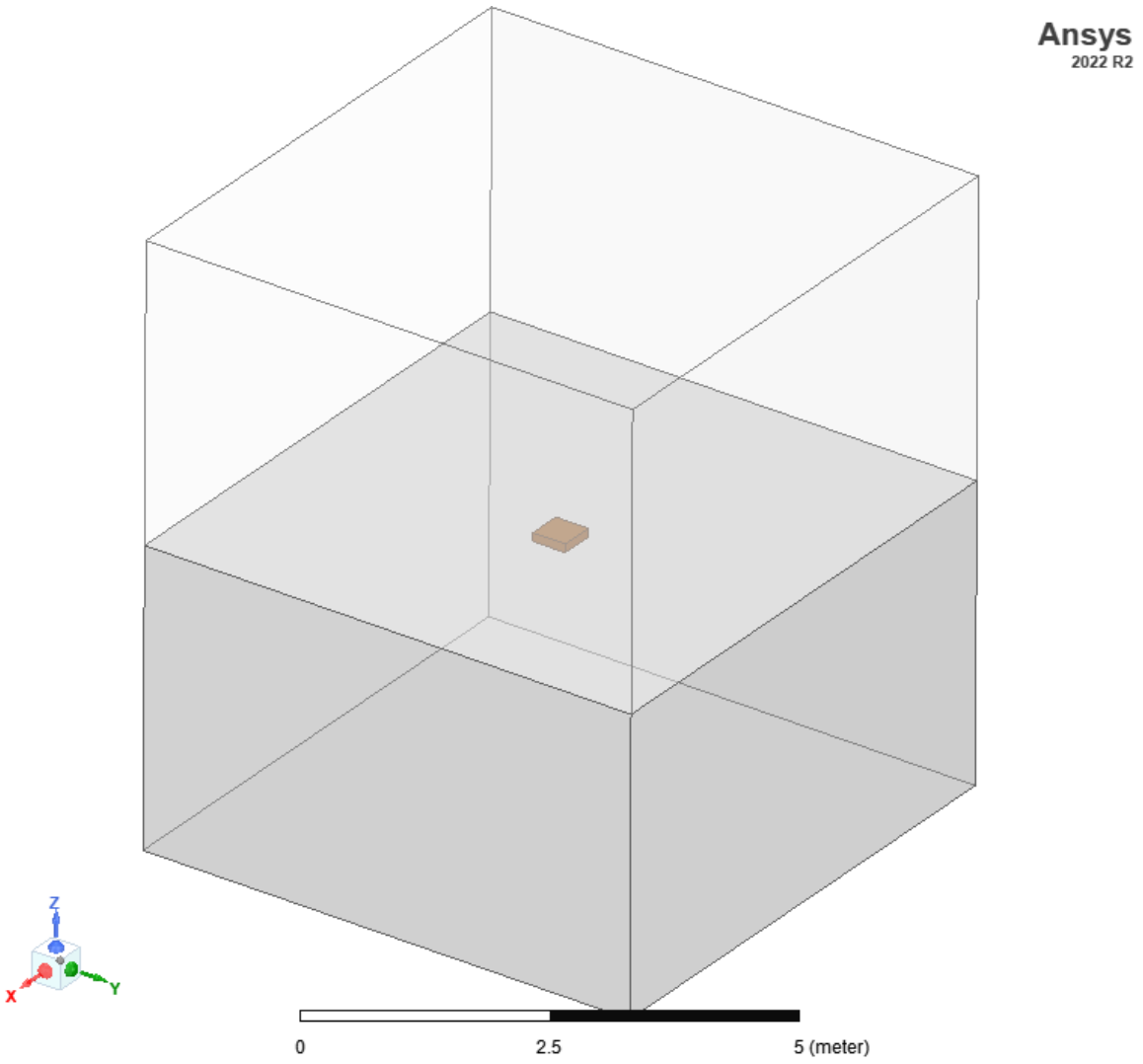

Fig. 3.7: Ansys model for block of loss within concrete

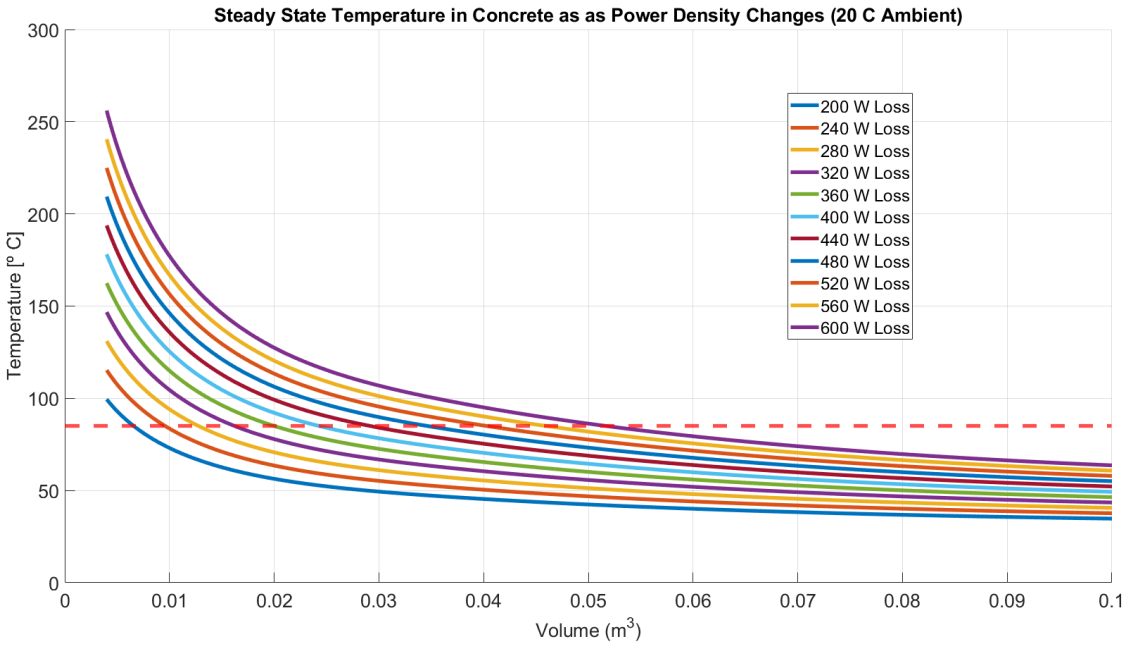

Fig. 3.8: Steady-state temperature of block of loss within concrete with changing power density

3.2.5 Identify anticipated DWPT utilization profiles and determine transient temperature rise requirements

The transient temperature rise of a solid body, considering material properties and conduction heat transfer with a lumped system analysis, is shown in equation (3.8).

$$T(t) = (T_i - T_\infty)e^{-t/\tau} + T_\infty \tag{3.8}$$

Where $T(t)$ is the temperature at time t, T_i is the initial uniform temperature of the body, T_∞ is the steady state or final temperature of the body, and τ the time constant is given by equation (3.9).

$$\tau = \frac{\rho V C_p L}{kA} \tag{3.9}$$

where ρ is the density of the body, V is the volume of the body, C_p is the specific heat of the body, L is the characteristic length of the body, A is the surface area of the body, and k is the thermal conductivity of the surrounding material. This equation shows that as

the thermal mass of the body increase, the time constant increases, meaning it takes longer for the system to reach steady state. As the surface area of the body increases, the time constant decreases.

When components are encapsulated in epoxy, the thermal mass of the system is increased and it can take hours for the system to reach steady state. When these components are embedded in concrete, the expected transient temperature rise will continue to slow to time periods of potentially days. Considering the large volume and density of the roadway and the corresponding large time constants, optimal system design will factor in transient temperature rise.

The transient temperature rise of the generic component block model was simulated in Ansys Icepak with continuous maximum loss. These results shown in Fig. 3.9 suggest that roadway-embedded DWPT systems will rarely operate at steady-state temperatures. Reaching steady-state temperature would require over a full day of non-stop charging which is an unlikely utilization scenario. Instead, the system may reach a quasi-steady-state temperature based on the average utilization of the system.

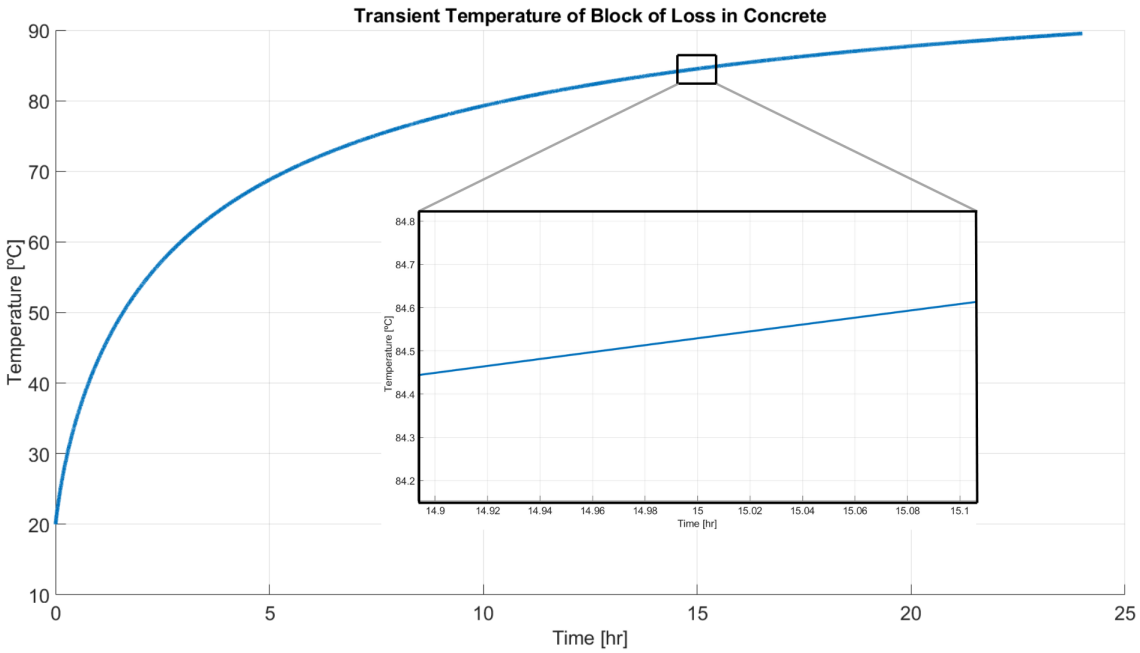

Fig. 3.9: Transient temperature rise of block of loss within concrete

To observe these quasi-steady-state results, we can set specific duty cycles and periods during which our system will operate, reflecting its utilization. For instance, a 50% duty cycle every second can simulate a car driving over the system on a freeway, followed by the interval between subsequent cars. Alternatively, we could implement a 12-hour on-off duty cycle, representing high utilization during daytime when more cars are on the road and low utilization at night. The transient temperature rise for both of these situations was simulated in Ansys and is shown in Fig. 3.10.

By simply reducing the utilization to a 50% duty cycle for the entire day, the temperature after 24 hours decreases from $90°C$ down to $55°C$. Additionally, when the system has time at night to cool, a significant portion of the heat can dissipate away from the electronics allowing the system to return to $28°C$.

Incorporating PCM materials complicates the analysis by introducing heat storage into the system. This additional material alters the transient temperature rise by storing heat during the phase change, thereby lengthening the temperature rise time and fall times. While analytical modeling of this phenomenon can be challenging, the thermal properties of PCM materials can be defined within FEM software and simulated to understand the changes in transient temperature rise.

3.2.6 Select embedded-electronic components and packaging

The thermal design of components and packaging can we simplified to a series of thermal circuit components as shown in Fig. 3.11 with the circuit component descriptions listed in Table. 3.1, where R_{th} and C_{th} are given in equation (3.10).

$$R_{th}(Convection) = \frac{L}{hA}, \quad R_{th}(Conduction) = \frac{L}{kA}, \quad C_{th} = mC_p \tag{3.10}$$

The thermal resistance can also be calculated by taking the difference in temperature between steady state and ambient and dividing that change in temperature by the power loss as shown in equation (3.11)

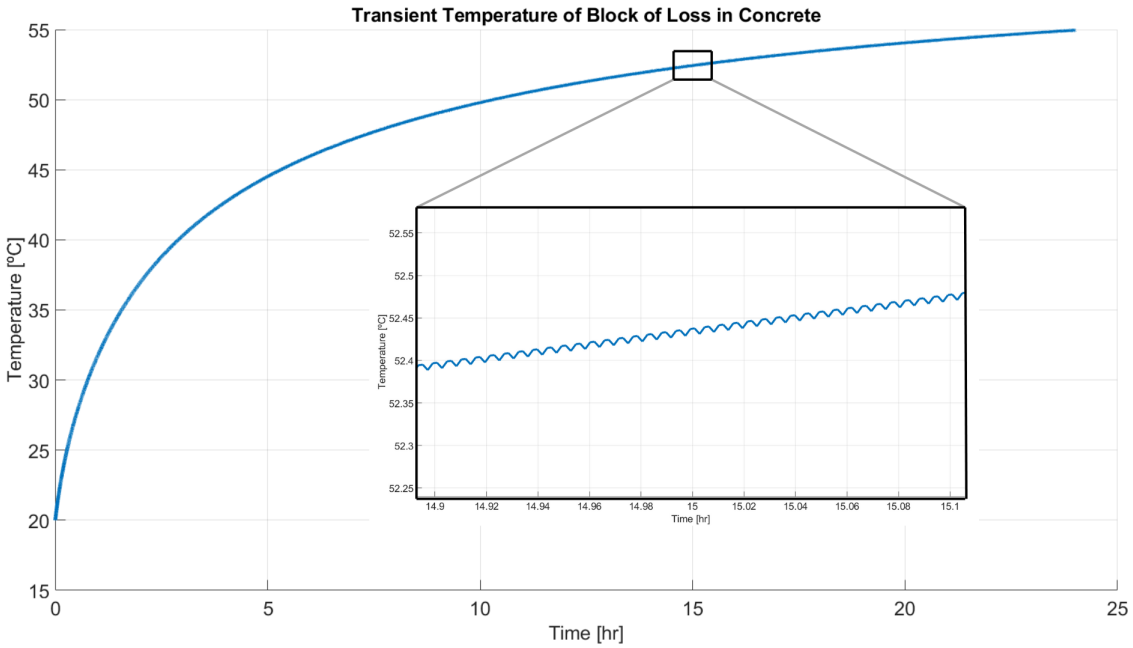

(a) Transient temperature rise of block of loss within concrete given 50% utilization

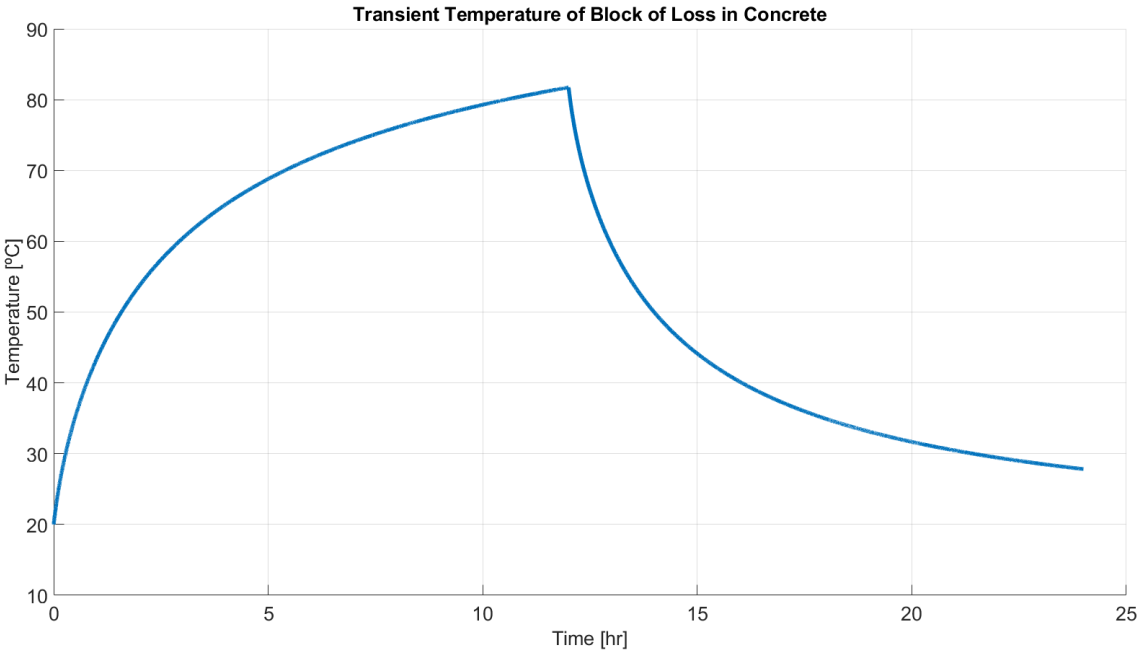

(b) Transient temperature rise of block of loss within concrete 12 hrs on 12 hrs off

Fig. 3.10: Transient temperature rise given different DWPT utilization profiles

$$R_{th} = \frac{T_\infty - T_A}{W} = \frac{\Delta T}{W} \tag{3.11}$$

In our roadway-embedded thermal management design, the goal is to reduce the thermal resistance within our system to achieve a lower steady-state temperature and increase the thermal capacitance to acheive a larger transient time constant.

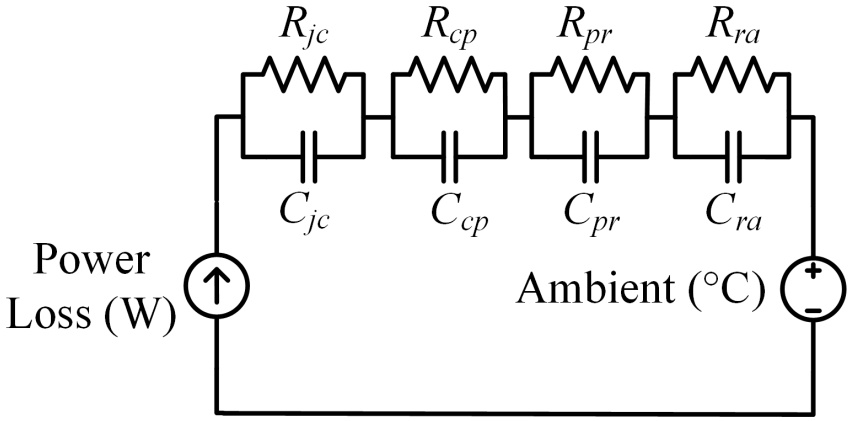

Fig. 3.11: Thermal circuit diagram showing thermal resistance and thermal capacitance of the roadway-embedded DWPT electronics

Table 3.1: Thermal circuit components descriptions

R_{jc} & C_{jc}	R_{cp} & C_{cp}	R_{pr} & C_{pr}	R_{ra} & C_{jc}
R_{th} and C_{th} from the junction of the device to the case of the device	R_{th} and C_{th} from the case of the device to the device packaging	R_{th} and C_{th} from the device packaging to the roadway	R_{th} and C_{th} from the roadway to the ambient environment

The selection of components depends on factors such as power density, cost, temperature operation, and reliability. Greater component numbers typically enhances current sharing capabilities and increases C_{jc}, while higher-priced components tend to offer greater reliability and lower R_{jc} packaging.

The selection of packaging includes the choice of heat sinks, thermal interface materials, and thermal pads that reduce R_{cp}, but also provide required electrical isolation. A larger

heat sink can provide increased C_{cp} and decreased R_{cp} but increase the overall size and cost of the system. Packaging material should include materials with high thermal conductivity characteristics to reduce both R_{cp} and R_{pr}.

Potting and encapsulation materials have different viscosity's and electrical and thermal conductivity's which will impact their feasibility for certain designs. Power-electronic packaging should protect the electronics from the elements such as water, humidity, and strain while reducing R_{pr}. The greater surface area of the potting material in contact with the roadway allows for lower R_{pr} but may lead to increased costs.

The thermal circuit components R_{ra} and C_{ra} primarily depend on the materials used for roadway construction, the burial depth of embedded electronics, and the roadway layer stack-up. Concrete and asphalt mixtures with better thermal properties can be used improve these thermal circuit parameters.

3.2.7 Prototype power electronics within sand

Given the costly and time-consuming nature of prototyping power electronics in concrete, sand can serve as an initial embedded medium for conducting thermal testing. Sandtastik sand was chosen for all of the embedded experiments in this thesis for its lack of metal, small particle size, uniformity of particle size, and minimal crystalline silica [52]. The thermal properties of this sand compared to other roadway materials are shown in Table. 3.2 [21, 43, 53–56].

Table 3.2: Thermal properties of sand compared to other roadway materials

Material	**Thermal Conductivity** (k) W/mK	**Density** (ρ) kg/m^3	**Specific heat** (C_p) J/kgK	**Thermal Diffusivity** (α) m^2/s
Sand	0.27	1700	800	1.985×10^{-7}
Aggregate	0.71	2780	600	4.257×10^{-7}
Asphalt	1.6	2282	959	7.311×10^{-7}
Concrete	1.8	2738	775	8.483×10^{-7}

The lower thermal conductivity of sand compared to other roadway materials suggests

that the steady-state temperature of embedded electronics in sand will be higher than in other roadway materials. The lower thermal diffusivity of sand compared to other roadway materials suggests that the transient temperature rise time constant will be larger in sand than in other roadway materials. Despite these differences, sand experiments give an estimate for the results we could expect in roadway-embedded scenario.

The sandbox constructed for thermal testing is approximately 1130 mm in width and length and 290 mm tall. The sandbox was filled with varying levels of sand, but for a majority of the experiments conducted in this thesis, the sandbox was filled to a depth of about 220mm. A picture of the sandbox testing setup is shown in Fig. 3.12.

Fig. 3.12: Sandbox for thermal testing of power electronics

To make testing in sand even easier, the sandbox was designed with liquefaction capabilities. By pumping air through holes in a PVC pipe grid at the bottom of the sandbox, illustrated in Fig. 3.13, the upward flow of air creates a liquid-like state in the sand [57]. In a liquefaction state, power electronics can be easily inserted and removed. This liquefaction process also helps ensure that sand is able to fill in all of the gaps that exist within electronic components.

Fig. 3.13: Sandbox PVC pipe grid for liquefaction of sandbox

Sand experiments can be conducted in an environment with a constant ambient temperature or with changing ambient temperatures to reflect daily and seasonal temperature variations.

Once results from sand have been obtained and simulations in Ansys Icepak successfully mirror those results, the Ansys Icepak simulations can be modified with various ambient temperatures, roadway materials, and packaging materials to assess how those design changes affect on the thermal management of the electronics.

CHAPTER 4

Current 100 kW DWPT Power Electronics

4.1 Overview of Utah State University DWPT System

Utah State University currently has a 100 kW DWPT prototype system which contains both a ground assembly and a vehicle assembly. This system uses a double-sided split LCCL tuning topology as shown in Fig. 4.1 with the component values detailed in Table. 4.1.

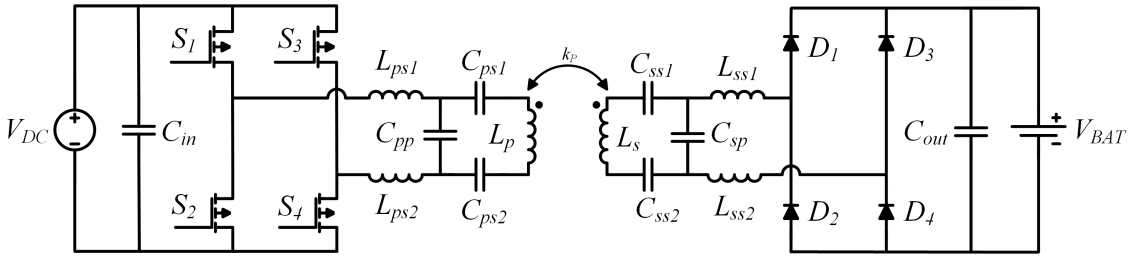

Fig. 4.1: Circuit diagram and configuration of the current DWPT capacitor bank

Table 4.1: Hardware component values for original DWPT capacitor bank

Component	Hardware Value
V_{DC}	800 V
f_s	85 kHz
C_{in}	400 uF
L_{ps1}&L_{ps2}	2.81 uH
C_{ps1}&C_{ps2}	830 nF
C_{pp}	630.8 nF
L_p	13.36 uH
k_P	0.197
L_s	7.26 uH
C_{sp}	1.04 uF
C_{ss1}&C_{ss2}	1.9 uF
L_{ss1}&L_{ss2}	1.677 uH
C_{out}	400 uF
V_{BAT}	800 V

The power electronics in this system were originally designed to be air-cooled within a roadside cabinet. The goal of this analysis is to determine the feasibility of embedding these power electronics into the roadway given their current design. It aims to identify necessary packaging requirements, achievable utilization levels, and potential failure points. Additionally, the analysis seeks to propose simple modifications to the current DWPT system that would better prepare these electronics for being embedded in the roadway.

Both the inverter and capacitor bank are relatively expensive compared to the inductors in the LCCL network, warranting their detailed analysis. The inverter is analyzed first since it is the power electronic component with the highest risk of failure and the cause of failure in the formerly-embedded DWPT system. Following this, the capacitor bank is evaluated, as it has the lowest temperature rating and is therefore likely to fail at lower temperatures than other embedded components.

4.2 Current DWPT Inverter Thermal Management

The current DWPT Inverter consists of two Cree CAB450M12XM3 MOSFET half bridges, each paired with a CREE CGD12HBXMP gate drive board. An image of one of these half-bridge modules is shown in Fig. 4.2

Fig. 4.2: Inverter half-bridge module

The complete inverter incorporates these MOSFET modules and gate driver boards on a power PCB, which also includes DC input capacitors, a control board, an FPGA controller,

and a heat sink. The inverter is designed to operate with ZVS over the entire operating range and features fiber optic communication. The full inverter is shown in Fig. 4.3

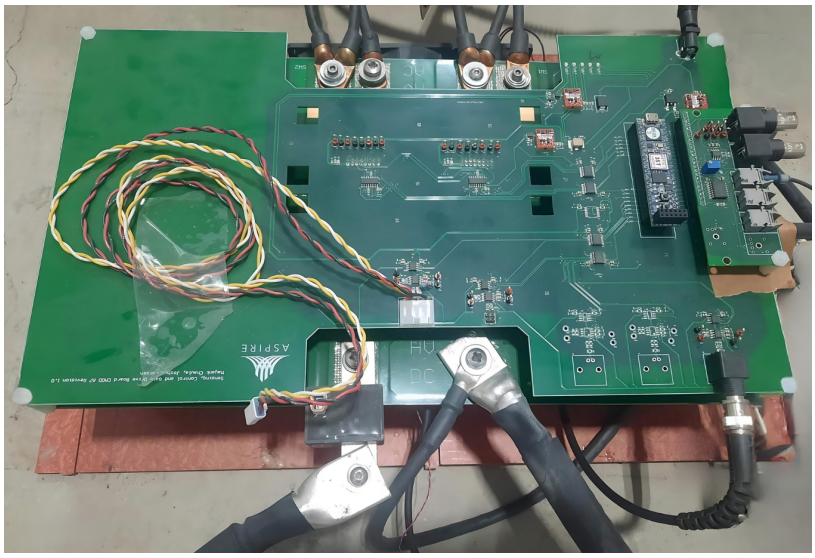

Fig. 4.3: Full DWPT inverter

4.2.1 Inverter Experiments

The inverter was tested at 100 kW with fans to evaluate the system's thermal performance with the current design. The test setup is shown in Fig. 4.4. Fans directed air through the heat sink attached to the base plate of the MOSFET modules. The inverter gate drivers operated at 50% duty cycle with an 85 kHz gate signal, and the inverter appeared to be soft switching. The inverter ran continuously for approximately 15 minutes until the temperatures appeared to stabilize. Thermal images were captured using a FLIR thermal camera after steady-state operation was reached. These images taken at full power operation are shown in Fig. 4.5 and Fig. 4.6

The results indicate that despite the current cooling system, parts of the inverter board still reach temperatures as high as $60°C$. The bleeder resistors on the board appear to be the hottest components, while the DC input capacitors are among the coolest parts of the board. To better prepare this inverter for an embedded scenario, all auxiliary components,

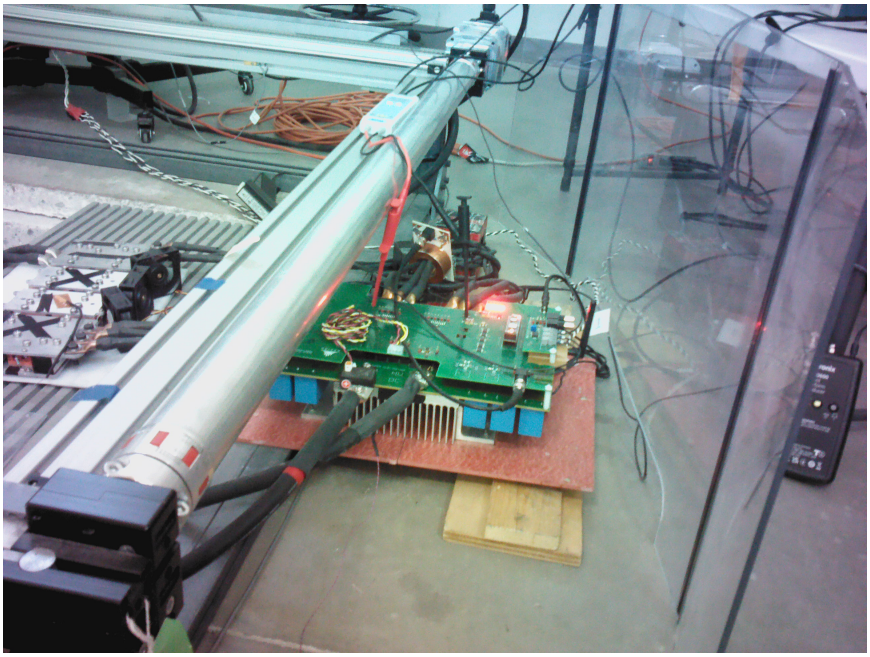

Fig. 4.4: Inverter 100 kW test setup

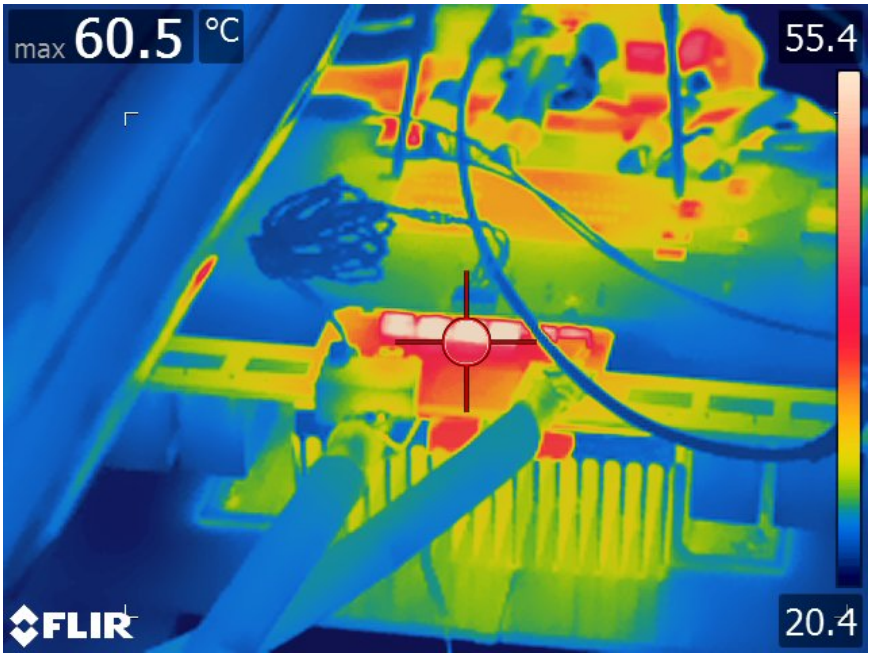

Fig. 4.5: Inverter FLIR thermal camera image with bleeder resistors in focus

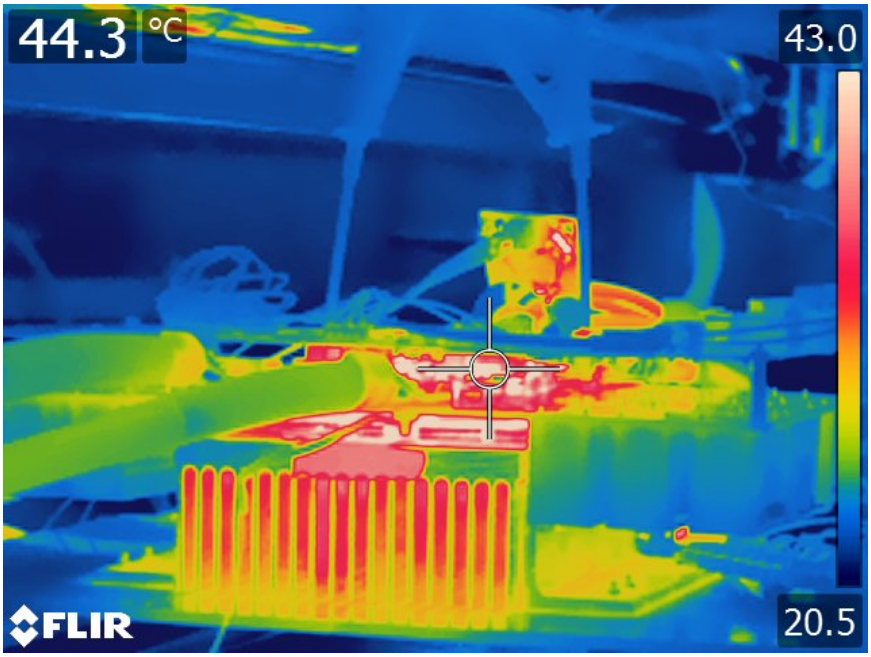

Fig. 4.6: Inverter FLIR thermal camera image with gate driver boards in focus

including bleeder resistors, power supplies, ICs, and sensing components, should be sized appropriately so their temperature rise remains low relative to the rest of the board. Optimal component selection may involve choosing less power-dense alternatives, as many auxiliary components are typically designed with high power density, assuming natural convection cooling conditions. Additionally, a custom gate drive board should be designed specifically for an 85 kHz switching frequency to enhance the efficiency of gate drive circuitry, thereby reducing losses.

The majority of heat loss occurs within the MOSFET modules. Since the formerly-embedded inverter was not fully validated before it failed, further research is needed to understand how the temperature rise of these MOSFET modules changes in a roadway-embedded scenario. Further analysis can determine the optimal heat sink size and packaging materials for effectively dissipating heat in a passively-cooled embedded environment.

Since the full inverter is expensive and difficult to handle, smaller-scale equivalent loss devices were created. The first device features resistors in the place of MOSFET modules. The second device uses a single MOSFET module instead of two modules. Both of these

devices provide a similar thermal response while being more affordable and easier to simulate compared to the full inverter.

4.2.2 Resistor Heat Sink Thermal Experiments and Simulations

The equivalent resistor device was designed to produce the same amount of loss as MOSFET modules within a similar area and attached to similar size heat sink. The resistors were calibrated to produce a loss equivalent to analytical calculated conduction losses based on the current flowing through the MOSFET and the MOSFETs $R_{DS(on)}$ value. The switching losses are considered negligible since the MOSFET modules are normally operated with soft switching. With approximately 100 A RMS at full power operation and an $R_{DS(on)}$ value of 2.6 $m\Omega$, the estimated conduction losses are 26 W per module or roughly 52 W per half bridge. The "resistor heat sink" device was tested at a slightly lower power level of 45 W per resistor. The resistor heat sink device is shown in Fig. 4.7

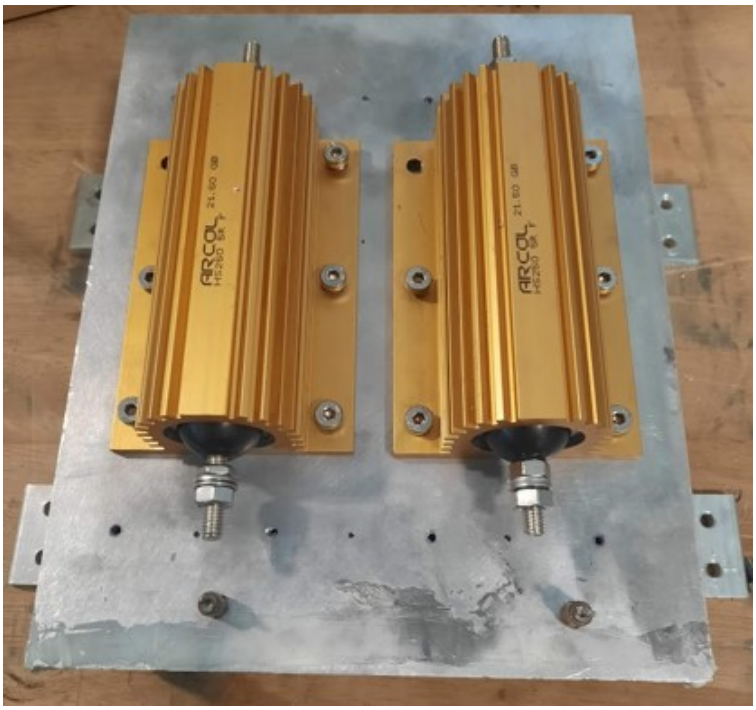

Fig. 4.7: Resistor heat sink device

T-type thermocouples were placed atop each resistor and on the top and side of the heat sink to monitor temperature changes. The resistors were connected in series and supplied power by a DC power supply set to 30 V. Each resistor, rated at 5 Ω, received three amps of current, generating 45 W of loss in each. The resistor heat sink device was tested in both air and sand environments to compare the thermal response of embedded and non-embedded conditions. Both scenarios were then simulated in Ansys Icepak, with the simulations refined based on experimental results.

Resistor Heat Sink Air Tests

An image depicting the air test setup is shown in Fig. 4.8. The cooling of this device primarily occurs through natural convection around the resistors and heat sink.

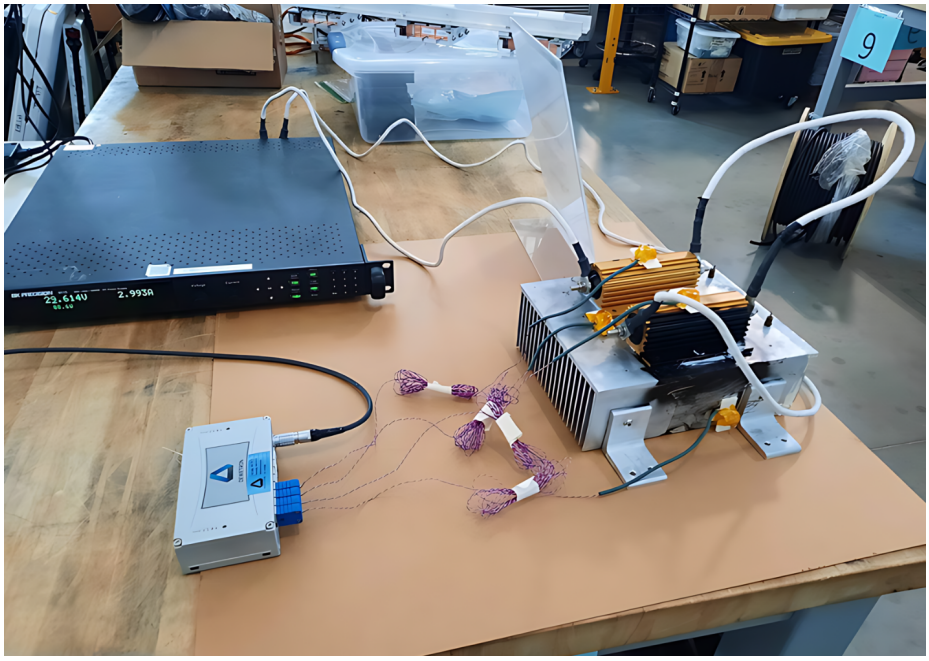

Fig. 4.8: Resistor heat sink air test setup

The device was turned on at full power losses for 1.5 hours. The setup was then turned off and the temperature of the device was measured for another 1.25 hours. This device was modeled in Ansys Icepak with the same heat sink dimensions. Simplifications were made to

the resistors in the Ansys model to simplify meshing. The air density and ambient conditions within the simulation were modified to reflect the elevation of Logan Utah and the $21°C$ lab-measured ambient temperature. Natural convection defaults were chosen to model the air around the device and constant ambient temperature opening boundary conditions were selected to mirror the experimental setup. A screenshot of the Ansys model is shown in Fig. 4.9

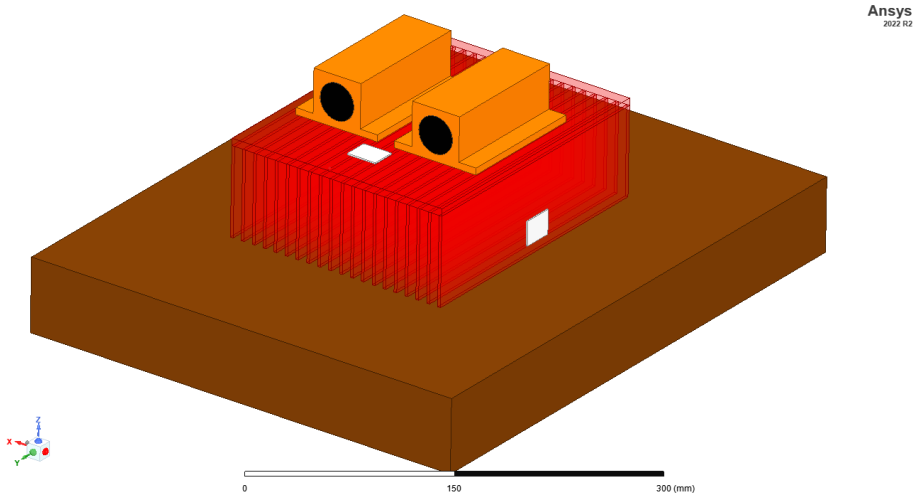

Fig. 4.9: Resistor heat sink air Ansys model

The thermocouple measurements and Ansys simulation results for the resistor heat sink device during the test duration are shown in Fig. 4.10. After 1.5 hours, the top of the resistors reached a temperature of approximately $68.5°C$. It appears that the steady-state temperature would reach around $70°C$ if the setup were run for a longer period of time. Based on this estimated steady-state temperature, the thermal resistance from the top of the resistor to ambient is approximately $R_{th} = \frac{70°C - 21°C}{45\,W} \approx 1.09\,\frac{°C}{W}$

The Ansys model predicts the temperature rise of the heat sink reasonably well, but it is less accurate at predicting the resistor temperature compared to experimental data. Discrepancies between simulation and experiment are likely due to simplifications to the resistors within the Ansys model and differences in the thermal properties of the aluminum

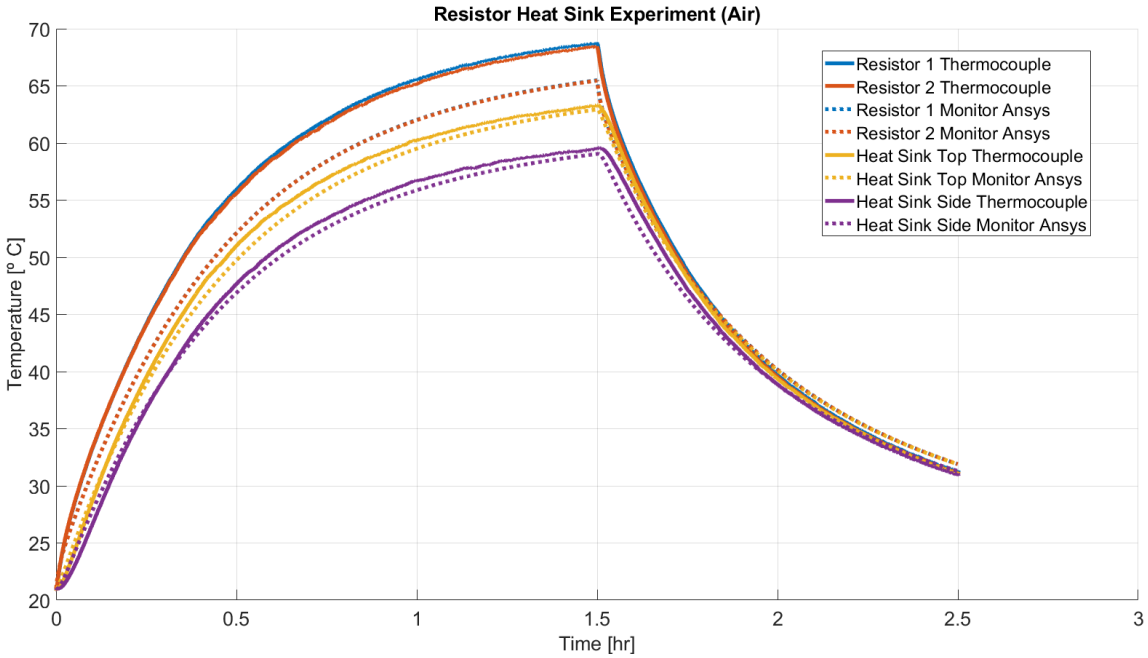

Fig. 4.10: Resistor heat sink air test results

material. With additional time and more accurate measurements of the thermal material properties, it is likely that these simulation results could be improved to align more closely with experimental results.

Resistor Heat Sink Sand Test

An image depicting the sand test setup is shown in Fig. 4.11. The resistor heat sink device was buried 60 mm below the surface of the sand and was buried near the corner of the sandbox for convenience. The cooling of this device primarily occurs through conduction from the heat sink and resistors to the surrounding sand.

The setup was turned on at full power losses for 7 hours. This device was modeled in Ansys Icepak with the same heat sink and resistor dimensions as in the air model. The ambient conditions were adjusted to $20°C$, and sand properties were inputted based on estimated analytical values. Natural convection defaults were chosen to model the heat transfer above the sandbox and constant temperature wall boundary conditions were selected to model the edges of the sandbox. A screenshot of the Ansys model is shown in

Fig. 4.11: Resistor heat sink sand test setup

Fig. 4.12

The thermocouple measurements and Ansys simulation results for the resistor heat sink device during the test duration are shown in Fig. 4.13. After 7 hours, the top of the resistors reached a temperature of approximately $120°C$. Due to the thermal mass of the sand, the system did not reach steady-state temperature and it would require a longer time period for the system to fully stabilize.

The Ansys model predicts the temperature rise of the heat sink and resistor temperature reasonably well compared with experimental results. The transient temperature rise curve from the Ansys simulation seems to have a slightly higher slope than seen in experimental results. The discrepancies between the simulation and experiment are likely due to the same simplifications made to the geometry within the model as well as potential differences in the thermal properties of the aluminum and the sand.

Although the Ansys simulation results differ slightly from the true temperature measurements, these results are sufficiently accurate to provide insights for analyzing the inverter design. By extrapolating these simulation results from sand to concrete and adding

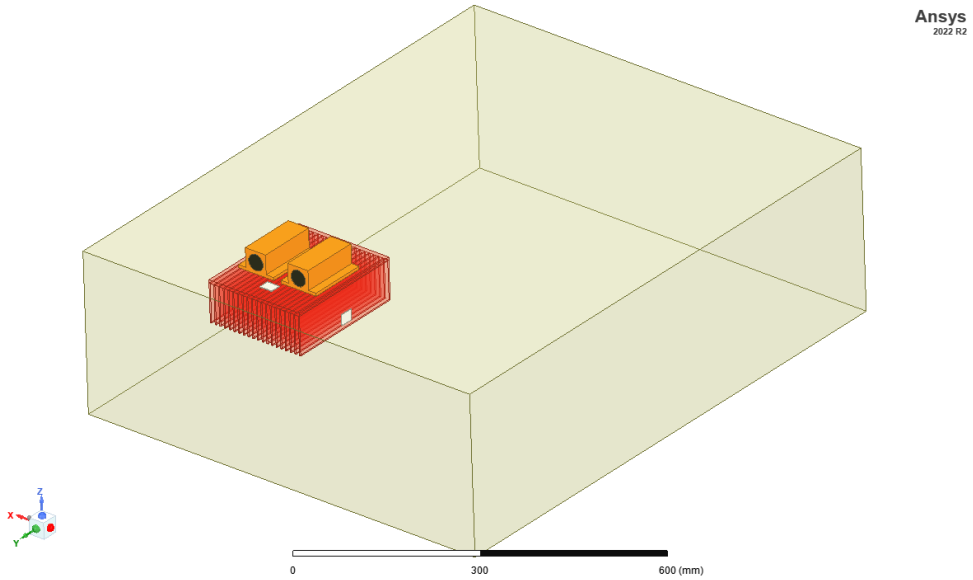

Fig. 4.12: Resistor heat sink sand Ansys model

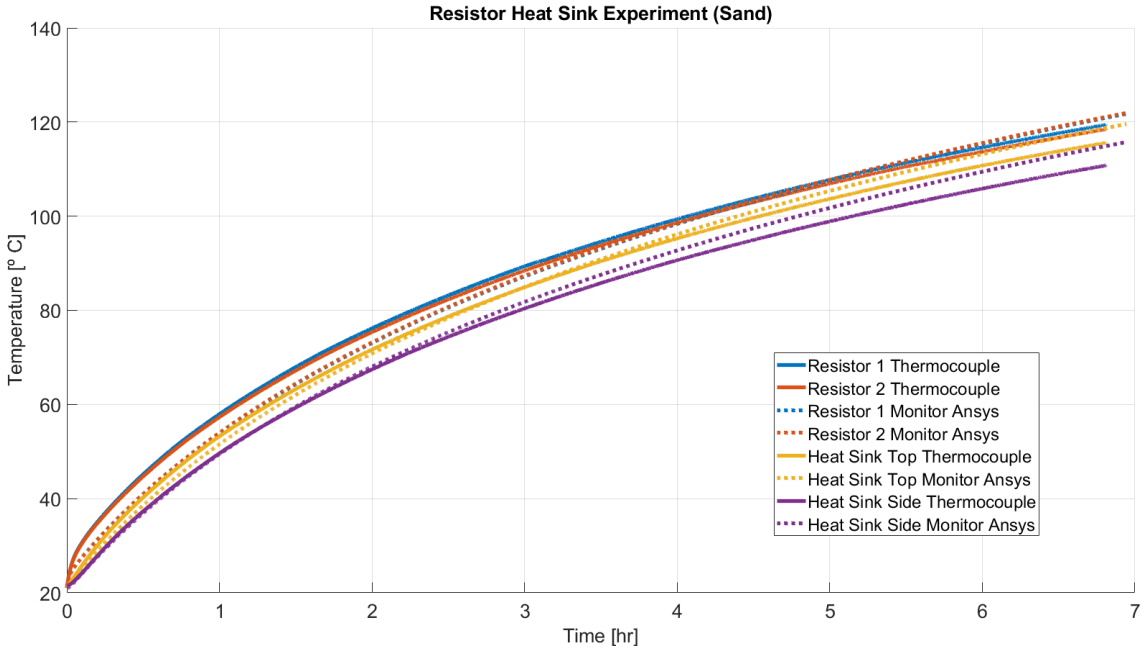

Fig. 4.13: Resistor heat sink sand test results

epoxy encapsulation material around the resistor heat sink device, we can estimate the temperature of the MOSFET modules in a roadway-embedded environment. The Ansys model for this setup is shown in Fig. 4.14. The epoxy block includes Epoxy-50-2151FR potting material that surrounds the resistor heat sink device with a thickness of 20 mm on all sides. The top of the epoxy block is 250 mm from the surface of the concrete and the sides of the epoxy block are approximately 2.8 meters from the edge of the concrete block on all sides. The simulation setup is set to natural convection defaults for the air above the concrete block and the edges of this concrete block are wall boundary conditions with a constant ambient temperature. The Ansys simulation results for this model are shown in Fig. 4.15

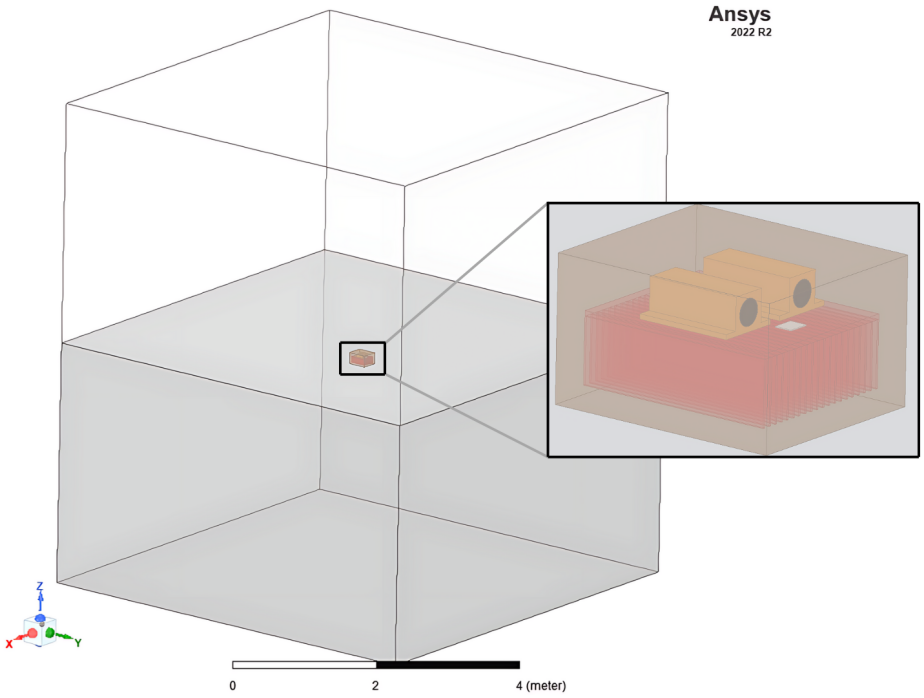

Fig. 4.14: Resistor heat sink Ansys model in concrete with epoxy potting

It appears that this device, which has similar losses to the inverter MOSFET modules, could be embedded in the roadway when thermally-conductive epoxy is used. The steady-state temperature approaches a reasonable operating temperature at moderate ambient conditions even at 100% utilization.

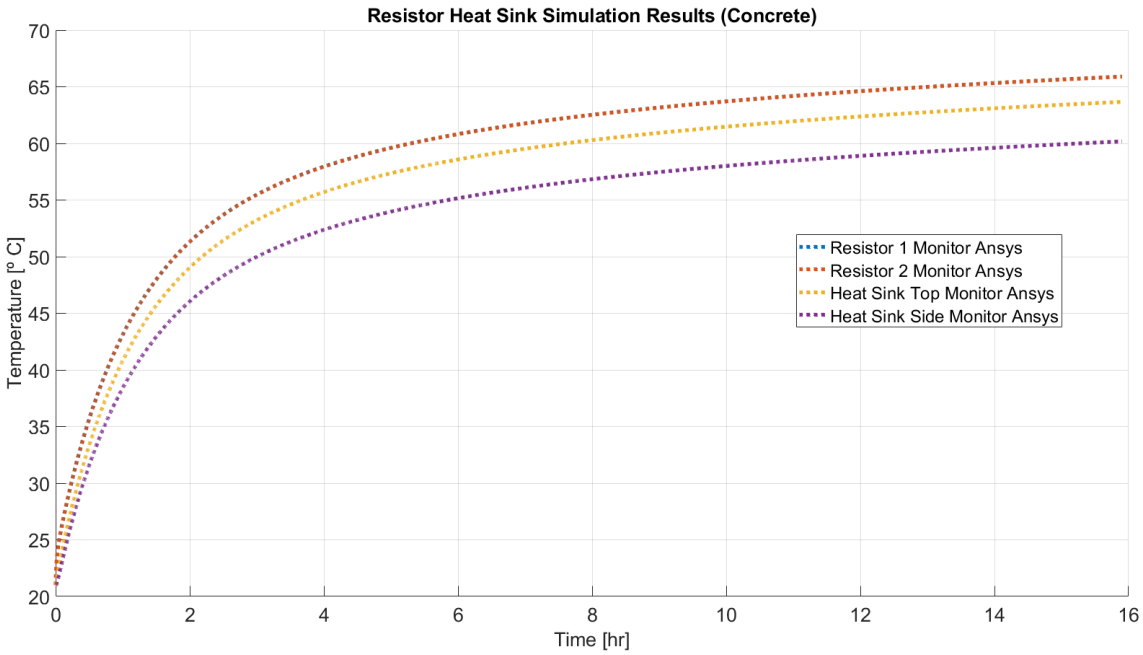

Fig. 4.15: Resistor heat sink roadway-embedded simulation results

A PCM heat sink was not modeled within Ansys Icepak, but this could be explored in future simulations to enhance the transient thermal response of the inverter. Additionally, testing epoxy materials with different thermal properties could help assess their heat extraction effectiveness and determine the optimal thermal conductivity of packaging material in a roadway-embedded environment. This simulation could also be modified to account for higher ambient temperatures, higher power losses, and lower utilization rates to predict MOSFET module performance across various deployment scenarios.

Additionally, testing epoxy materials with different thermal properties could help assess their heat extraction effectiveness and identify the optimal thermal conductivity for packaging materials in a roadway-embedded environment

4.2.3 MOSFET Heat Sink Thermal Experiments

The equivalent MOSFET device was configured with a single MOSFET module device and a slightly smaller heat sink compared to the resistor heat sink device. While the reduced size of the heat sink will result in less effective heat transfer, this device is still expected to

perform similarly to the resistor heat sink device. This device was tested with additional amounts of power loss and compared with the resistor heat sink device to show how the the heat transfer differs. Thermocouples were attached to the base plate of the MOSFET module and the heat sink beneath it. Additionally, the NTC temperature of the MOSFET module was monitored. The MOSFET module device is shown in Fig. 4.16

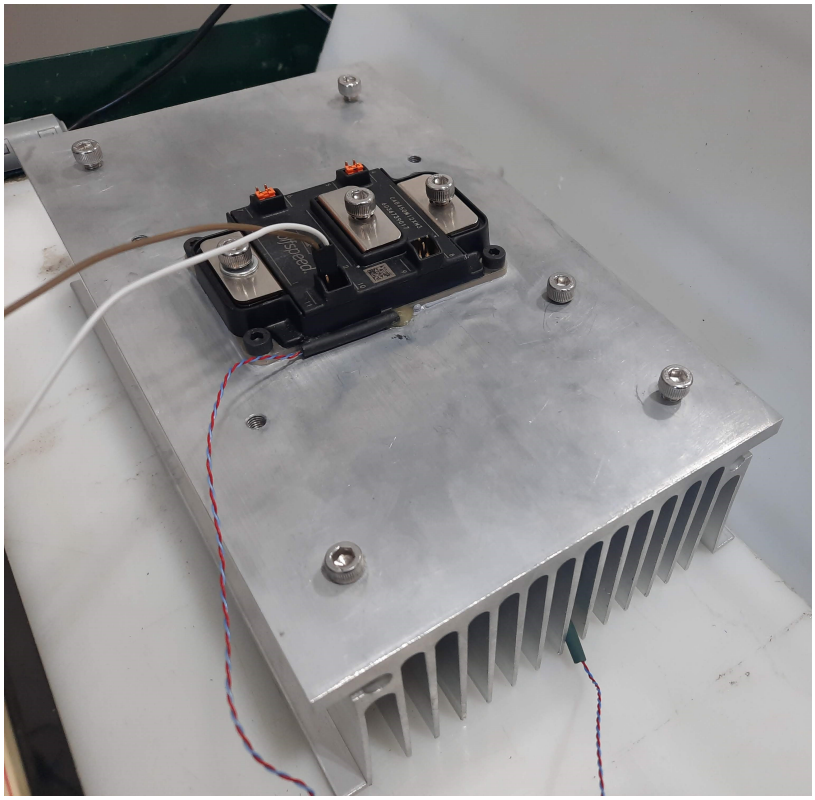

Fig. 4.16: MOSFET heat sink device

Generating loss through the $R_{DS(on)}$ of the MOSFET requires high currents. To simplify the loss generation, the DC voltage applied to the MOSFET module was reversed, forward-biasing the body diodes of the MOSFET half bridge and causing loss through the body diodes. The voltage drop across the body diode and the current flowing through it were measured to produce the equivalent loss expected in the MOSFET module during normal operation in a full DWPT system. The circuit diagram for testing this MOSFET module is shown in Fig. 4.17 where the red dotted line indicates the current flow path. Since

the current is DC and no gate signal is applied to the switches, all the current is expected to flow through the body diodes.

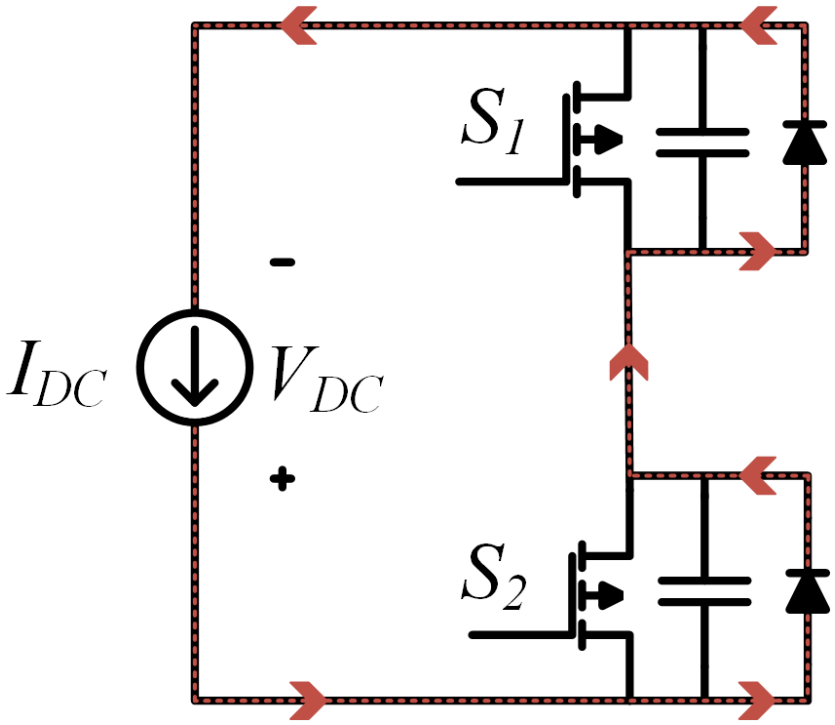

Fig. 4.17: MOSFET heat sink test circuit

MOSFET Heat Sink Air Tests

A picture of the air test setup is shown in Fig. 4.18. The cooling of this device primarily occurs through natural convection, similar to the resistor heat sink device. However, with the MOSFET modules, less heat is transferred through the tops of the device. Instead, more heat is directly conducted to the heat sink via the MOSFET base plate, where the silicon dies are mounted.

The MOSFET heat sink device was tested at three different power levels to observe the temperature differences at varying conditions. Since the $R_{DS(on)}$ of the MOSFET can increase with temperature, the 100 kW operating point was tested with two different hypothetical $R_{DS(on)}$ values, with power loss calculated based on an 800 V DC link and

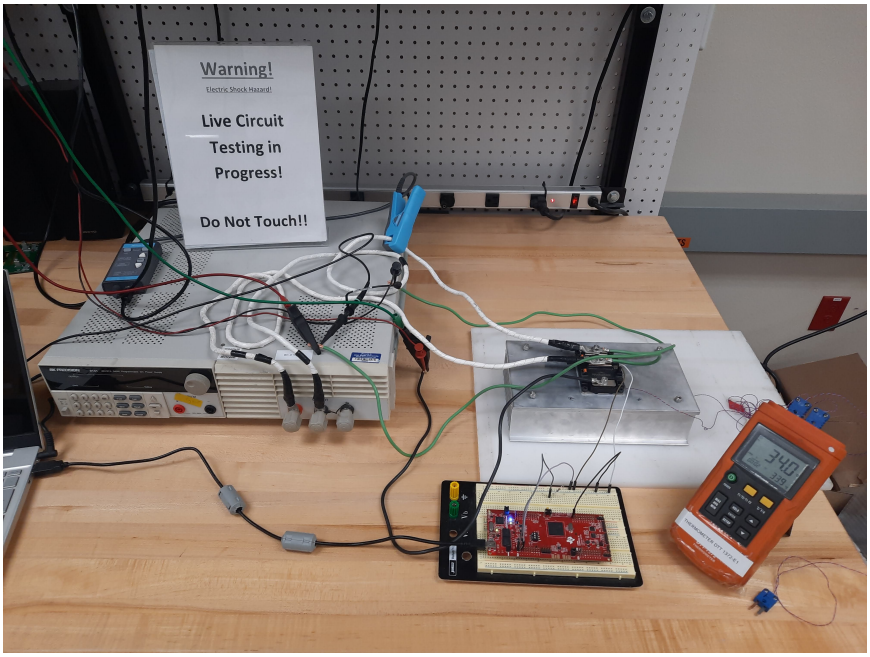

Fig. 4.18: MOSFET heat sink air test setup

100 A RMS current through the MOSFET modules. Table. 4.2 displays these different power loss conditions, where I_{DC} is the current through the devices and V_{DC} is the average diode voltage drop across the devices. The voltage drop across this MOSFET body diode decreases with temperature, so with consistent DC current, the power losses reduce slightly over the test duration. The average voltage drop and average power losses through the device are listed in the table.

Table 4.2: Power loss conditions for MOSFET heat sink device experiments

Power Level	$R_{DS(on)}$	Power Loss	I_{DC}	V_{DC}
50 kW	2.6 $m\Omega$	28 W	7.6 A	3.68 V
100 kW	2.6 $m\Omega$	52 W	13.5 A	3.85 V
100 kW	3.95 $m\Omega$	79 W	20 A	3.95 V

The setup was run at full power for about 1.5 hours. The setup was then turned off and the temperature of device was measured for another 1.5 hours. The ambient temperature remained at approximately 20.5°C throughout each of the three tests. The thermocouple

measurements and NTC temperature measurements are shown in Fig. 4.19. The temperature rise of the resistor heat sink device in air is included for reference.

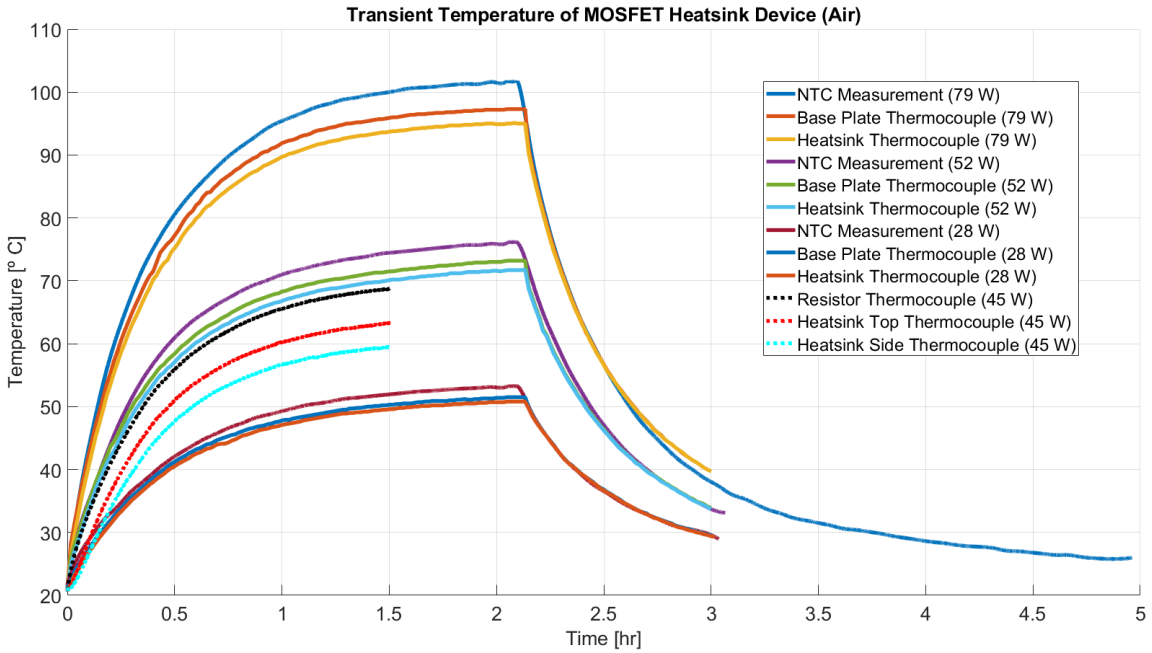

Fig. 4.19: MOSFET heat sink air test results

The thermal resistance from the NTC to ambient is estimated to be on average $R_{th} \approx 1.1\,\frac{^\circ C}{W}$. Since temperature scales approximately linearly with an increase in power loss, this thermal resistance can be used to estimate the steady-state temperature of the NTC at higher power loss conditions. For instance, at the worst case $R_{DS(on)}$ of $4.6\,m\Omega$, the estimated power loss at the 100 kW operating condition is 92 W. Given the thermal resistance from NTC to ambient, that gives an expected steady-state temperature of $T_\infty = 92\,W \times 1.1\,\frac{^\circ C}{W} + 20.5^\circ C = 121.7^\circ C$. This estimated steady-state temperature at 92 W of loss is lower than the maximum operating temperature of $175^\circ C$ listed in the MOSFET module datasheet, but continued operation at this high temperature could significantly decrease in the lifetime of the device.

The comparison between the resistor heat sink device and MOSFET heat sink device shows that their thermal resistances are quite similar. Each resistor generates a heat load of

45 W, totaling to 90 W throughout the entire device. However, the steady-state temperature rise of the resistor heat sink device aligns with what is expected for a 45 W heat dissipation in a single MOSFET module. By distributing the loss between two devices instead of one, the thermal resistance from the case to heat sink of a single device is in parallel with itself, effectively halving the thermal resistance and thus halving the steady-state temperature. This reduction in total thermal resistance is due to the increased surface area of the devices in contact with the heat sink, allowing more paths for the heat to dissipate.

The transient time constants and shape of the transient RC curves are also similar between the two devices, despite differences in shape and location of the devices when connected to their respective heat sinks. The difference in heat sink temperature measurements on the resistor heat sink device vs the MOSFET heat sink device is due to the varying thermocouple placements on each heat sink. If the thermocouples were moved to the same locations on each heat sink, the temperatures are expected to more closely align.

MOSFET Heat Sink Sand Test

A picture of the sand test setup is shown in Fig. 4.20. The MOSFET heat sink device was buried 70 mm below the surface of the sand. The cooling of this device primarily occurs through conduction from the heat sink and module to the surrounding sand, similar to the resistor heat sink device. However, with the MOSFET modules, less heat is transferred through the tops of the device. Instead, more heat is directly conducted to the heat sink via the MOSFET base plate, where the silicon dies are mounted. Heat is then transferred from the heat sink to the surrounding sand.

This sand experimental setup was only run at the 28 W average power dissipation operating point. The setup was turned on at full power losses for about 24 hours and then turned off for about 36 hours. The ambient temperature was measured to be approximately $20°C$ over the duration of the test. The NTC measurements of the MOSFET module over that time period are shown in Fig. 4.21

The figure shows that the MOSFET heat sink device failed to reach steady state even after 24 hours of continuous operation. The temperature of the MOSFET NTC approached

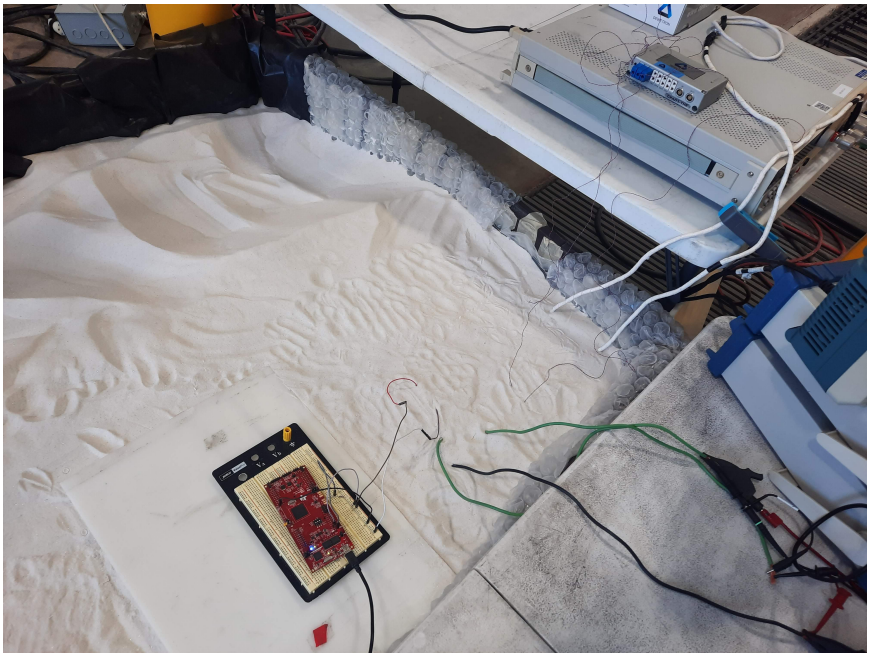

Fig. 4.20: MOSFET heat sink sand test setup

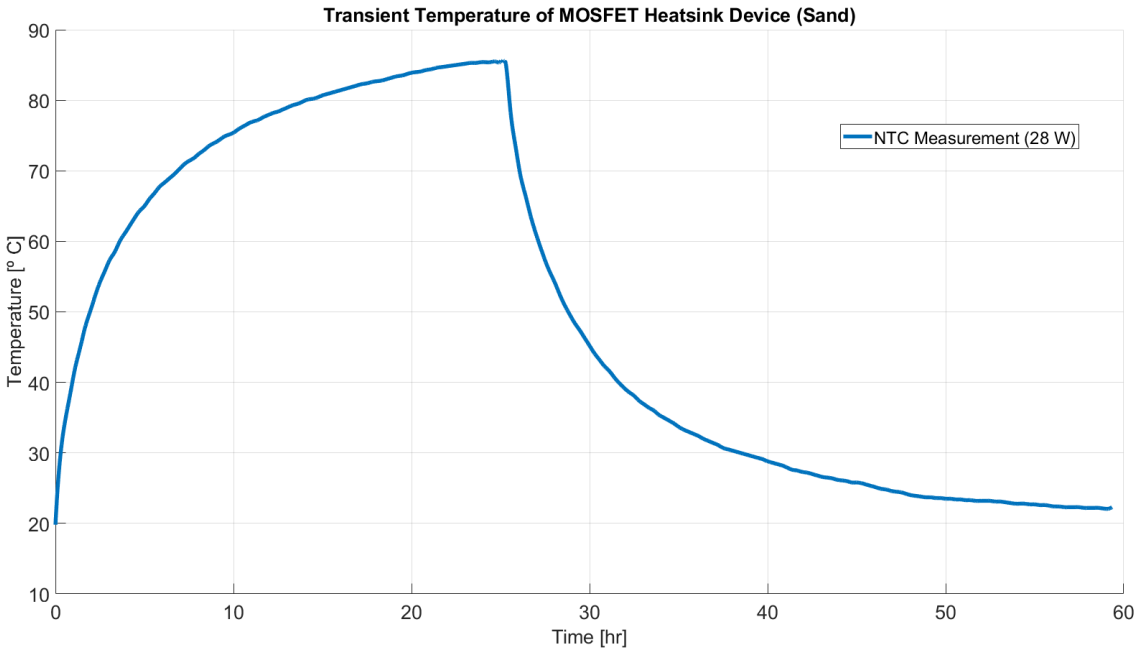

Fig. 4.21: MOSFET heat sink sand test results

approximately $85°C$ after 24 hours, and it appears that the final steady-state temperature would be slightly higher, around $87°C$.

The estimated steady-state temperature of the MOSFET heat sink device at 28 W is approximately $34°C$ higher than at the same power level in air. Since temperature scales linearly with an increase in power loss due to the mostly constant thermal resistance, a similar temperature difference is expected between the air and sand experiments at higher power levels. The thermal resistance from the NTC to ambient is estimated to be $R_{th} \approx 2.39\ \frac{°C}{W}$. The estimated steady-state temperature of the MOSFET heat sink module in sand at higher power losses is given in Table. 4.3.

Table 4.3: Power loss conditions for MOSFET heat sink device experiments

Power Level ($R_{DS(on)}$)	Power Loss	Estimated NTC Steady-State Temperature
50 kW ($2.6\,m\Omega$)	28 W	$87°C$
100 kW ($2.6\,m\Omega$)	52 W	$124°C$
100 kW ($3.95\,m\Omega$)	79 W	$189°C$
100 kW ($4.6\,m\Omega$)	92 W	$220°C$

This table shows that at higher power losses, the single MOSFET module in a roadway-embedded environment has potential to overheat. In lower DWPT utilization scenarios, the steady-state temperature may not be reached due to the large time constant, allowing higher power losses or higher ambient temperatures. Additionally, the use of effective epoxy encapsulation material and a PCM heat sink could further increase the lifetime of the roadway-embedded inverter or allow increased utilization and higher ambient temperatures. In the case of high power loss, ambient temperature, or utilization, two inverters could be put in parallel to process the power. By splitting the power loss into two modules rather than one, we can expect the steady-state temperature to reduce by nearly half, as shown previously.

4.3 Current DWPT Capacitor Bank Thermal Management

The current DWPT capacitor bank consists of Celem film power capacitors used in parallel and series. A single one of these Celem capacitors is shown in Fig. 4.22

Fig. 4.22: Celem film power capacitor

The complete capacitor bank consists of 18 Celem film capacitors connected together with aluminum bus bars. This setup includes three Celem capacitors in parallel to make the C_{ps1} and C_{ps2} capacitor and ten Celem capacitors in a parallel and series combination to make the C_{pp} capacitor. Two T-type thermocouples were attached to the capacitor bank, positioned as shown in Fig. 4.23. According to the Celem capacitor datasheet, the maximum operating temperature for these capacitors is $85°C$.

4.3.1 Celem Capacitor Bank 100 kW Experiments and Simulations

The capacitor bank was first tested at 100 kW to evaluate the system's thermal performance with the current design. It was tested without fans to determine if it could sustain full-power operation without active cooling. This test setup is shown in Fig. 4.24. The capacitor bank was tested within the same double-sided LCCL tuning network as the inverter, operating at a 50% duty cycle with an 85 kHz square wave applied to its input terminals.

The transient temperature rise of the DWPT capacitor increased rapidly, indicating that the capacitor bank would overheat if allowed to reach steady state. Consequently, the test was only conducted for 10 minutes at full power operation. The capacitor bank was

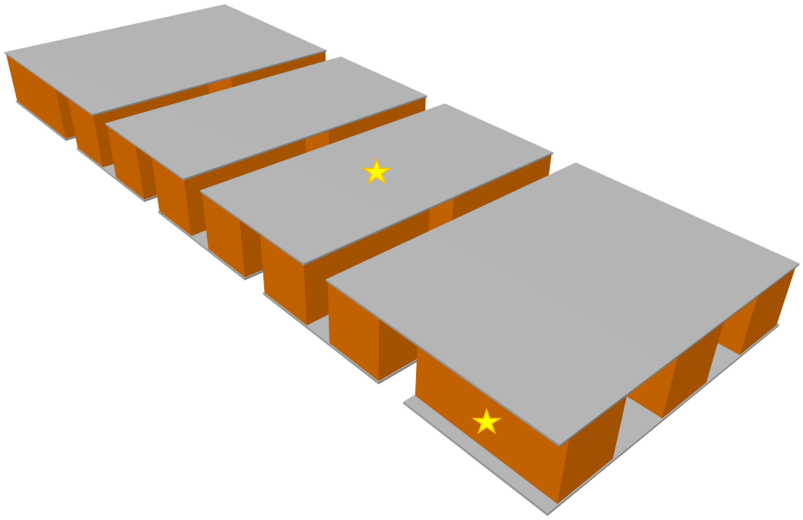

Fig. 4.23: Celem capacitor bank. Yellow stars represent where thermocouples were attached during thermal testing

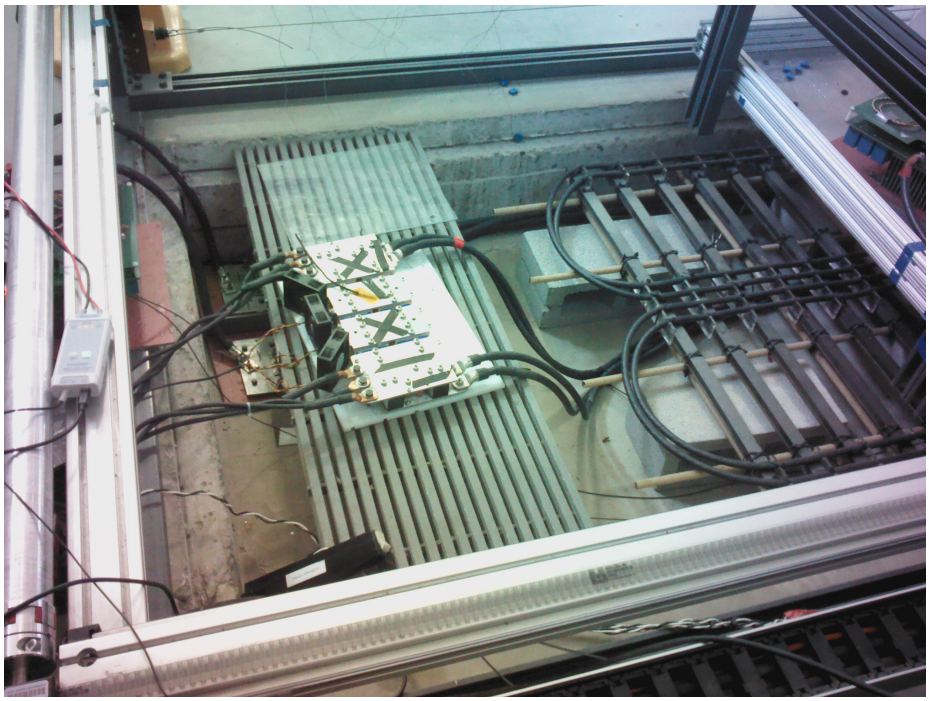

Fig. 4.24: DWPT capacitor bank 100 kW test setup

modeled in Ansys Icepak for an extended duration to predict what its steady-state temperature would reach under natural convection cooling. The simulation used natural convection defaults and constant ambient temperature opening boundaries to mirror the experimental setup. Simplifications such as removing screws and terminals were made within the Ansys model to simplify meshing. The capacitors were modeled as simple rectangular blocks of copper and the losses were inputted as block excitations based on analytical estimations. While the Celem capacitor website suggests calculating losses using 1% of the reactive power, only half of those analytical losses were used in the Ansys simulation as shown in Table. 4.4. It seems that the Celem website suggested loss calculations are generous and we are experiencing nearly 50% less loss than analytically calculated. A screenshot of the Ansys model is shown in Fig. 4.25.

Table 4.4: Electrical measurements and power losses in Celem capacitor bank at 100 kW

Component	Voltage V_{RMS}	Current I_{RMS}	Power Loss (W)	Ansys Losses (W)
C_{ps1}	514	244	117.12	58.56
C_{ps2}	514	244	117.12	58.56
C_{pp}	790	271	210.26	105.13

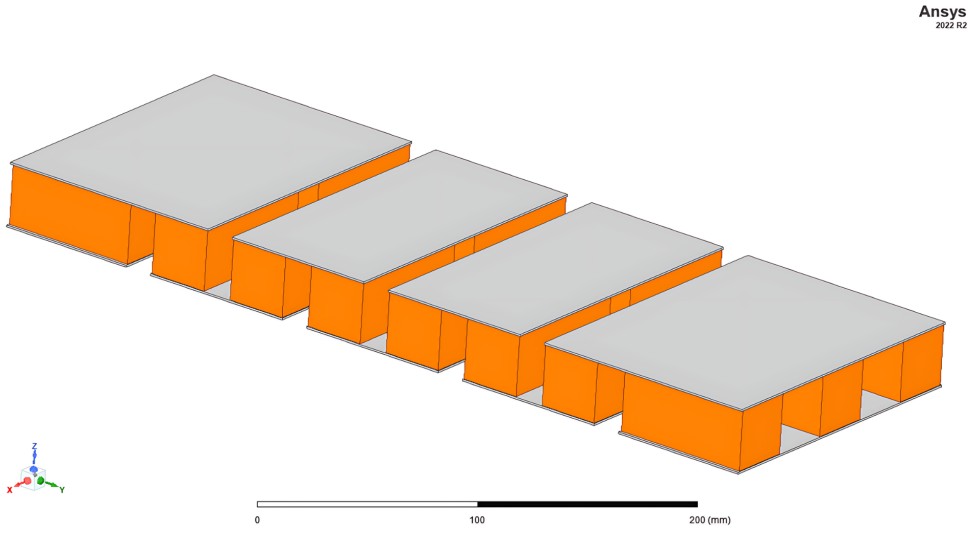

Fig. 4.25: Celem capacitor bank Ansys model

The experimental results and Ansys Icepak simulation results are shown in Fig. 4.26. The experimental results only reach a temperature of around $45°C$, but given more time, the Ansys Icepak results predict a steady-state temperature of around $105°C$. These results indicates that without active cooling, the capacitor bank is expected to overheat beyond its maximum rated operating temperature.

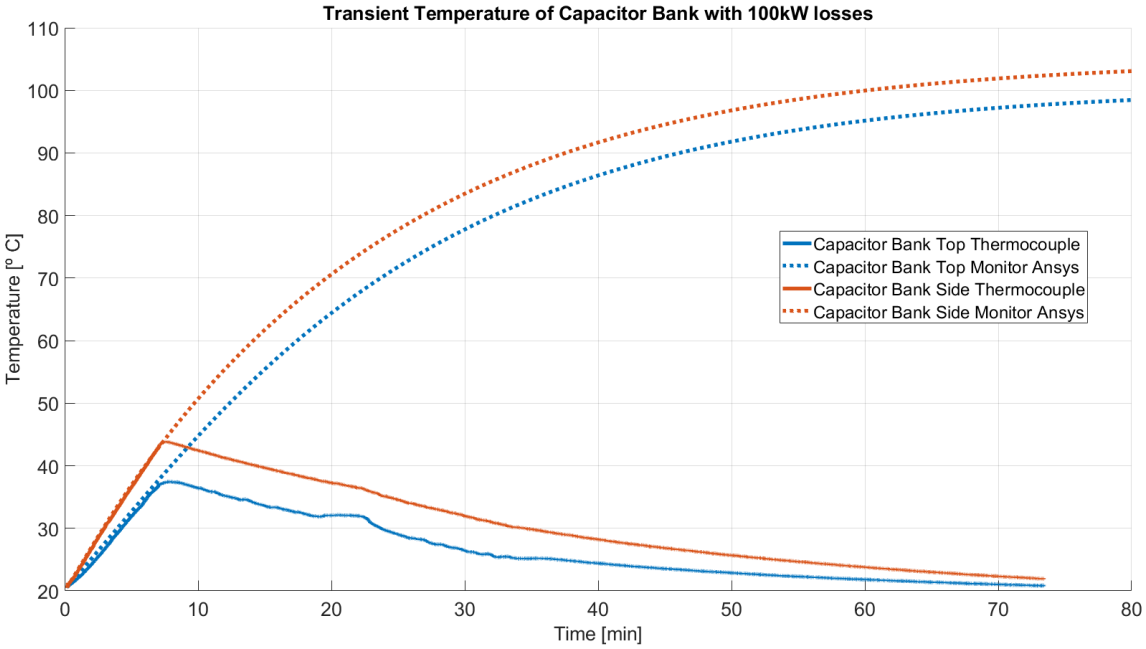

Fig. 4.26: Celem capacitor bank transient temperature results at 100 kW power losses in air

The same capacitor bank was simulated in concrete within Ansys Icepak to observe the impact of embedding the device. In the simulation, the capacitor bank was first encased in an epoxy potting material, then surrounded by concrete. A screenshot of the Ansys model is shown in Fig. 4.27. The epoxy block includes Epoxy-50-2151FR potting material, encasing the capacitor bank with a thickness of 20 - 40 mm on all sides. The top of the epoxy block is 250 mm from the surface of the concrete, and the sides of the potted capacitor bank are approximately 2.5 meters from the edges of the concrete block on all sides. The simulation setup uses natural convection defaults for the air above the concrete block and constant ambient temperature boundary conditions set to $20°C$. The edges of the air are modeled

with an opening boundary condition and the edges of the concrete block are modeled with wall boundary conditions. The Ansys results from this simulation are shown in Fig. 4.28

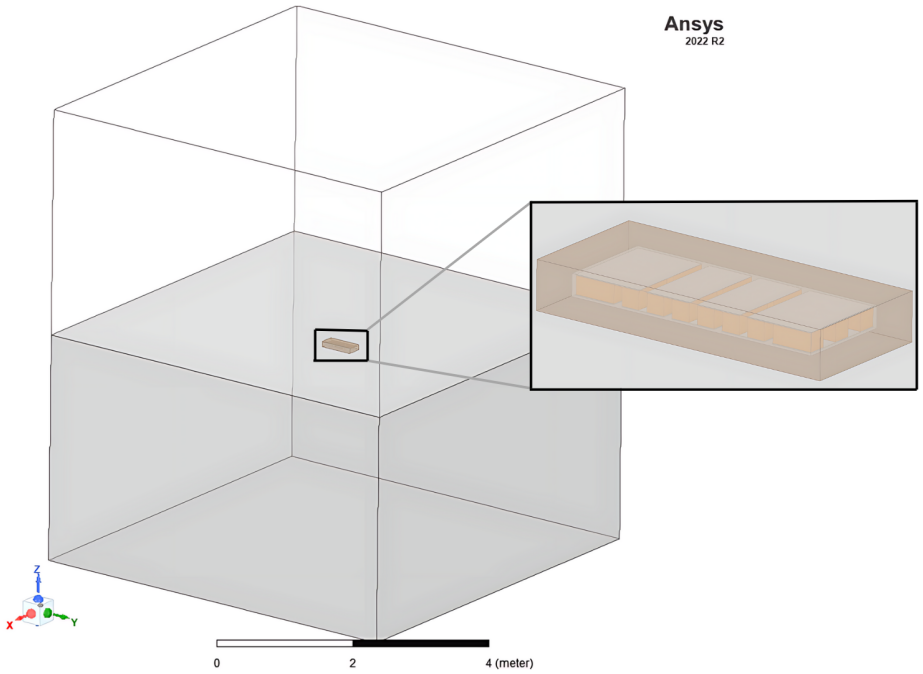

Fig. 4.27: Ansys Icepak model for Celem capacitor bank encapsulated in epoxy and embedded in concrete

These results predict that the steady-state temperature in concrete is expected to reach over $100°C$ after 24 hours. It appears that it takes about 9 hours for the temperature of the concrete-embedded capacitor bank to reach the same steady-state temperature as it does in air. These results suggest that the long transient time constant could be used to effectively cool the device in scenarios with lower DWPT system utilization. The difference between the capacitors' temperature and the temperature outside the epoxy block highlights the significant impact of thermal resistance between components and packaging. The more thermally conductive the epoxy potting material and the greater the surface area of the components in contact with the packaging material, the lower the thermal resistance and, consequently, the lower the capacitors' steady-state temperatures.

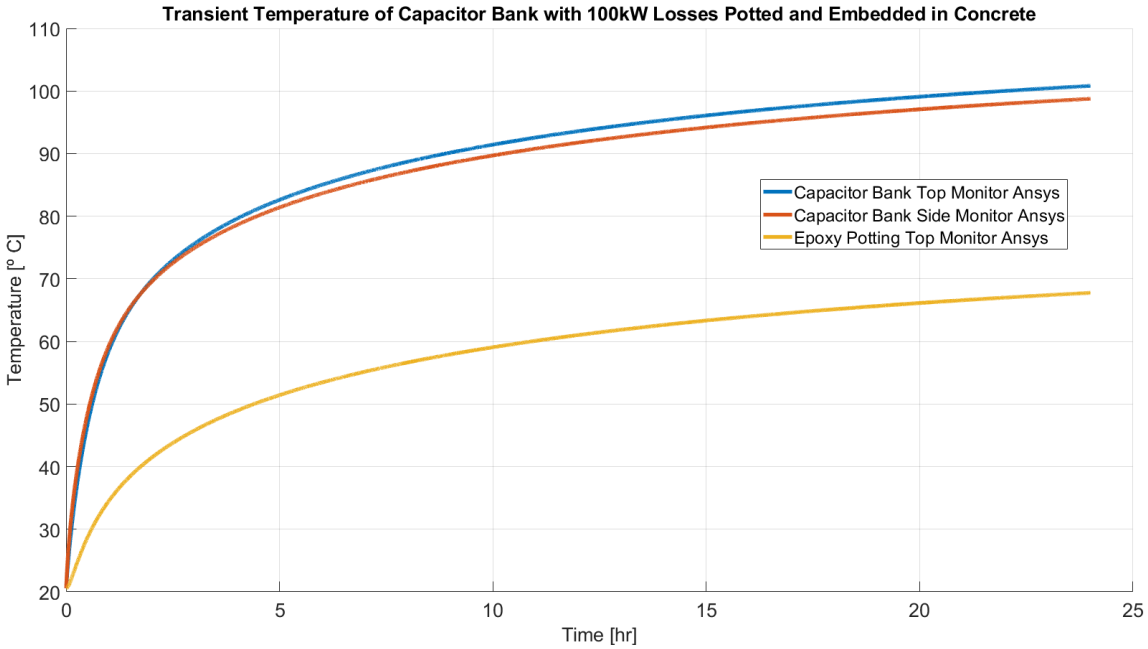

Fig. 4.28: Celem capacitor bank transient temperature results at 100 kW power losses embedded in concrete

4.3.2 Celem Capacitor Bank 20 kW Experiments and Simulations

Since the capacitor bank could not be operated until steady state at full power, it was tested at a lower power level to observe the full temperature rise characteristics. The test setup for the 20 kW power level was slightly modified by placing the capacitor bank underneath the transmitter pad instead of positioning it at the same level. An image of the experimental setup is shown in Fig. 4.29.

The capacitor bank was turned on at full power for 2 hours, after which it was turned off and the natural convection cooling of the device was measured for 2 hours. The experimental results over this longer period are simulated in Ansys. The thermocouple measurements of the capacitor bank during this period along with the corresponding Ansys results are shown in Fig. 4.30.

After two hours, the hottest part of the capacitor bank reached approximately $47°C$, which was not yet at steady-state temperature. The Ansys results predict a similar temperature on the top of the capacitor bank and a slightly lower temperature on the side compared to the experimental results. This discrepancy is likely due to the simplifications

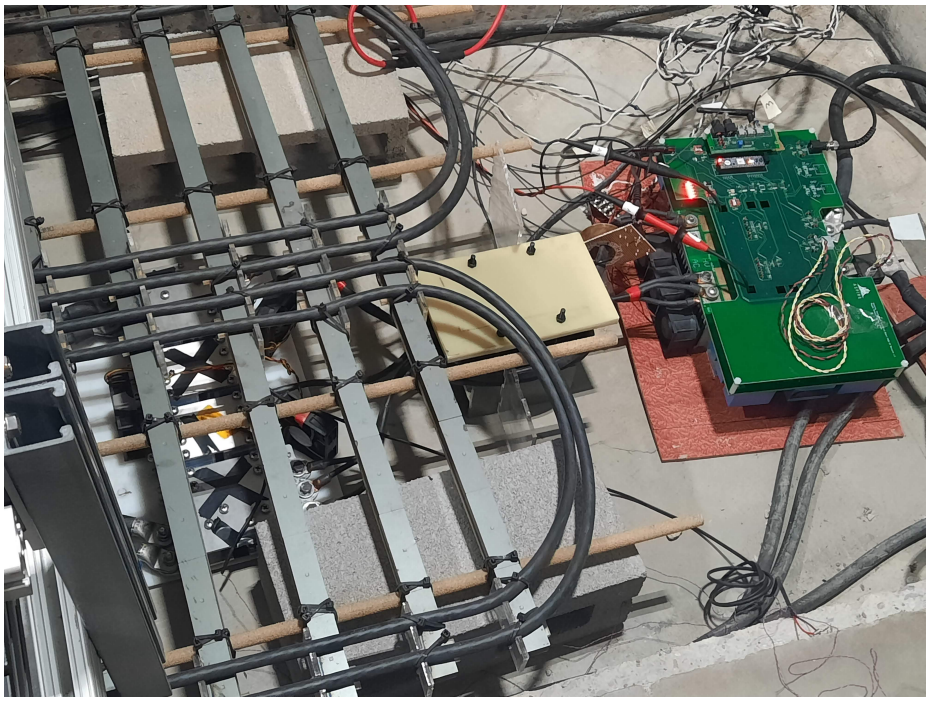

Fig. 4.29: DWPT capacitor bank 20 kW test setup

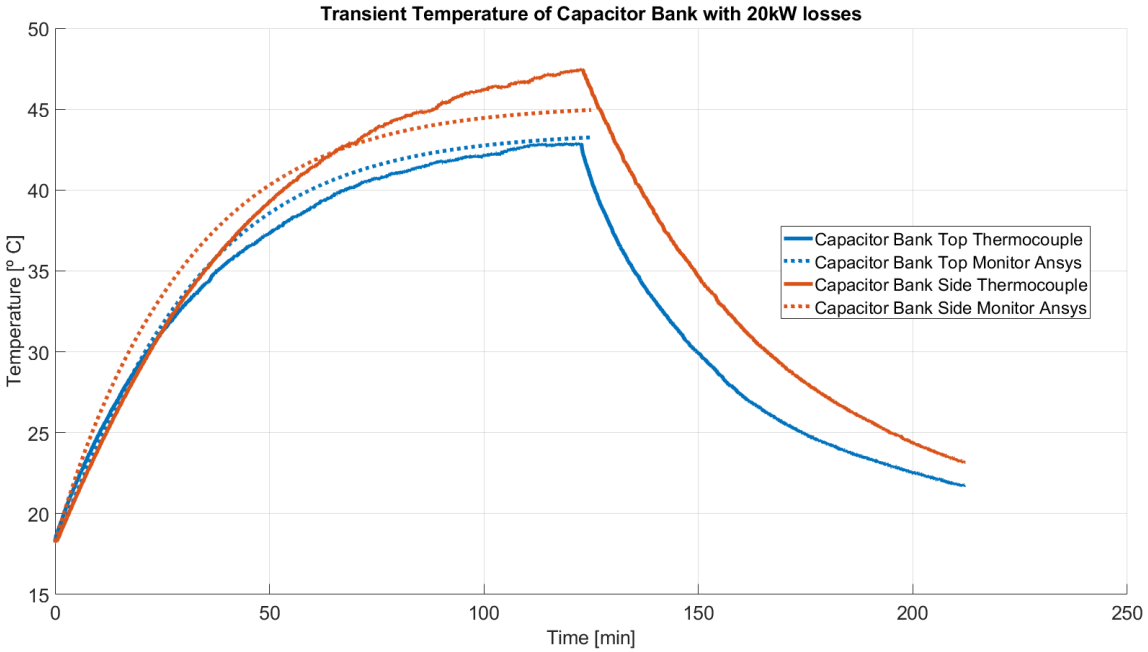

Fig. 4.30: Celem capacitor bank transient temperature results at 20 kW power losses in air

in the Ansys model. For example, the model does not include the terminals, which get quite hot where the litz wire connects. This terminal temperature likely increases the temperature of the capacitor closest to it, affecting the side thermocouple readings.

The results indicate that the Celem capacitor bank could be embedded in the roadway but only under low utilization conditions and low ambient temperatures. Using more thermally conductive epoxy or PCM could allow for increased utilization or operation at higher ambient temperatures, but the high-temperature operation would still result in lower component lifetime. Exploring alternative capacitor bank designs may be beneficial for roadway-embedded environments involving higher ambient temperatures or increased utilization.

CHAPTER 5

Proposed DWPT Roadway-Embedded Power Electronics

5.1 Overview of Proposed Roadway-Embedded Electronics

In the previous chapters, we explored how we can lower the steady-state temperature of components by reducing power density or increasing surface area of components in contact with the roadway. Additionally, increasing thermal mass extends the time a system can run before reaching steady state. This low-power-density, high-thermal-mass design approach is recommended for roadway-embedded power electronics, since there is ample space beneath the transmitter coil to allow for larger power electronics. In this chapter, we propose a new capacitor bank design and discuss how it can be integrated into a complete roadway-embedded DWPT system.

5.2 Proposed DWPT Capacitor Bank Design

The proposed DWPT capacitor bank uses polypropylene metallized film capacitors selected for their low cost, self-healing properties, and stable capacitance value with changing temperatures. TDK capacitors were specifically chosen for their high voltage and temperature ratings. The specific B32672L series capacitors in this design have a 2000 V DC voltage rating and a maximum operating temperature of $125°C$. A picture of one of these TDK capacitors is shown in Fig. 5.1

Fig. 5.1: TDK metallized film capacitor

These TDK capacitors, which have low individual current ratings, are soldered directly onto PCBs and are connected in parallel to increase their current-carrying capabilities. Bleeder resistors are also included on each board for safety. An example of one of these capacitor boards is shown in Fig. 5.2. Each capacitor board is soldered directly into top and bottom base board PCBs, enabling further parallel connections while maintaining a low-inductance footprint.

Fig. 5.2: TDK film capacitor PCB board

The proposed capacitor bank is designed to completely replace the current DWPT Celem capacitor bank. To achieve this, the C_{ps1}, C_{ps2}, and C_{pp} capacitor values were each individually constructed. Each capacitor in the LCCL tuning network must handle the full 100 kW of power and have a distinct capacitance value. By utilizing multiple small, low-tolerance TDK capacitors, we can construct each series and parallel capacitor independently with high precision and then combine these capacitance values to form the complete DWPT capacitor bank.

The 3D model of an LCCL capacitor rated for 100 kW is shown in Fig. 5.3. This full-size capacitor consists of 24 parallel-connected capacitor boards, each containing 16 capacitors in parallel with 2 in series. This configuration results is 32 capacitors per capacitor board and 768 capacitors total. This full-size capacitor is designed so that each individual TDK capacitor is handling up to 50% of its maximum rated RMS voltage and 80% of its maximum rated current at full power.

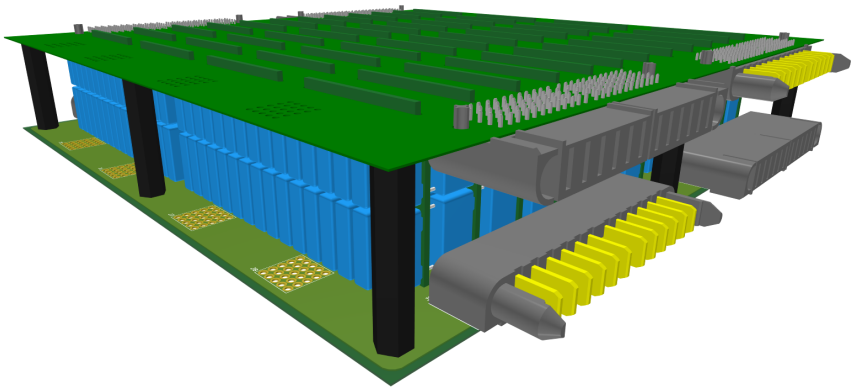

Fig. 5.3: Full-size 100kW rated TDK capacitor

The complete DWPT capacitor bank combines two full-size series capacitors and one full-size parallel capacitor, as shown in Fig. 5.4. For size comparison, the original Celem capacitor bank is also included in the image. This proposed TDK capacitor bank comprises a total of 2,304 small TDK capacitors to form the entire DWPT capacitor bank.

Even with hundreds of capacitors connected in parallel, the overall TDK capacitor bank is expected to be more cost-effective than the Celem capacitor bank. The availability of various capacitance values in the same package also offers flexibility in tuning design while maintaining the same footprint and using the same PCBs. A comparison of costs and power density between these boards is shown in Table. 5.1.

Type of Capacitor	TDK Capacitor	Celem Capacitor
Amount Required	2304	18
Cost for Capacitors	\$298.13	\$2908
Cost for PCB's and Connectors	\$726.3	\$154.1
Total Cost	\$1024.422	\$3062.1
Power Density (cm^3)	8219.6	2453.5

Table 5.1: Comparison between the cost and size of the TDK and Celem capacitor boards

This table shows that the proposed capacitor bank is nearly four times larger than the previous capacitor bank, but it is also three times cheaper. The table does not account for the necessary potting/packaging material. Since the proposed capacitor bank is larger, the packaging will likely be more expensive, but it is still expected to cost at least half as

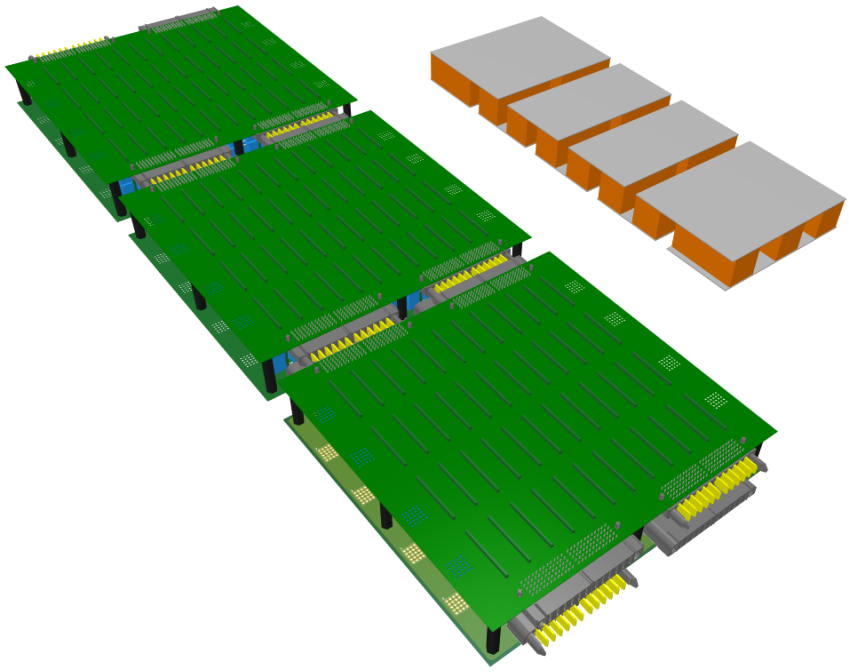

Fig. 5.4: Proposed capacitor bank compared with original capacitor bank

much as the Celem capacitor bank. The use of many capacitors raises reliability concerns. However, it will be demonstrated later that although an increase in the number of components increases the potential for failure, the decrease in temperature compensates for this, maintaining a similar reliability.

To evaluate the effectiveness of the proposed design, a prototype version of the board was created. This prototype, shown in Fig. 5.5, is one-quarter the size of the C_{pp} capacitor in the LCCL circuit. By using 3.3 nF and 2.7 nF capacitors in parallel and series, this prototype achieves a capacitance of 156 nF, which is approximately one-quarter of the original C_{pp} capacitance.

5.2.1 Prototype Capacitor Bank Experiments and Simulations

The TDK prototype capacitor bank was tested in both air and sand to compare its temperature rise characteristics with the Celem capacitors. The experimental setups were then modeled in Ansys Icepak and extrapolated to provide insight into its potential effectiveness in a roadway-embedded environment.

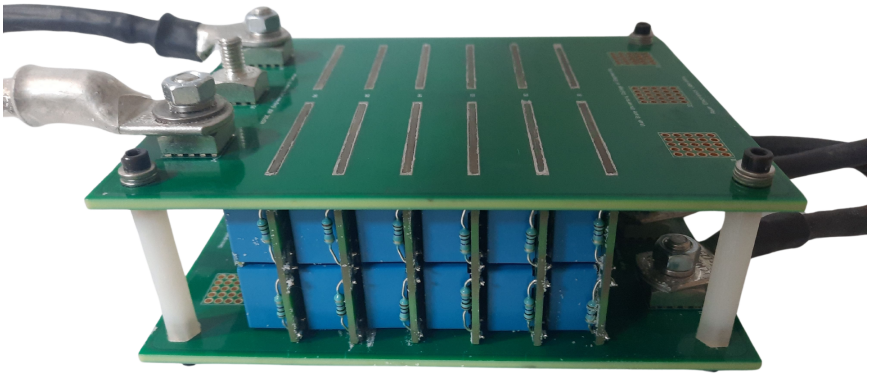

Fig. 5.5: TDK film capacitor prototype board

To effectively test the prototype, the same proportional power levels expected in the full 100 kW design were used. Since the prototype is one-fourth the size of the C_{pp} capacitor in the LCCL circuit, it was designed to handle one-fourth of the rated power. A high current AC waveform was achieved using a resonant circuit test setup with the inductor tuned to 85 kHz. An inverter generated the 85 kHz square wave, which was then connected to the series-tuned resonant circuit, as shown in Fig. 5.6. The component values for this circuit are listed in Table. 5.2.

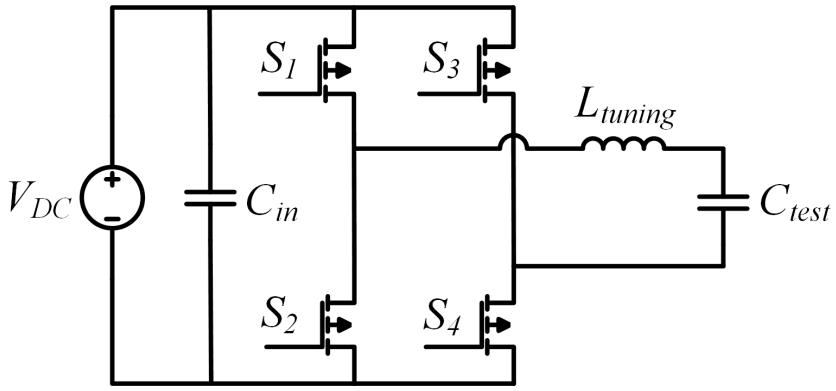

Fig. 5.6: TDK film capacitor prototype board test circuit

The prototype was tested at three different operating conditions to compare its transient temperature rise characteristics at various power levels. The power levels were adjusted by varying the DC input voltage, which altered the current through and voltage across the

Table 5.2: Hardware component values for TDK prototype board test setup

Component	Hardware Value
V_{DC}	55 - 80 V
f_s	85 kHz
C_{in}	208 uF
L_{tuning}	24.3 uH
C_{test}	157.5 nF

capacitor bank. These operating conditions were represented in terms of scaled equivalent power. For example, during 100 kW operation, the full-size C_{pp} capacitor experiences approximately 268 A RMS and 800 V RMS. For the scaled-down prototype capacitor bank, the 100 kW-equivalent power corresponds to 67 A RMS and 800 V RMS. Table. 5.3 shows the different test conditions for this prototype capacitor bank.

Power Level	C_{test} Voltage	C_{test} Current	Reactive Power	Power Losses (Estimated)
100 kW Power	800 V RMS	67 A RMS	53.6 kVAR	26.8 W
70 kW Power	700 V RMS	56 A RMS	39.2 kVAR	19.6 W
45 kW Power	542 V RMS	45 A RMS	24.4 kVAR	12.2 W

Table 5.3: Three operating points for prototype capacitor bank testing

During the experiments, thermocouples were used to measure the temperature at three different locations on the prototype capacitor bank. One thermocouple was placed in the middle of the prototype on top of a capacitor. Another thermocouple was positioned at the corner of the prototype on top of a capacitor. The final thermocouple was attached to the PCB.

Prototype Capacitor Bank Air Experiments

The capacitor prototype air test setup is shown in Fig. 5.7. Due to the compact arrangement of the capacitors within the prototype board, there is minimal space for air to circulate between the paralleled capacitor boards. Therefore, while natural convection may contribute to cooling the PCBs and edges of the boards, most of the heat transfer within the capacitor bank likely occurs through conduction. An Ansys Icepak model was

developed to simulate these conditions, and the results were compared with experimental data. Simplifications were made to the Ansys model including modeling the PCBs as basic rectangles of FR4 material, omitting the capacitor leads, and representing the capacitors as solid rectangular blocks of polypropylene. The analytical losses were inputted as block excitations and calculated based on 0.05% of the reactive power. The ambient temperature was set to the experimentally measured ambient temperature of $21°C$, and the boundary conditions were setup similar to previous air models. A screenshot of the Ansys Icepak model within air is shown in Fig. 5.8

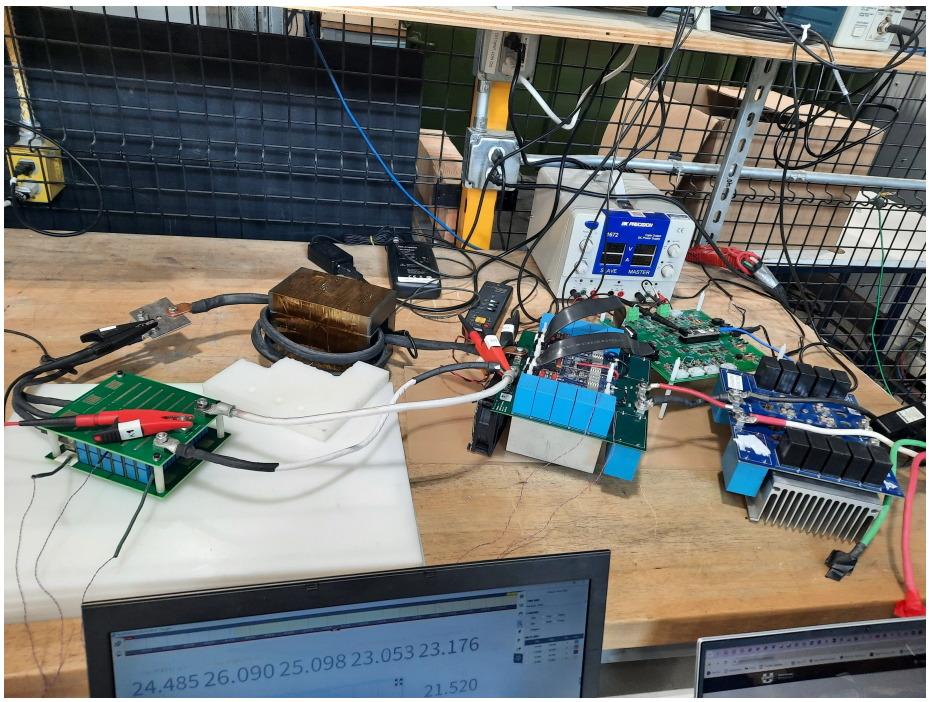

Fig. 5.7: TDK film capacitor prototype board air test setup

The prototype was first tested at the 100 kW-equivalent operating point corresponding to 67 A through the capacitor bank. The system was turned on at full power losses for 47 minutes, after which it was turned off and the natural cooling of the device was measured for 53 minutes. The thermocouple measurements of the capacitor bank during this period along with the corresponding Ansys results are shown in Fig. 5.9. The steady-state temperature of the middle capacitor thermocouple appears to approach approximately $75°C$ which is

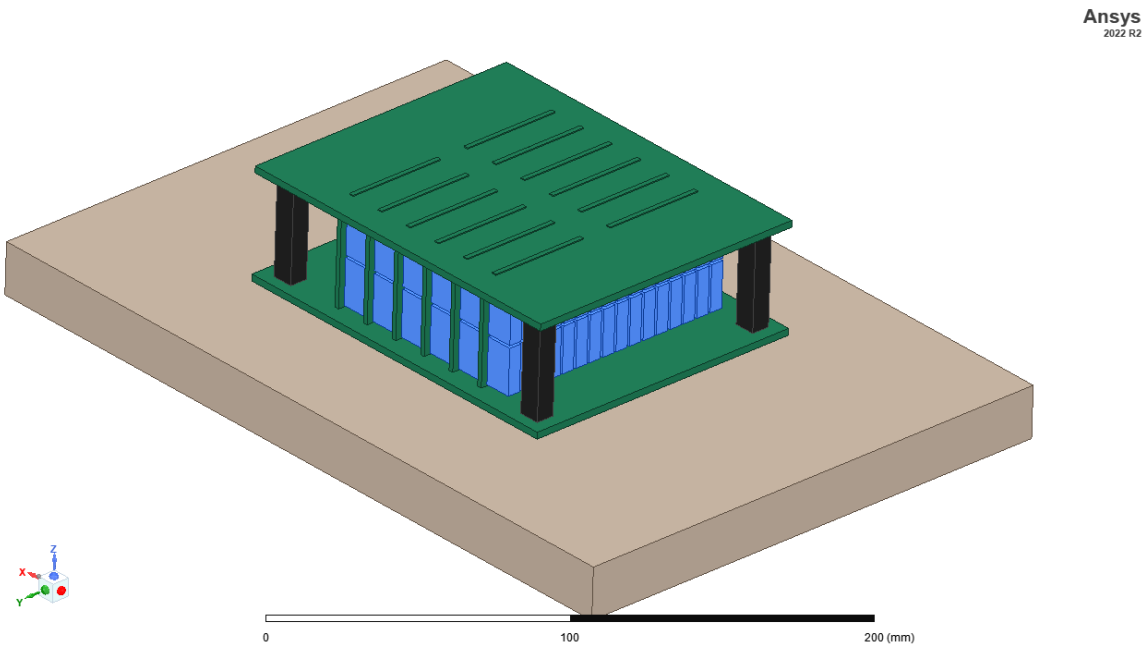

Fig. 5.8: Ansys Icepak model for prototype capacitor board in air

$30°C$ lower than the Celem capacitor bank at the same power level.

These results indicate a significant temperature gradient between the capacitors positioned on the outer edge and those in the middle of the the capacitor bank. The Ansys results correspond well for the PCB and edge capacitors, but the model predicts higher temperatures for the middle capacitors compared to the observed experimental results. This discrepancy between experimental results and simulation results is likely due to the simplifications in the Ansys model. The greater inaccuracy in the center of the capacitor bank is likely because more heat transfer is occurring through conduction in this location and the model simplifications have a greater impact upon conduction heat transfer through the capacitor bank than convective heat transfer around the outside of the capacitor bank.

The capacitor bank was next tested at the 56 A and 45 A operating points, equivalent to 70 kW and 45 kW scaled power levels, respectively. The system was turned on for approximately 1.75 hours at 56 A and 2 hours at 45 A. Both tests were then turned off and the cool down was measured. The temperature measurements from the thermocouples for the 45 A experiment along with Ansys simulation results are shown in Fig. 5.10.

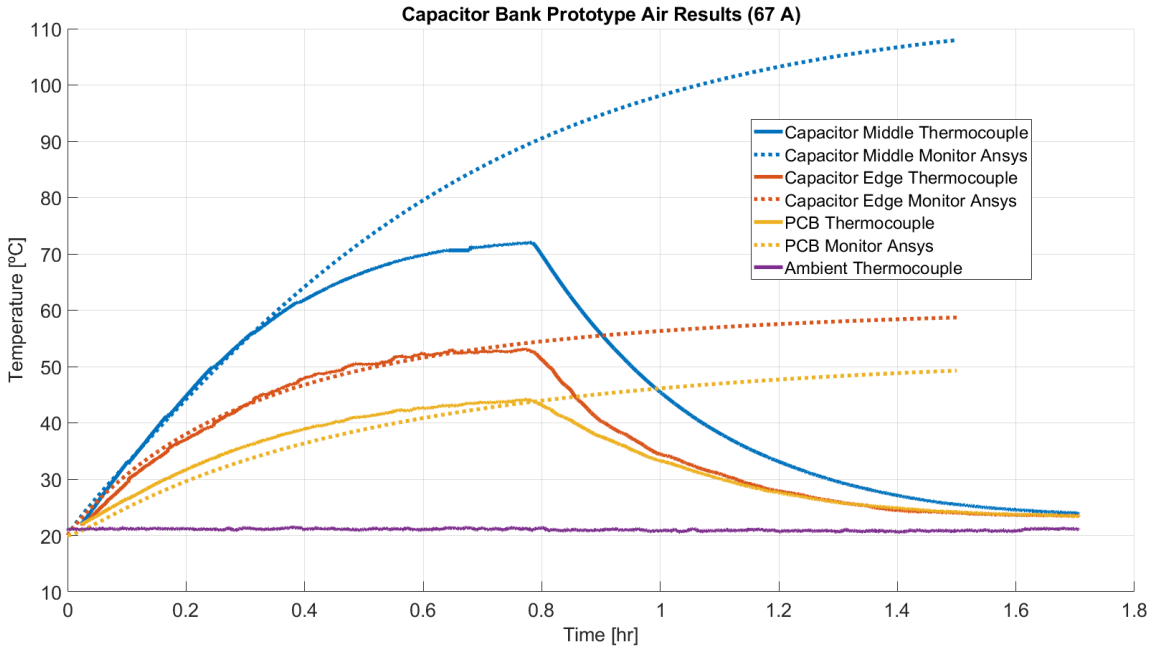

Fig. 5.9: TDK film capacitor prototype board air test at 100 kW equivalent power (67 A)

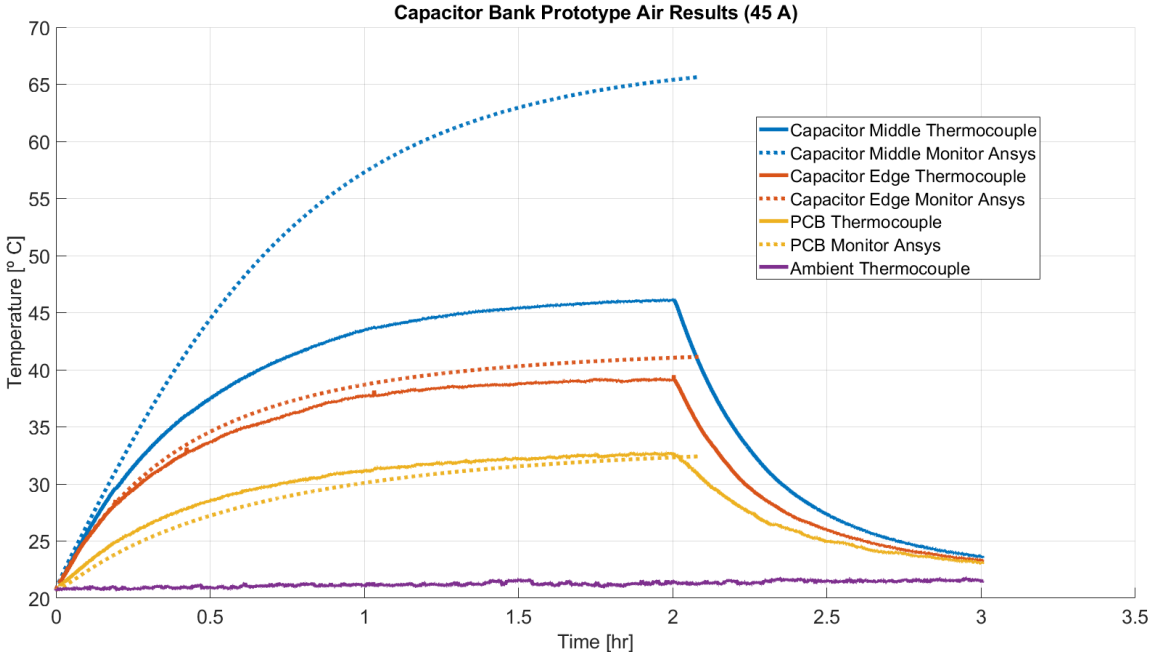

Fig. 5.10: TDK film capacitor prototype board air test at 45 kW equivalent power (45 A)

A graph comparing the temperature rise at the thermocouple located in the middle of the capacitor bank for all three tests is shown in Fig. 5.11. Based on these results, the thermal resistance to ambient for the middle of the capacitor bank is estimated to be on average approximately $R_{th} \approx 2.01 \frac{^\circ C}{W}$. Since the steady-state temperature scales linearly with an increase in power, this value can be used to predict the temperature of the capacitor bank at higher power levels. For instance, at 200 kW, the power loss through the capacitor bank is expected to be around 53.6 W. At this higher power level, the expected temperature rise in the middle of the capacitor bank would be approximately $53.6\,W \times 2.01 \frac{^\circ C}{W} + 21^\circ C = 128.74^\circ C$, which is only a few degrees higher than the maximum rated operating temperature of these devices.

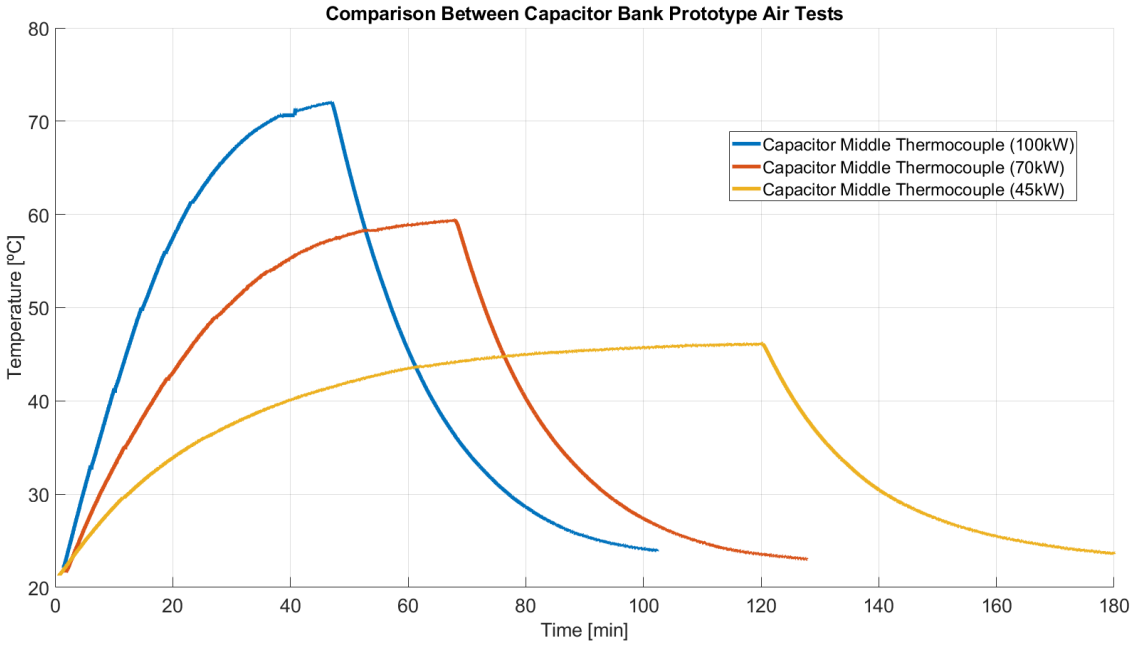

Fig. 5.11: TDK film capacitor prototype board air tests comparison

Prototype Capacitor Bank Sand Experiments

The capacitor prototype sand test setup is shown in Fig. 5.12. The capacitor bank was buried 55 mm below the surface of the sand. The cooling of this device primarily

occurs through conduction from the capacitor bank to the surrounding sand. The capacitor bank was modeled in Ansys Icepak using the same dimensions as the air model and the same sandbox size and boundary conditions as in previous sand models, with the ambient temperature set to $19°C$. The Ansys model is shown in Fig. 5.13.

When the capacitor bank was inserted into the sand, efforts were made to fill all the cracks and crevices between the capacitor boards and the capacitors. However, it is unlikely that all air gaps were eliminated. These remaining air gaps between capacitors within the prototype board lead to greater error between simulation and experimental results.

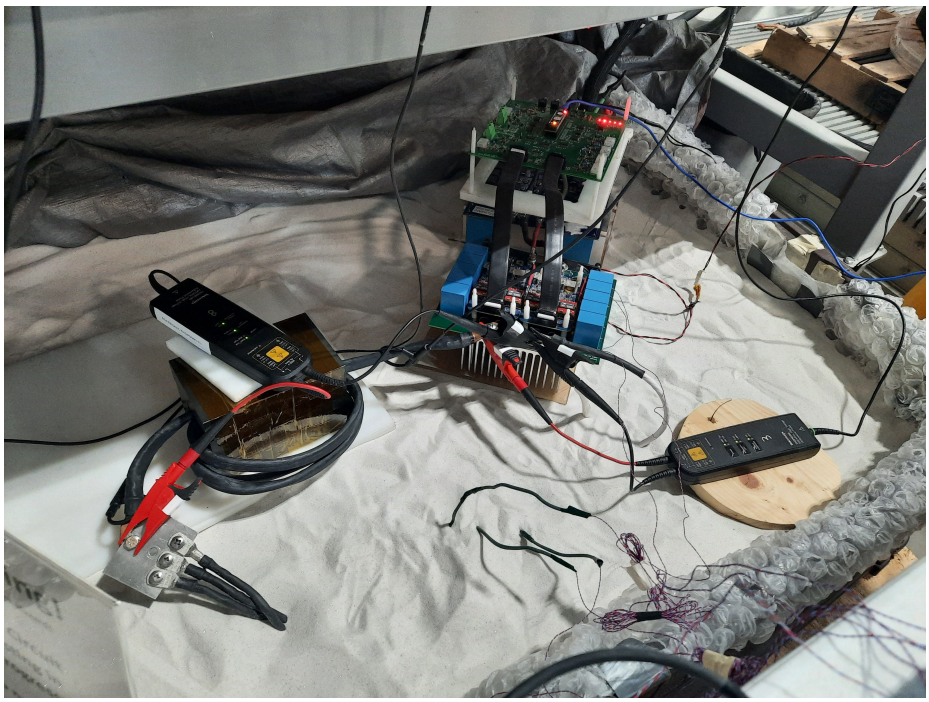

Fig. 5.12: TDK film capacitor prototype board sand test setup

The prototype was first tested at the 100 kW-equivalent operating point corresponding with 67 A of current through the capacitor bank. The system was turned on at full power losses for approximately 8 hours. The thermocouple measurements of the capacitor bank during this period along with the corresponding Ansys results are shown in Fig. 5.14.

The temperature gradient between the capacitor on the outer edge of the capacitor bank and the capacitor in the middle seems to have reduced after embedding the prototype

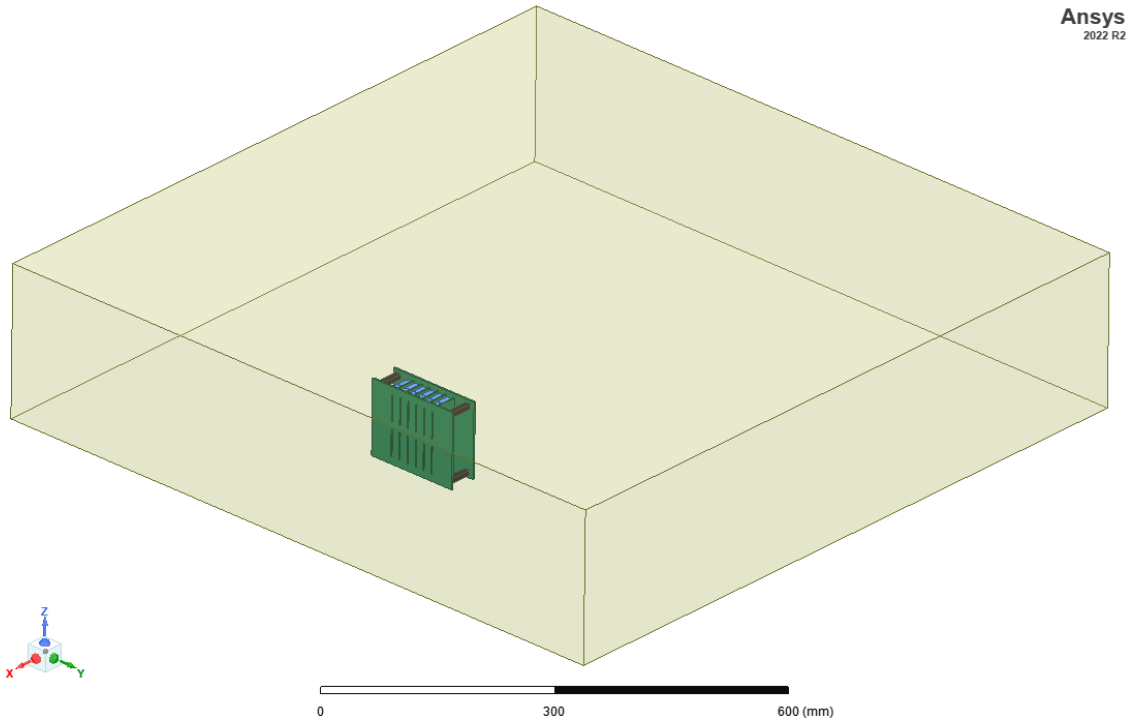

Fig. 5.13: TDK film capacitor prototype board sand Ansys model

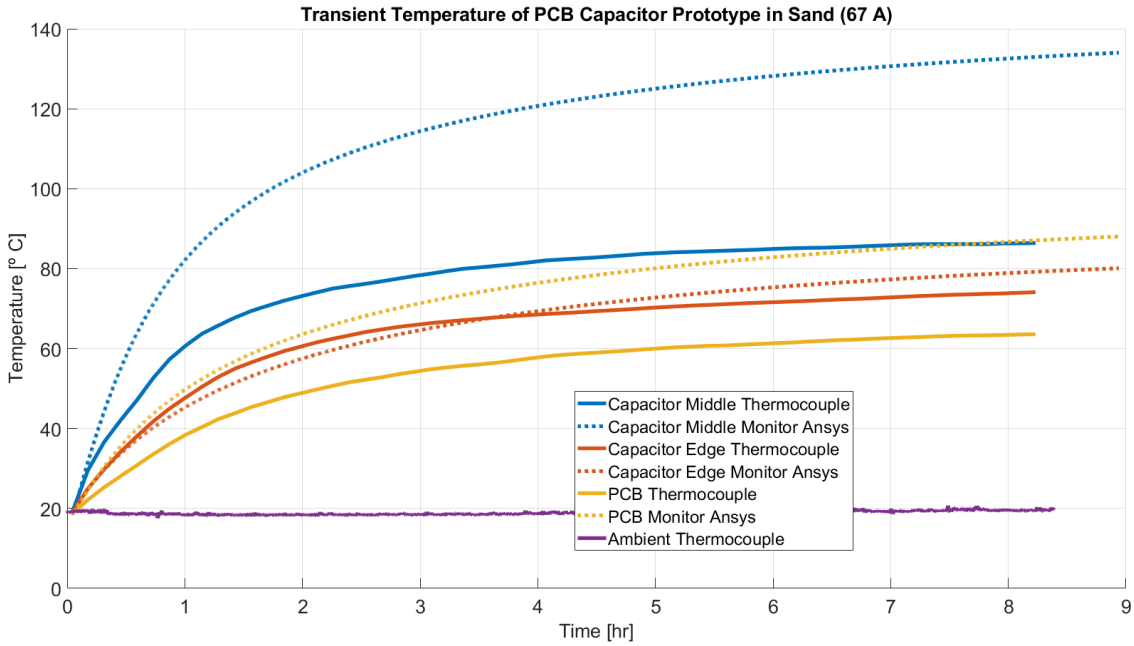

Fig. 5.14: TDK film capacitor prototype board sand test at 100 kW equivalent power (67 A)

in sand. The middle capacitor reaches only $10°C$ higher than the temperature observed in the air experiment.

The Ansys simulation results do a worse job predicting the temperature rise of the capacitor bank in the sand-embedded scenario. The Ansys simulation again predicts higher temperatures for the middle capacitors compared to the observed experimental results. Furthermore, the discrepancy between the edge capacitor and PCB temperatures has increased. Since the thermal properties of the sand were chosen based on analytical calculations rather than experimental measurements, it is likely that differences in the thermal properties of the sand are contributing to the increased error between the edge capacitor and PCB temperatures. Inaccurate modeling of the boundary conditions at the edge of the sandbox could also be contributing to these discrepancies.

The capacitor bank was next tested at the 56 A and 45 A operating points corresponding to 70 kW and 45 kW equivalent power operation. These tests were turned on at full power losses for 9 hours and 7.25 hours respectively. When comparing the middle capacitor thermocouple across the three different tests, the temperature appears to be approximately $10°C$ higher than the air experiment at each power level. A comparison between the middle capacitor thermocouple for the three different tests is shown in Fig. 5.15. Based on these results, the thermal resistance to ambient for the middle of the capacitor bank in sand is calculated to be approximately $R_{th} \approx 2.54 \frac{°C}{W}$. Since the steady-state temperature scales linearly with the increase in power, if we were to again produce 53.6 W of loss thorough the capacitor bank, we can estimate the steady-state temperature at this 200 kW operating point to be approximately $53.6\,W \times 2.54 \frac{°C}{W} + 19°C = 155.14°C$. These results show how the calculated thermal resistances can be used to optimize the design of roadway-embedded power electronics given various ambient temperatures, power losses, and utilization scenarios.

5.2.2 Full-Size Capacitor Bank Simulation Results

Despite the differences between simulation and experimental results for the air and sand-embedded experiment, the 100 kW-equivalent losses can still be used in ANSYS Icepak

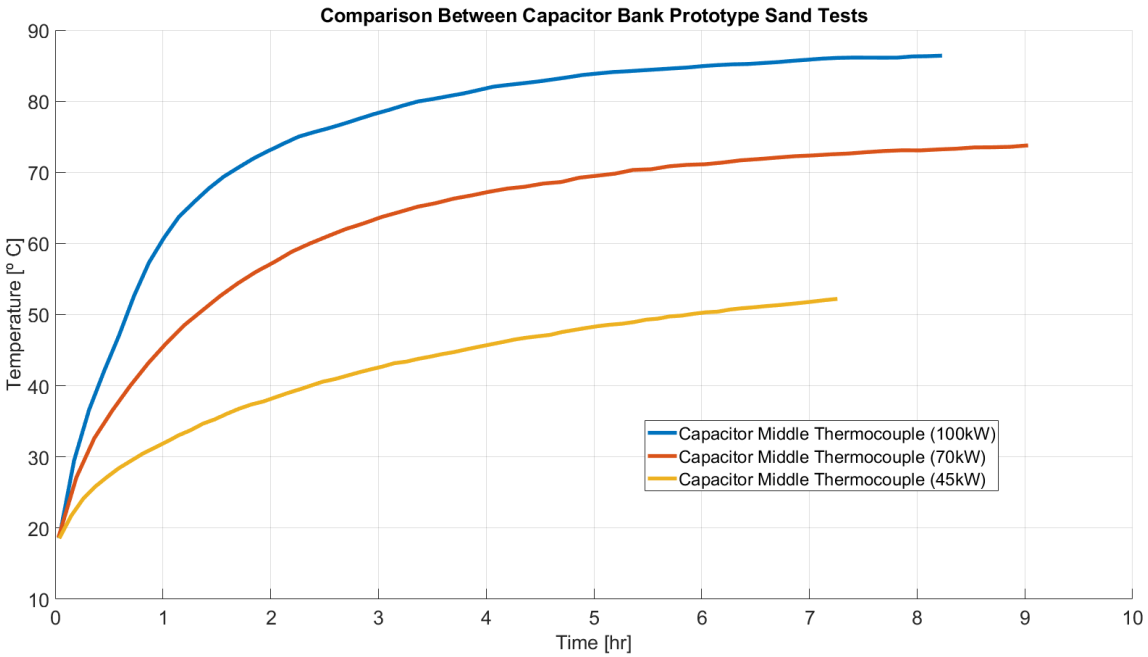

Fig. 5.15: TDK film capacitor prototype board sand tests comparison

to predict the temperature of the full-size capacitor. The full-size capacitor was modeled in Ansys Icepak for both air and sand scenarios. The Ansys model for the air simulation is shown in Fig. 5.16. The sand simulation utilized the same capacitor dimensions, sandbox size, boundary conditions, and ambient temperatures as in the previous prototype capacitor bank sand models. The simulation results were conducted with a steady-state solution type instead of a transient solution type.

The results for the air and sand Ansys models were adjusted based on experimental results to remove the steady-state error. Those modified steady-state temperatures for the full-size capacitor bank compared to the prototype capacitor bank are shown in Table. 5.4.

Capacitor Bank Version	Steady-State Temperature (Air)	Steady-State Temperature (Sand)
TDK Prototype Capacitor Bank	$75°C$	$85°C$
TDK Full-size Capacitor Bank	$80°C$	$95°C$

Table 5.4: Comparison between the steady-state temperatures of prototype capacitor bank and the full-size capacitor bank temperatures in air and sand at 100 kW

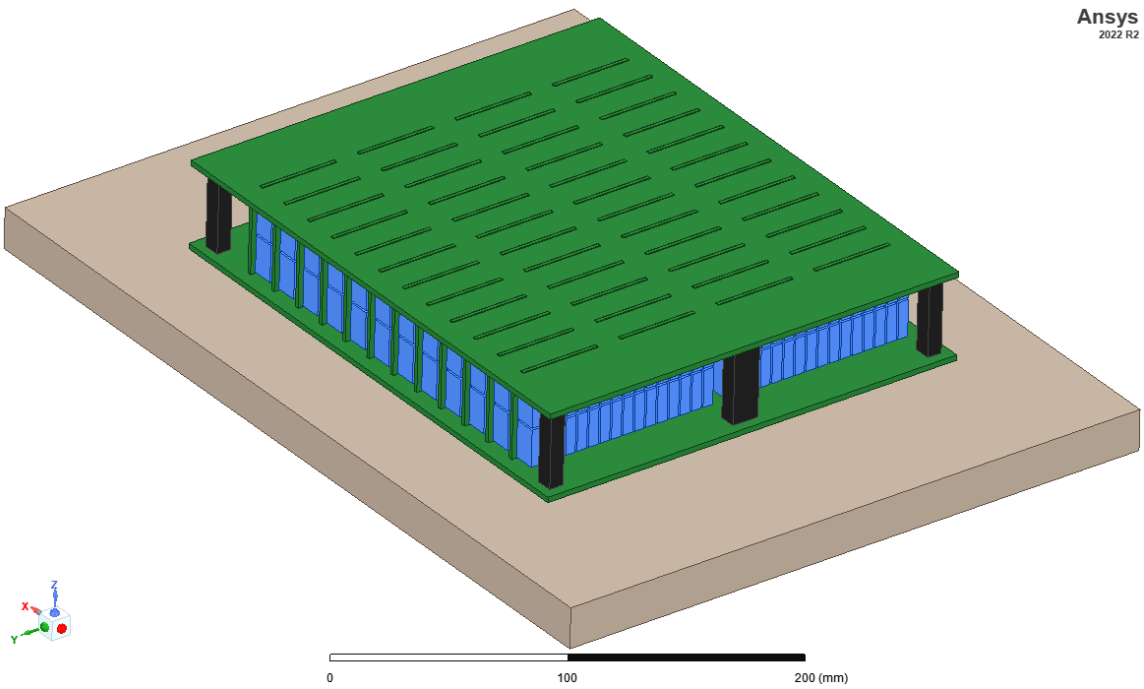

Fig. 5.16: Proposed full-size capacitor bank prototype Ansys model in air

These results predict that when scaled to the full-size, the capacitor bank has a worst-case temperature increase of approximately $5°C$ higher in the air scenario and $10°C$ in the sand scenario. This maximum temperature of $95°C$ is below the $125°C$ maximum rated temperature of the TDK capacitor, even at 100% utilization. Although the temperature is expected to increase at higher ambient temperatures, the capacitor bank has sufficient margin to accommodate these increases.

If both the proposed TDK capacitor bank and the Celem capacitor bank were operated in the same environment at the same utilization, the higher operating temperature of the Celem capacitor bank would result in a greater risk of capacitor failure. Conversely, the increased number of components in the TDK capacitor bank also elevates the risk of failure.

A failure analysis was conducted for the TDK capacitor bank, using the MTTF listed in the datasheet. This analysis used the predicted temperatures and estimated voltages at steady-state operation in air and sand. This failure analysis considers a lifetime for when a single capacitor is predicted to fail and where 1% of the capacitors within the bank have failed. This failure analysis is summarized in Table. 5.5.

Capacitor Bank Scenarios	Average operating temperature	Estimated lifetime given a single capacitor failure	Estimated lifetime given 1% capacitor failures
TDK Full-size Capacitor Bank (Air)	$80°C$	6.3 years	98.9 years
TDK Full-size Capacitor Bank (Sand)	$95°C$	2.3 years	36.3 years

Table 5.5: Estimated failure rate of the full-size TDK capacitor bank in air vs sand

The TDK polypropylene film capacitors are most likely to fail open, meaning a single capacitor failure would not lead to a complete system failure, but would simply reduce the overall capacitance of capacitor bank. Therefore, despite the increased potential for individual capacitor failures due to the use of thousands of capacitors, the overall lifetime of the TDK capacitor bank, assuming 1% component failures, is beyond the necessary lifetime requirements. 1% capacitor failures is 23 capacitors within the full-size capacitor bank. Assuming all of these capacitor fail open, the reduction in capacitors means that all other capacitors will be sharing a slightly higher current. The capacitor bank was designed based on 80% current derating from suggested maximum, so there is margin for capacitors to handle a slight increase in current over the lifetime of the system.

Additionally, this failure analysis assumes that the steady-state operating temperature at 100% utilization is the average operating temperature for these components, which is the worst-case scenario. The average operating temperature will decrease with lower utilization and with the addition of thermally conductive packaging material.

5.2.3 Roadway-Embedded Electronics Design Example

Given the simulation and experimental results of the proposed capacitor bank as well as the inverter experiments in the previous chapter, we now explore a design example to illustrate how these results can be used to integrate power electronics into a fully-embedded DWPT system.

The specific use case for this roadway-embedded power electronics design example includes location, utilization, roadway stack-up, burial depth, and lifetime requirements.

The location is a roadway at the Utah Inland port near Salt Lake City, Utah. The DWPT system will service class 8 truck fleet vehicles running routes between the rail yard and surrounding warehouses. The system's utilization is expected to be low but consistent throughout the day and year. The selected roadway in this area has a roadway stack-up of 150 mm of asphalt followed by sub-base material. Given the size of the transmitter coil and the construction of the roadway, the embedded electronics will need to placed within the sub-base layer, between 150 - 250 mm deep. The average maximum ambient temperature at this depth during the summer months is estimated to be around $44°C$. The DWPT system needs a minimum lifetime of 20 years to align with roadway maintenance schedules, but a lifetime of 25-30 years is preferred. Each power electronic component will first be encapsulated in its own individual epoxy potting material and then embedded in the sub-base of the roadway.

The entire roadway-embedded DWPT system is designed to cover approximately a quarter mile of roadway. Each individual ground assembly is structured according to the block diagram shown in Fig. 5.17

An Ansys Icepak model was developed for the proposed complete capacitor bank and resistor heat sink device, with roadway layers, burial depth, and ambient temperatures updated based on the specific parameters outline in this example. The simulations were run at steady-state operation to observe the worst-case operation, but it is expected that at the utilization of 2 seconds on and 5 seconds off over a 24-hour period, the temperature would reach a steady-state value of at least half the predicted 100% utilization steady-state temperature. While actual temperatures may vary throughout the day, an average ambient temperature of $44°C$ is assumed for simplicity throughout the simulation. The Ansys model for the roadway-embedded capacitor bank is shown in Fig. 5.18. The Ansys model for the roadway-embedded resistor heat sink model is shown in Fig. 5.19. These models assume that the roadway boundaries are at a constant ambient temperature, although in reality, the edges of the roadway may influence the temperature rise results to a minimal extent.

The steady-state operating temperature of the capacitor bank at 100% utilization

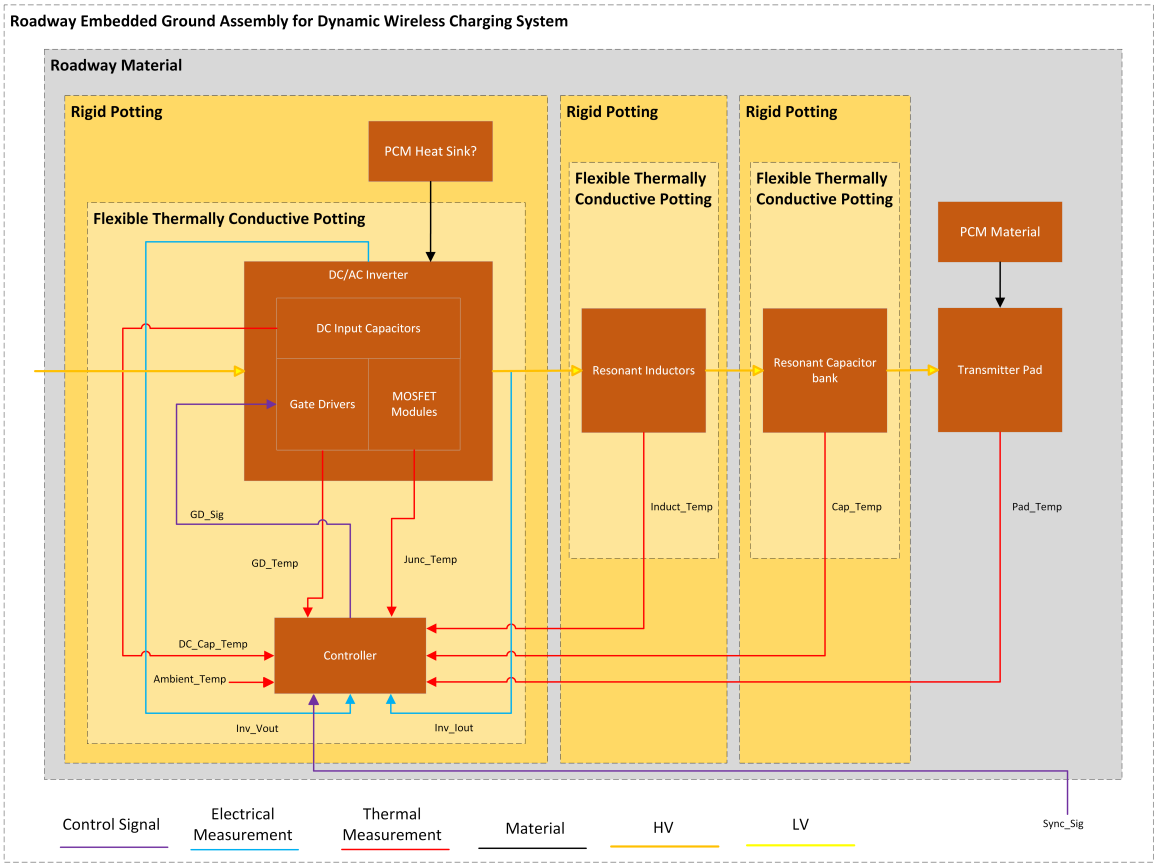

Fig. 5.17: Roadway-embedded power electronics block diagram

reaches 142°C and the steady-state operating temperature of the resistor heat sink device at 100% utilization reaches 146°C.

At the specified lower utilization, the temperatures of these components are expected to reach at least half the steady-state temperature. This means the capacitor bank would reach a steady-state temperature of approximately 70°C and the resistor heat sink device would reach a steady-state temperature of approximately 75°C. These results indicate that the proposed TDK capacitor bank and inverter MOSFET modules can be utilized within a roadway-embedded DWPT system and obtain the given lifetime requirements under the specified utilization scenario. This example also shows how the tools discussed in this thesis can be utilized to accelerate the design of roadway-embedded power electronic systems.

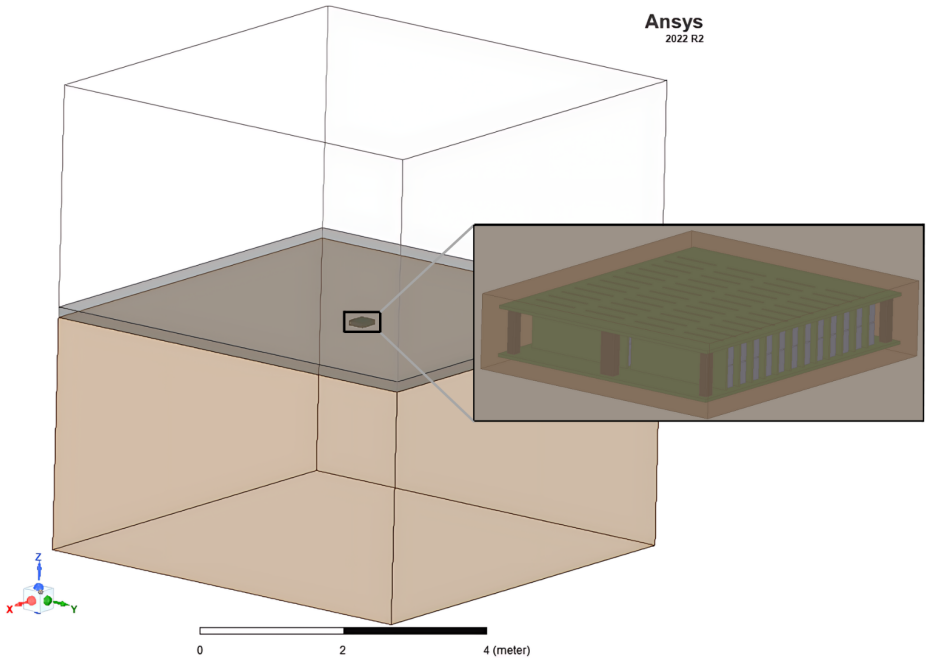

Fig. 5.18: Proposed full-size capacitor bank prototype Ansys model in Utah inland port roadway

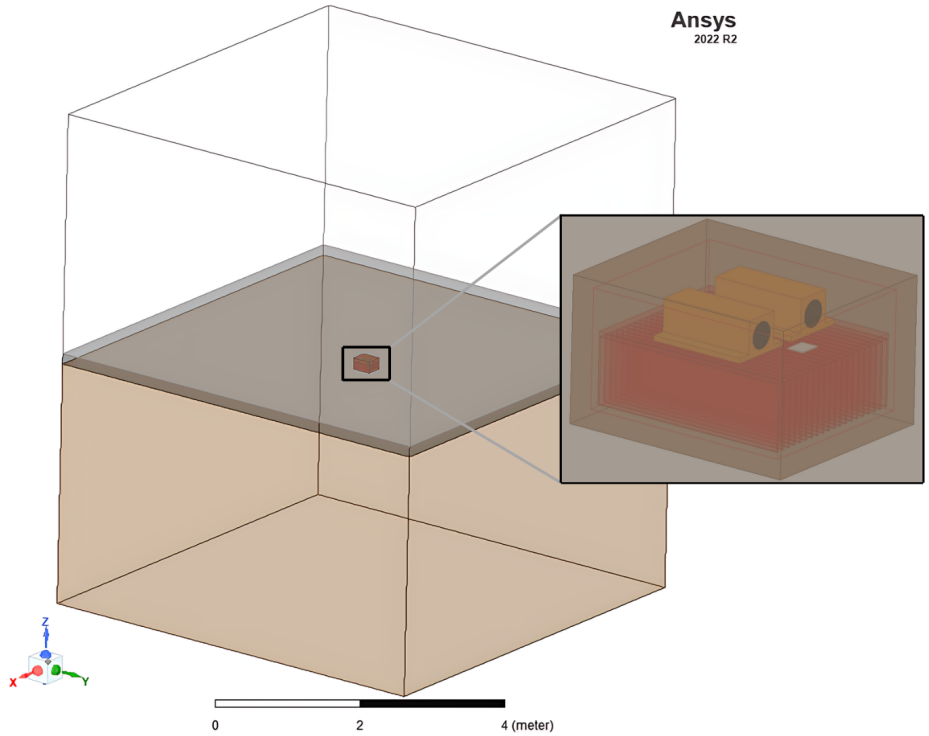

Fig. 5.19: Resistor heat sink device Ansys model in Utah inland port roadway

CHAPTER 6

Conclusion and Future Work

6.1 Conclusion

The research conducted for this thesis provides guidelines and design practices for integrating power electronics in a roadway-embedded environment. The thesis explores the balance between minimizing costs, achieving high power density, and maintaining reliability when designing roadway-embedded electronics. Practical considerations gained during this research, along with specific thermal management recommendations and techniques, have been detailed and documented.

A new capacitor bank is proposed using the techniques mentioned in this thesis. This capacitor bank is validated at a prototype level and suggestions for integrating this new capacitor bank into a full DWPT system are mentioned.

The temperature considerations discussed in this thesis for roadway-embedded DWPT systems provide innovative new ways of designing the thermal management of electronics, improving the field of knowledge in this area. Embedding power electronics in roadways will not only enhance the installation process of DWPT systems but also lower cost and improves efficiency, thereby promoting wider adoption across various roadway applications.

6.2 Future Work

6.2.1 Roadway-embedded electronics packaging

Future research should be conducted on roadway-embedded power electronics packaging, specifically determining optimal thermally conductive potting materials and researching the trade-offs of using PCM material. Research can be done to reduce the thermal resistance of electronics to packaging as well as from packaging to the roadway. Research can

also be done to optimize the thermal capacitance of packaging material based on varying utilization scenarios.

The choice of potting material can be influenced by properties such as thermal conductivity, viscosity, thermal expansion coefficient, water penetration through epoxy, and epoxy hardness. The use of PCM heat sinks can be determined by investigating heat sink size, fin size, fin distance, PCM material, and ratio between PCM and heat sink material.

Furthermore, the inverter, capacitor bank, and tuning inductors can be encapsulated in their own individual packaging or these components could be integrated into more complex combined packaging to both protect these devices from the environment and provide increased ease in manufacturing.

6.2.2 Temperature implications of closely-embedded electronics

When multiple power electronic components are embedded in close proximity, the heat from each component will affect the surrounding components, likely resulting in a temperature increase for all embedded electronics.

Further research should be conducted analyzing the temperature profile throughout the roadway from closely-embedded electronics and how the design of the entire DWPT system can be electrically and thermally optimized.

6.2.3 Reliability of connections between roadway-embedded electronics

Future research should also include analyzing the reliability of the connections between electronics within the roadway. Connections between power electronics can be made prior to encapsulation, with the connections being encapsulated along with the electronics. Alternatively, connections can be made during the installation of the electronics in the roadway.

6.2.4 Ansys Icepak model improvement

Certain Icepak simulation models mentioned in this thesis were simplified to allow for ease of meshing and to reduce simulation time. Some of these simplifications led to a reduction in accuracy between simulation and experimental results. Furthermore, certain

thermal properties and thermal boundary conditions were estimated instead of being experimentally measured. In the future, thermal properties of the test sand can be measured in order to create a more accurate model. More complex models could also be created that more accurately model both the conductive and convective properties of these electronics within a roadway-embedded environment.

6.2.5 On-line temperature monitoring

Improved thermal monitoring techniques can be researched to determine methods that function well in a roadway-embedded environment. Thermal monitoring needs to be accurate and reliable without dramatically increasing the number of measurement tools or circuits in the system. Research in this area could help reduce the cost of the system while providing more on-line monitoring of the system for lifetime estimates and safety limits.

Thermocouples/thermistors and the inverter MOSFET NTCs can be can be fed as an input to the inverter controller to monitor temperatures. If the temperature reaches levels which are deemed unsafe, then the controller could either lower the duty cycle thus lowering the power level in the system, or the system could be shut off completely to ensure that thermal failure does not occur. Optimization of these control algorithms can be researched to determine the best limits and controls for prolonging system lifetime.

6.2.6 Component lifetime monitoring

Lifetime monitoring of these embedded systems as well as effective repair and replacement of embedded systems are also topics that require additional research. If DWPT systems have on-line lifetime monitoring, this can inform a timeline for the appropriate replacement or repair of these systems. Potential scenarios can be investigated to reduce the costs and time associated with the replacement and repair of these systems. For instance, electronics could potentially be embedded in something other than epoxy which is easier to remove. Additionally, different roadway construction or repair techniques can be investigated to improve the ease of access to roadway-embedded electronics.

Future work can also be conducted analyzing failures caused by vibrations from earthquakes and water damage from flooding. These situations can be analyzed and their affect on the functionality and lifetime of power electronic components can be determined. Different types of packaging and or installation techniques can be investigated to solve these practical challenges.

6.2.7 Encapsulated and roadway-embedded experiments

Each individual electronic component will eventually require validation in electronic packaging within the actual roadway. Power electronics can be encapsulated in their own separate blocks of varying materials to compare the thermal resistance of different packaging methods. Similarly, encapsulated components can be embedded in varying blocks of roadway material to measure how their thermal characteristics differ compared to sand experiments.

The results of encapsulated and roadway-embedded experiments can be compared with analytical estimations and Ansys simulations. These systems can be tested for various utilization scenarios and varying loading conditions to extrapolate the results to all possible use cases.

The roadway-embedded power electronics can be tested within a full DWPT system including the embedded transmitter pad. Various ambient temperatures and environmental conditions can be tested to analyze their affect on the temperature rise of the electronics. Additionally, the electronics can be monitored to ensure that the wet concrete or hot asphalt does not damage the electronics during installation.

REFERENCES

[1] EPA, "Inventory of U.S. Greenhouse Gas Emissions and Sinks: 1990-2022," U.S. Environmental Protection Agency, EPA, Tech. Rep., 2024. [Online]. Available: https://www.epa.gov/ghgemissions/draft-inventory-us-greenhouse-gas-emissions-and-sinks-1990-2022

[2] EIA, "Electric Power Monthly," U.S. Energy Information Administration, EIA, Tech. Rep., 2023. [Online]. Available: https://www.eia.gov/energyexplained/electricity/electricity-in-the-us.php

[3] IEA, "Comparative life-cycle greenhouse gas emissions of a mid-size BEV and ICE vehicle," International Energy Agency, IEA, Tech. Rep., 2021. [Online]. Available: https://www.iea.org/data-and-statistics/charts/comparative-life-cycle-greenhouse-gas-emissions-of-a-mid-size-bev-and-ice-vehicle

[4] A. Burnham, L. Gohlke, David amd Rush, T. Stephens, Y. Zhou, M. A. Delucchi, A. Birky, C. Hunter, Z. Lin, S. Ou, F. Xie, C. Proctor, S. Wiryadinata, N. Liu, and M. Boloor, "Comprehensive total cost of ownership quantification for vehicles with different size classes and powertrains. united states," U.S. Department of Energy, Office of Scientific and Technical Information, Tech. Rep., 2021. [Online]. Available: https://www.osti.gov/biblio/1780970/

[5] IEA, "Top 5 barriers to EV adoption reported by EV100 member companies," International Energy Agency, IEA, Tech. Rep., 2021. [Online]. Available: https://www.iea.org/data-and-statistics/charts/top-5-barriers-to-ev-adoption-reported-by-ev100-member-companies

[6] SAE, "New sae wireless charging standard is ev game-changer," *Automotive Engineering*, 2020. [Online]. Available: https://www.sae.org/news/2020/10/new-sae-wireless-charging-standard-is-ev-game-changer

[7] D. H. Nguyen, "Electric vehicle – wireless charging-discharging lane decentralized peer-to-peer energy trading," *IEEE Access*, vol. 8, pp. 179 616–179 625, 2020.

[8] X. Lu, P. Wang, D. Niyato, D. I. Kim, and Z. Han, "Wireless charging technologies: Fundamentals, standards, and network applications," *IEEE Communications Surveys & Tutorials*, vol. 18, no. 2, pp. 1413–1452, 2016.

[9] Z. Popovic, "Near- and far-field wireless power transfer," in *2017 13th International Conference on Advanced Technologies, Systems and Services in Telecommunications (TELSIKS)*, 2017, pp. 3–6.

[10] A. A. S. Mohamed, A. A. Shaier, H. Metwally, and S. I. Selem, "Wireless charging technologies for electric vehicles: Inductive, capacitive, and magnetic gear," *IET Power Electronics*, vol. n/a, no. n/a, 2023. [Online]. Available: https://ietresearch.onlinelibrary.wiley.com/doi/abs/10.1049/pel2.12624

[11] A. C. Bagchi, A. Kamineni, R. A. Zane, and R. Carlson, "Review and comparative analysis of topologies and control methods in dynamic wireless charging of electric vehicles," *IEEE Journal of Emerging and Selected Topics in Power Electronics*, vol. 9, no. 4, pp. 4947–4962, 2021. [Online]. Available: https://doi.org/10.1109/JESTPE.2021.3058968

[12] S. Li, W. Li, J. Deng, T. D. Nguyen, and C. C. Mi, "A double-sided lcc compensation network and its tuning method for wireless power transfer," *IEEE Transactions on Vehicular Technology*, vol. 64, no. 6, pp. 2261–2273, 2015.

[13] H. Bray, "This Watertown company wants to charge your EV wirelessly." Boston Globe, Tech. Rep., 2023. [Online]. Available: https://www.bostonglobe.com/2023/08/22/business/watertown-wireless-ev-charger/

[14] B. J. Varghese, A. Kamineni, N. Roberts, M. Halling, D. J. Thrimawithana, and R. A. Zane, "Design considerations for 50 kw dynamic wireless charging with concrete-embedded coils," in *2020 IEEE PELS Workshop on Emerging Technologies: Wireless Power Transfer (WoW)*, 2020, pp. 40–44. [Online]. Available: https://doi.org/10.1109/WoW47795.2020.9291275

[15] K. Hanawa, T. Imura, and N. Abe, "Basic evaluation of electrical characteristics of ferrite-less and capacitor-less coils by road embedment experiment for dynamic wireless power transfer," in *2021 IEEE PELS Workshop on Emerging Technologies: Wireless Power Transfer (WoW)*, 2021, pp. 1–5. [Online]. Available: https://doi.org/10.1109/WoW51332.2021.9462862

[16] K. Hanawa, T. Imura, Y. Hori, and N. Abe, "Proposal of coil embedment method by pouring resin materials for dynamic wireless power transfer," in *2022 Wireless Power Week (WPW)*, 2022, pp. 761–765. [Online]. Available: https://doi.org/10.1109/WPW54272.2022.9901360

[17] B. J. Varghese, "Roadway-embedded transmitters and multi-pad receivers for high power dynamic wireless power transfer," Ph.D. dissertation, Utah State University, Logan, UT, 2021. [Online]. Available: https://doi.org/10.26076/6c1c-3335

[18] S. Kim, M. Amirpour, G. Covic, and S. Bickerton, "Thermal characterisation of a double-d pad," in *2019 IEEE PELS Workshop on Emerging Technologies: Wireless Power Transfer (WoW)*, 2019, pp. 1–5. [Online]. Available: https://doi.org/10.1109/WoW45936.2019.9030613

[19] S. Kim, M. Amirpour, T. Dharmakeerthi, V. Z. Barsari, G. Covic, S. Bickerton, and D. Thrimawithana, "Thermal evaluation of an inductive power transfer pad for charging electric vehicles," *IEEE Transactions on Industrial Electronics*, vol. 69, no. 1, pp. 314–322, 2022. [Online]. Available: https://doi.org/10.1109/TIE.2021.3055186

[20] R. Wojda, V. P. Galigekere, J. Pries, and O. Onar, "Thermal analysis of wireless power transfer coils for dynamic wireless electric vehicle charging," in *2020 IEEE Transportation Electrification Conference & Expo (ITEC)*, 2020, pp. 835–838. [Online]. Available: https://doi.org/10.1109/ITEC48692.2020.9161453

[21] A. N. Barnes, "Thermal modeling and analysis of roadway embedded wireless power transfer modules," Master's thesis, Utah State University, Logan, UT, 2020. [Online]. Available: https://doi.org/10.26076/7005-1a78

[22] R. Tavakoli and Z. Pantic, "Analysis, design, and demonstration of a 25-kw dynamic wireless charging system for roadway electric vehicles," *IEEE Journal of Emerging and Selected Topics in Power Electronics*, vol. 6, no. 3, pp. 1378–1393, 2018. [Online]. Available: https://doi.org/10.1109/JESTPE.2017.2761763

[23] A. Dosetareh, "Personal email communication with Electreon employee," August 2023, contacted via website. [Online]. Available: https://electreon.com/contact-us

[24] E. Gurpinar, M. Mohammad, U. Kavimandan, E. Asa, V. P. Galigekere, B. Ozpineci, S. Mukherjee, L. Tolbert, H. Bai, and Y. Liu, "Failure modes and effects analysis for wireless and extreme fast charging," Oak Ridge National Laboratory and University of Tennessee, Knoxville, Tech. Rep., 2021.

[25] E. Alawadhi and C. Amon, "Performance analysis of an enhanced pcm thermal control unit," in *ITHERM 2000. The Seventh Intersociety Conference on Thermal and Thermomechanical Phenomena in Electronic Systems (Cat. No.00CH37069)*, vol. 1, 2000, pp. 283–289.

[26] A. Ridge, S. Konaklieva, S. Bradley, R. McMahon, and K. Kumar, "Power electronics packaging for in-road wireless charging installations," in *2021 IEEE PELS Workshop on Emerging Technologies: Wireless Power Transfer (WoW)*, 2021, pp. 1–6. [Online]. Available: https://doi.org/10.1109/WoW51332.2021.9462857

[27] H. Polat, F. Hosseinabadi, M. M. Hasan, S. Chakraborty, T. Geury, M. El Baghdadi, S. Wilkins, and O. Hegazy, "A review of dc fast chargers with bess for electric vehicles: Topology, battery, reliability oriented control and cooling perspectives," *Batteries*, vol. 9, no. 2, 2023. [Online]. Available: https://www.mdpi.com/2313-0105/9/2/121

[28] M. Mohammad, O. C. Onar, V. P. Galigekere, G.-J. Su, and J. Wilkins, "Thermal design and optimization of high-power wireless charging system," in *2022 IEEE Applied Power Electronics Conference and Exposition (APEC)*, 2022, pp. 480–485.

[29] S. Christian, R. Fantino, R. Amir Gomez, and J. Carlos Balda, "Inductor encapsulation-based thermal management enabling increased power density," in *2022 IEEE 13th International Symposium on Power Electronics for Distributed Generation Systems (PEDG)*, 2022, pp. 1–5.

[30] K. Lafdi, O. Mesalhy, and A. Elgafy, "Merits of Employing Foam Encapsulated Phase Change Materials for Pulsed Power Electronics Cooling Applications," *Journal of Electronic Packaging*, vol. 130, no. 2, p. 021004, 04 2008. [Online]. Available: https://doi.org/10.1115/1.2912185

[31] ACT, "PCM heat sinks," Advanced Cooling Technologies, Tech. Rep., 2024. [Online]. Available: https://www.1-act.com/thermal-solutions/passive/pcm/heat-sinks/#:~:text=PCM%20Modules%20are%20also%20used,Spacecraft%20market%20for%20thermal%20control

[32] J. B. Larsen, A. Kamineni, N. Roberts, M. Halling, P. Vaikasi, and A. Barnes, "Test platform to evaluate pavement embedded wireless charging pads," in *2022 Wireless Power Week (WPW)*, 2022, pp. 861–866. [Online]. Available: https://doi.org/10.1109/WPW54272.2022.9901325

[33] V. Blasko, R. Lukaszewski, and R. Sladky, "On line thermal model and thermal management strategy of a three phase voltage source inverter," in *Conference Record of the 1999 IEEE Industry Applications Conference. Thirty-Forth IAS Annual Meeting (Cat. No.99CH36370)*, vol. 2, 1999, pp. 1423–1431 vol.2. [Online]. Available: https://doi.org/10.1109/IAS.1999.801687

[34] A. Sangwongwanich, H. Wang, and F. Blaabjerg, "Reduced-order thermal modeling for photovoltaic inverters considering mission profile dynamics," *IEEE Open Journal of Power Electronics*, vol. 1, pp. 407–419, 2020. [Online]. Available: https://doi.org/10.1109/OJPEL.2020.3025632

[35] C.-K. Liu, P.-K. Chiu, S.-F. Hsu, H.-L. Wu, S.-T. Wu, W.-S. Lai, H.-H. Liu, and M.-T. Lee, "Effects of thermal characteristics of power module on electric vehicle inverter," in *2021 16th International Microsystems, Packaging, Assembly and Circuits Technology Conference (IMPACT)*, 2021, pp. 143–146. [Online]. Available: https://doi.org/10.1109/IMPACT53160.2021.9696922

[36] M. Ghorbani, H. Wang, and N. Roberts, "Analytical and numerical modeling of phase change material and hybrid pcm-heat sinks for high-power wireless ev charging," *International Communications in Heat and Mass Transfer*, vol. 154, p. 107460, 2024. [Online]. Available: https://www.sciencedirect.com/science/article/pii/S0735193324002227

[37] A. Roßkopf, C. Joffe, and E. Bär, "Calculation of ohmic losses in litz wires by coupling analytical and numerical methods," in *2014 4th International Electric Drives Production Conference (EDPC)*, 2014, pp. 1–6.

[38] M. Amirpour, S. Kim, M. P. Battley, P. Kelly, S. Bickerton, and G. Covic, "Coupled electromagnetic-thermal analysis of roadway inductive power transfer pads within a model pavement," *Applied Thermal Engineering*, vol. 189, p. 116710, 2021. [Online]. Available: https://www.sciencedirect.com/science/article/pii/S1359431121001654

[39] S. Niu, H. Yu, S. Niu, and L. Jian, "Power loss analysis and thermal assessment on wireless electric vehicle charging technology: The over-temperature risk of ground assembly needs attention," *Applied Energy*, vol. 275, p. 115344, 2020. [Online]. Available: https://www.sciencedirect.com/science/article/pii/S0306261920308564

[40] K.-Y. Li, T. Allen, S. Bickerton, and P. Kelly, "Thermal-mechanical behaviour of road-embedded wireless charging pads for evs," *Applied Sciences*, vol. 13, no. 23, 2023. [Online]. Available: https://www.mdpi.com/2076-3417/13/23/12766

[41] V. Lakshminarayanan and N. Sriraam, "The effect of temperature on the reliability of electronic components," in *2014 IEEE International Conference on Electronics, Computing and Communication Technologies (CONECCT)*, 2014, pp. 1–6.

[42] Z. Ni, X. Lyu, O. P. Yadav, B. N. Singh, S. Zheng, and D. Cao, "Overview of real-time lifetime prediction and extension for sic power converters," *IEEE Transactions on Power Electronics*, vol. 35, no. 8, pp. 7765–7794, 2020.

[43] J. Côté and J.-M. Konrad, "Thermal conductivity of base-course materials," *Canadian Geotechnical Journal*, vol. 42, no. 1, pp. 61–78, 2005. [Online]. Available: https://doi.org/10.1139/t04-081

[44] W. Kim, J.-W. Bae, I.-D. Choi, and Y.-S. Kim, "Thermally conductive emc (epoxy molding compound) for microelectronic encapsulation," *Polymer Engineering & Science*, vol. 39, no. 4, pp. 756–766, 1999. [Online]. Available: https://4spepublications.onlinelibrary.wiley.com/doi/abs/10.1002/pen.11464

[45] A. D. Brovont, D. Aliprantis, S. D. Pekarek, C. J. Vickers, and V. Mehar, "Magnetic design for three-phase dynamic wireless power transfer with constant output power," *IEEE Transactions on Energy Conversion*, vol. 38, no. 2, pp. 1481–1484, 2023.

[46] L. Xue, V. Galigekere, G.-j. Su, R. Zeng, M. Mohammad, E. Gurpinar, S. Chowdhury, and O. Onar, "Design and analysis of a 200 kw dynamic wireless charging system for electric vehicles," in *2022 IEEE Applied Power Electronics Conference and Exposition (APEC)*, 2022, pp. 1096–1103.

[47] A. Baig, A. Zahid, J. B. Larsen, A. Kamineni, and R. Zane, "Investigation of split lccl tuning network for high power wpt systems," in *2023 IEEE Wireless Power Technology Conference and Expo (WPTCE)*, 2023, pp. 1–6.

[48] O. Ozgener, L. Ozgener, and J. W. Tester, "A practical approach to predict soil temperature variations for geothermal (ground) heat exchangers applications," *International Journal of Heat and Mass Transfer*, vol. 62, pp. 473–480, 2013. [Online]. Available: https://www.sciencedirect.com/science/article/pii/S001793101300238X

[49] A. B. M. Alves and A. L. Schmid, "Cooling and heating potential of underground soil according to depth and soil surface treatment in the brazilian climatic regions," *Energy and Buildings*, vol. 90, pp. 41–50, 2015. [Online]. Available: https://www.sciencedirect.com/science/article/pii/S0378778814010767

[50] *TDK, Film Capacitors, Metallized Polypropylene Film Capacitors (MKP), Series/Type B32671L, B32672L.*

[51] *TDK, Film Capacitors, Quality.*

[52] *Sandtastik, Sparkling White Play Sand, Details.*

[53] S. A. Tan, T. F. Fwa, C. T. Chuai, and B. H. Low, "Determination of thermal properties of pavement materials and unbound aggregates by transient heat conduction," *Journal of Testing and Evaluation*, vol. 25, pp. 15–22, 1997. [Online]. Available: https://api.semanticscholar.org/CorpusID:136950931

[54] I. Hamdhan and C. Barry, "Determination of thermal conductivity of coarse and fine sand soils," *Bali, Indonesia: Proceedings World Geothermal Congress*, 01 2010.

[55] H. V. Vo, D. W. Park, W. J. Seo, and J. S. Im, *Effect of Conductive Filler Size and Type on Thermal Properties of Asphalt Mixtures*. ASCE Library, 2015, pp. 1–7. [Online]. Available: https://ascelibrary.org/doi/abs/10.1061/9780784479278.001

[56] P. Pan, S. Wu, X. Hu, G. Liu, and B. Li, "Effect of material composition and environmental condition on thermal characteristics of conductive asphalt concrete," *Materials*, vol. 10, no. 3, 2017. [Online]. Available: https://www.mdpi.com/1996-1944/10/3/218

[57] M. Rober, "Liquid Sand Hot Tub - Fluidized air bed," Youtube, Tech. Rep., 2017. [Online]. Available: https://www.youtube.com/watch?v=My4RA5I0FKs

APPENDIX

Dynamic Wireless XFC (22–120 KW) Concept System, Subsystem, and Components
FMEA worksheet for heavy-duty dynamic wireless charger (22–120 kW) concept system, subsystem, and components.
***For embedded and non embedded applications (LCC-series and LCC-LCC* tuning)**

No.	Component	Component description	Component function	Potential failure mode	Cause of failure modes	Likelihood score	Failure mode consequences	Consequence score	Risk score	Controls/Detection
A. Grid interface subsystem										
A.1.	Common-mode choke	Multi-turn common-mode inductor made of toroidal core and Litz wire usually	Filter inductor for conductive and differential emissions	High voltage insulation breakdown	Over voltage operation due to grid surge, voltage sag, transient, and so on Mechanical deformation Improper manufacturing design Over temperature Aging of insulation	1	Insulation breakdown between windings might cause electrical arc Significant damage such as fire with the other components and subsystems Increase high current at the grid and power losses at the PFC Increase of conductive and differential emissions User electrical and thermal safety hazard and excessive energy exposure	4	4	Current and temperature sensors Electrical and mechanical design requirements Safety and quality operating conditions Shielded enclosure to limit user access
				Electrical open circuit	Over temperature and breakdown winding Mechanical failure (e.g., break of winding, disconnect from the circuit board) Over pressure during manufacturing of windings	1	Open circuit between live terminals might cause an electrical arc and over voltage Significant damage such as fire with the other components and subsystems Electrical and thermal safety hazard User safety hazard	4	4	Current, temperature, and voltage sensors Electrical and mechanical design requirements Safety and quality operating conditions
				Electrical short circuit	Improper manufacturing electrical or mechanical design High voltage breakdown of insulation wire Improper isolation clearance between active wires High temperature across the winding leading to insulation degradation	1	Significant damage such as fire with the other components and subsystems Electrical and thermal safety hazard Increase high current at the grid and power losses at the PFC Increase of conductive and differential emissions, User safety hazard and energy exposure	4	4	Current, temperature, and voltage sensors Electrical and mechanical design requirements Safety and quality operating conditions
				High temperature	High core losses due to improper design Degraded electrical property of core material Conductivity degradation of wire High conduction losses due to high current Improper thermal management and design Excessively high ambient temperature (e.g., operating outside recommended operating range)	1	High temperature might break the winding insulation and increase the possibility of short between turns and windings Significant damage such as fire with the other components and subsystems Electrical and thermal safety hazard Increase high current at the grid and power losses at the PFC Increase of conductive and differential emission User safety hazard and excessive energy exposure	4	4	Current, voltage, and temperature sensors Electrical and mechanical design requirements Safety and quality control during manufacturing
				Mechanical failure	Crash-induced mechanical failure Degradation due to external factors (e.g., temperature, humidity, water, air pressure) Aging of electrical and mechanical components Excessive vibration due to transportation and mounting Fragile components subject to mechanical shocks (e.g., crash, vibration, collapse, drop off) Improper assembly and soldering during manufacturing Improper mechanical design	1	Mechanical damage Potential short circuit Significant damage such as fire with the other components and subsystems Electrical and thermal safety hazard Increase high current at the grid and power losses at the PFC Increase of conductive and differential emissions User safety hazard and energy exposure	4	4	Current, voltage, and temperature sensors Electrical and mechanical design requirements Safety and quality control during manufacturing
				Component performance degradation	High over temperature Mechanical breakdown Insulation failure Core saturation High voltage breakdown Reduced current, voltage, and power handling capability	1	Conductivity degradation might cause increased and power losses Core saturation may lead to excessive current at grid Increase high current at the grid and power losses at the PFC Significant damage such as fire with the other components and subsystems Electrical and thermal safety hazard User safety hazard and excessive energy exposure	4	4	Current, voltage, and temperature sensors Electrical and mechanical design requirements Safety and quality control during manufacturing Lifetime assessment and estimation during the design stage
A.2.	Y capacitor	Film or ceramic capacitor	Filter capacitor for common-mode emission	High temperature	High ripple current Improper design, placement, and assembly Improper capacitor derating during the design stage	1	High temperature might cause derating, short, open circuit, reduced lifetime, and so on Improper functionality and damage to other components and subsystems Electrical and thermal safety hazard Increased ripple current and power losses Increase of conductive and differential emissions User safety hazard	3	3	Voltage, current, and temperature sensors Electrical and mechanical design requirements Safety and quality control during manufacturing
				Electrical open circuit	Over voltage failure due to oscillations between active phases and ground Over temperature High ripple current Mechanical failure (e.g., solder crack, disconnect from the board) Improper soldering and assembly during manufacturing Improper capacitor derating during the design stage	1	Improper functionality of the filtering Damage to the other components and subsystems Electrical and thermal safety hazard User safety hazard	3	3	Voltage, current, and temperature sensors Electrical and mechanical design requirements Safety and quality control during manufacturing
				Electrical short circuit	Over voltage failure due to oscillations between active phases and ground Over temperature Mechanical failure Improper design due to improper voltage clearance High ripple current Pressure, water exposure, humidity, and so on Improper capacitor derating during the design stage	1	Improper functionality of the filtering Damage to the other components and subsystems Increase ground currents Electrical and thermal safety hazard Increased ripple current and power losses Increase of conductive and differential emission User safety hazard	4	4	Voltage, current, and temperature sensors Electrical and mechanical design requirements Safety and quality control during manufacturing

				Mechanical failure, aging, deformation	Crash-induced mechanical failure Degradation due to external factors (e.g., temperature, humidity, water, air pressure) Aging of electrical and mechanical components Excessive vibration due to transportation and mounting Fragile components subject to mechanical shocks (e.g., crash, vibration, collapse, drop off) Improper assembly and soldering during manufacturing Improper mechanical design	1	Mechanical broken of the component Improper functionality of the system Damage to the components and subsystems Electrical and thermal safety hazard Increased ripple current and power losses Increase of conductive and differential emissions User safety hazard	3	3	Voltage, current, and temperature sensors Electrical and mechanical design requirements Safety and quality control during manufacturing
A.3.	X capacitor	Film capacitor	Filter capacitor for differential mode emission	High temperature	High voltage High ripple current Improper capacitor derating during the design stage Improper design	1	High temperature might cause reduced performance, short, open circuit, and so on Improper functionality and damage to other components and subsystems Electrical and thermal safety hazard Increased ripple current and power losses Increase of conductive and differential emission User safety hazard	3	3	Voltage, current, and temperature sensors Electrical and mechanical design requirements Safety and quality control during manufacturing
				Electrical open circuit	Excessive voltage due to grid voltage sag, surges, and so on Over temperature High ripple current Mechanical failure Improper soldering and assembly during manufacturing Improper capacitor derating during the design stage	1	Improper functionality of the filtering Damage to the other components and subsystems Electrical and thermal safety hazard User safety hazard	3	3	Voltage, current, and temperature sensors Electrical and mechanical design requirements Safety and quality control during manufacturing
				Electrical short circuit	Over temperature Mechanical failure, Improper design due to improper voltage clearance on the board High ripple current Pressure, water, humidity, and so on Improper capacitor derating during the design stage	1	Improper functionality of the filtering Damage to the other components and subsystems Electrical and thermal safety hazard Increased ripple current and power losses Increase of conductive and differential emissions User safety hazard	4	4	Voltage, current, and temperature sensors Electrical and mechanical design requirements Safety and quality control during manufacturing
				Mechanical failure, aging, deformation	Crash-induced mechanical failure Degradation due to external factors (e.g., temperature, humidity, water, air pressure) Aging of electrical and mechanical components Excessive vibration due to transportation and mounting Improper assembly and soldering during manufacturing	1	Physical damage to the component Improper functionality of the system Damage to the components and subsystems Electrical and thermal safety hazard Increased ripple current and power losses Increase of conductive and differential emissions User safety hazard	3	3	Voltage, current, and temperature sensors Electrical and mechanical design requirements Safety and quality control during manufacturing
A.4.	Shielding for EMI filter of the system	Aluminum or copper cover plate or housing	Absorbs and suppresses high-frequency EMFs for EMI filter circuit	Mechanical aging and deformation	Extreme temperature Mechanical stress Environmental conductions humidity, water, air pressure, and so on Improper mechanical design and installation Crash-induced damages Excessive vibration during transportation and operation, and so on	1	Mechanical deformation Malfunctioning of the filter, and increase of conductive and differential emissions Damage to the other components and subsystems Electrical and user safety hazard	3	3	Electrical and mechanical design requirements Safety and quality control during manufacturing
				High temperature	Improper thermal management Excessive loss on the shield due to high density eddy currents	1	Increase the temperature of other components Electrical and thermal safety hazard Increased power losses Increase of conductive and differential emissions User safety hazard due to high temperature exposure	3	3	Voltage, current, and temperature sensors Electrical and mechanical design requirements Safety and quality control during manufacturing
				Electrical short circuit	Contact to electrically live terminals and components Crash-induced damages Mechanical aging and deformation	1	Significant damage such as fire with the other components and subsystems Electrical and thermal safety hazard Increased current and power losses Increase of conductive and differential emissions User safety hazard and excessive energy exposure	4	4	Voltage, current, and temperature sensors Electrical and mechanical design requirements Safety and quality control during manufacturing
				Excessive emissions and loss in the shield	Mechanical breakdown, deformation, or crack in the shield Improper design Improper mechanical design and installation High eddy current loss in shield	1	Malfunctioning of the filter and increase of conductive and differential emissions Damage to other components and subsystems Increased current and power losses Electrical and user safety hazard Increased ambient temperature for other components Electrical and thermal safety hazard	3	3	Voltage, current, and temperature sensors Electrical and mechanical design requirements Safety and quality control during manufacturing
A.5.	Fuse	Low melting lead or zinc	Circuit current protection for high current conditions	Short circuit	Does not function Wrong type fuse selection Manufacturing design error Mechanical failure due to improper assembly or soldering	1	Damage to the other components and subsystems Electrical and thermal safety hazard User safety hazard	3	3	Using electronic fuse High voltage and current protection The input relay contactor in front stage with the fault signal Temperature sensors Electrical and mechanical design requirements Safety and quality operating conditions
A.6.	Contactor	Relay circuit with operating switches	Connects the system to the grid and energize the subsystem	Short circuit	Does not function Manufacturing design error Mechanical failure due to improper assembly or soldering	1	Damage with the other components and subsystems when the failure happens Electrical and thermal safety hazard User safety hazard	3	3	High voltage and current protection, Temperature sensors Electrical and mechanical design requirements Safety and quality control during manufacturing

A.7.	Soft start circuit	Electronic circuit charging the DC link capacitor slowly through analog and digital circuits	Ramping the DC Link voltage gradually to avoid grid instabilities and transients	Short circuit (not working properly)	Crash-induced mechanical failure Improper design during manufacturing Functionality is broken Exposure to temperature, humidity, water, air pressure, and so on Improper assembly and soldering during manufacturing	1	High voltage and current spikes during startup Damage to the other components and subsystems Electrical and thermal safety hazard User safety hazard	3	3	High voltage and current protection Temperature sensors Electrical and mechanical design requirements Safety and quality control during manufacturing
A.8.	Filter inductor	Multi-turn inductor	Filter inductor for high-frequency ripples on the grid side	High voltage insulation breakdown	Over voltage due to problems in the grid such as surge, voltage sag, transients, and so on Mechanical deformation (e.g., crash-induced damages) Improper mechanical design and installation Over temperature	1	Insulation breakdown between windings might cause electrical arc and short circuit Significant damage to the other components and subsystems Electrical and thermal safety hazard Increased current and power losses Damage to functionality of filtering and not complying with grid requirements User safety hazard and energy exposure	4	4	Voltage, current, and temperature sensors Electrical and mechanical design requirements Safety and quality control during manufacturing
				Electrical open circuit	Over temperature and breakdown winding Mechanical failure Improper assembly and soldering during manufacturing Improper mechanical design	1	Open circuit between active energy probes Damage to the functionality of the filter system, and other components and subsystems Electrical safety hazard User safety hazard	3	3	Voltage, current, and temperature sensors\ Electrical and mechanical design requirements Safety and quality control during manufacturing
				Electrical short circuit	Improper manufacturing and design for electrical or mechanical requirements High voltage breakdown of the wire insulation Improper isolation clearance between the wires	1	Damage to the functionality of the filter system, and other components and subsystems Electrical and thermal safety hazard Increased high current and power losses User safety hazard and energy exposure	4	4	Voltage, current, and temperature sensors Electrical and mechanical design requirements Safety and quality control during manufacturing
				High temperature	High core losses due to improper design Degraded electrical property of the core material High conduction losses due to high current and/or conductivity degradation of wire Improper thermal design	1	High temperature might break the wire insulation and increase the possibility of short circuit between windings Damage to the functionality of the filter system, and other components and subsystems Electrical and thermal safety hazard Increased high current and power losses, User safety hazard	4	4	Voltage, current, and temperature sensors Electrical and mechanical design requirements Safety and quality control during manufacturing
				Mechanical failure	Crash-induced mechanical failure Degradation due to external factors (e.g., temperature, humidity, water, air pressure) Aging of electrical and mechanical components Excessive vibration due to transportation and mounting Improper assembly and soldering during manufacturing	1	Mechanical damage Short circuit Damage grid filtering functionality and EMI filtering Electrical and thermal safety hazard Increased current and power losses User safety hazard	4	4	Voltage, current, and temperature sensors Electrical and mechanical design requirements Safety and quality control during manufacturing
A.9.	Filter capacitor	Film capacitor	Filter capacitor for high-frequency ripples on the grid side	Capacitor short circuit	Excessive voltage and current stresses High power losses and heat dissipation across the capacitor, which may lead to dielectric failure depending on capacitor properties Aging of the capacitor Mechanical failure due to improper assembly or soldering during manufacturing Improper design during manufacturing	1	The input of PFC will be shorted, resulting high current in the front stage and EMI filter Break the functionality of EMI with the other component and subsystems High power losses at the front stage High temperature in the components Electrical and thermal safety hazard User safety hazard	4	4	High voltage and current protection in front of the system The input relay contactor in front stage with the fault signal Temperature sensors Electrical and mechanical design requirements Safety and quality control during manufacturing
				Capacitor open circuit	Excessive voltage and current stresses across the capacitor Excessive heat dissipation Mechanical failure due to improper assembly or soldering during manufacturing Aging factors and lifetime Improper design during manufacturing	1	Damage to the functionality of the grid requirements and EMI filtering High power losses and temperature due to high ripple current Damage with the other components and subsystems Electrical and thermal safety hazard User safety hazard	2	2	High voltage and current protection The input relay contactor in front of the system for disconnection from the grid Temperature sensors Electrical and mechanical design requirements Safety and quality control during manufacturing
				High temperature	Excessive voltage and current stresses across the capacitor Mechanical failure due to improper assembly or soldering during manufacturing Aging factors and lifetime Improper design during manufacturing	1	High power losses at the front stage Damage to the other components and subsystems Electrical and thermal safety hazard User safety hazard	4	4	High voltage and current protection The input relay contactor in front of the system for disconnection from the grid Temperature sensors Electrical and mechanical design requirements Safety and quality control during manufacturing
A.10.	Rectifier module	Power module formed by housing and semiconductor diodes.	Rectifies AC voltage coming from the grid and forms DC voltage at the output.	One diode in the module shorted	High voltage and current stresses on the rectifier module High power losses Over temperature Mechanical failure due to improper assembly or soldering during manufacturing Aging, water flooding, pressure, humidity, and so on Improper design during manufacturing	2	The input AC grid half cycle will be shorted, resulting high current in the rectifier module It might damage the rectifier module Break the functionality of the PFC Excessive power losses in the rectifier module High temperature in the rectifier module Electrical and thermal safety hazard User safety hazard and energy exposure	3	6	High voltage and current protection at the input of rectifier module The input relay contactor in front of PFC turning off with the fault signal Temperature sensors Electrical and mechanical design requirements Safety and quality control during manufacturing
				Both diodes in the module shorted	High voltage and current stresses on the rectifier module High power losses Over temperature Mechanical failure due to improper assembly or soldering during manufacturing Aging, water flooding, pressure, humidity, and so on Improper design during manufacturing	2	The input AC grid will be shorted, resulting high current in the rectifier module Might damage the rectifier module Break the functionality of PFC High power losses in the rectifier module High temperature in the rectifier module DC link component failures due to short of the DC link terminals Electrical and thermal safety hazard User safety hazard and energy exposure	3	6	High voltage and current protection at the input of rectifier module The input relay contactor in front of PFC turning off with the fault signal Temperature sensors Electrical and mechanical design requirements Safety and quality control during manufacturing

				One diode in the module is open circuit	Mechanical failure due to improper assembly or soldering during manufacturing Aging factors Improper design during manufacturing	1	The input AC grid half cycle will be open Break the functionality of PFC Reduced DC link voltage due to limited rectification capability User safety hazard	3	3	High voltage and current protection in front of rectifier module The input relay contactor in front of PFC turning off with the fault signal Temperature sensors Electrical and mechanical design requirements Safety and quality control during manufacturing
				Both diodes in the module are open circuit	Mechanical failure due to improper assembly or soldering during manufacturing Aging factors Improper design during manufacturing	1	Open circuit to the output System will stop working and stop functionality of the system	3	3	High voltage and current protection in front of rectifier module The input relay contactor in front of PFC turning off with the fault signal Electrical and mechanical design requirements Safety and quality control during manufacturing
				High temperature	Excessive voltage and current stresses across the rectifier module Mechanical failure due to improper assembly or soldering during manufacturing Aging factors Improper design during manufacturing	1	High power losses in the rectifier module Damage to the other components and subsystems Electrical and thermal safety hazard User safety hazard and energy exposure	4	4	High voltage and current protection The input relay contactor in front of rectifier module turning off with the fault signal Temperature sensors Electrical and mechanical design requirements Safety and quality control during manufacturing
A.11.	DC link capacitor	Film or electrolytic	Filtering capacitor for DC link ripple voltages after rectification	Capacitor short circuit	Excessive voltage and current stresses High power losses and heat dissipation across the capacitor, which may translate in dielectric failure depending on capacitor properties Aging of the capacitor Mechanical failure due to improper assembly or soldering during manufacturing Improper design during manufacturing	1	The output of rectifier will be shorted, resulting high current in the rectifier module Might damage the rectifier module due to excessive energy Break the functionality of PFC and the overall system High energy dissipation across the rectifier module High temperature in the rectifier module, Electrical and thermal safety hazard User safety hazard and energy exposure	4	4	High voltage and current protection at the output of the rectifier The input relay contactor in front of PFC turning off with the fault signal Temperature sensors Electrical and mechanical design requirements Safety and quality control during manufacturing
				Capacitor open circuit	Excessive voltage and current stresses across the capacitor Excessive heat dissipation Mechanical failure due to improper assembly or soldering during manufacturing Aging factors Improper design during manufacturing	1	High voltage ripple at the DC link Might damage the functionality of the PFC High power losses and temperature in the PFC Damage to the other components and subsystems Electrical and thermal safety hazard User safety hazard and energy exposure	2	2	High voltage and current protection at the output of the rectifier The input relay contactor in front of PFC turning off with the fault signal Temperature sensors Electrical and mechanical design requirements Safety and quality control during manufacturing
				High temperature	Excessive voltage and current stresses across the capacitor Mechanical failure due to improper assembly or soldering during manufacturing Aging factors Improper design during manufacturing	1	High power losses in the rectifier module due to increased resistance in the capacitor Damage to the other components and subsystems Electrical and thermal safety hazard User safety hazard and energy exposure	4	4	High voltage and current protection The input relay contactor in front of rectifier module turning off with the fault signal Temperature sensors Electrical and mechanical design requirements Safety and quality control during manufacturing Proper derating during capacitor selection
A.12.	Heat sink	Heat sink structure made from aluminum or copper and uses air or liquid for heat transfer	Transfers the heat from power modules used in PFC and rectifier to the coolant	Mechanical failure of cold plate and coolant circulating unit	Mechanical shock or crack Leakage or loose contact between the cold plate and the circulating unit Improper design during manufacturing	1	Temperature control disrupted Lead to excessive heating of the electronic active and passive components Increased power loss across components Damage to the other components and subsystems	4	4	Temperature sensors to protect overheating The input relay contactor in front of PFC turning off with the thermal fault signal Electrical and mechanical design requirements Safety and quality control during manufacturing
				Failure of the coolant pump	Electrical failure of the pump motor Mechanical failure of the pump motor	2	Temperature control disrupted Lead to excessive heating of the electronic active and passive components Increased power loss across components Damage to the other components and subsystems	2	4	Temperature sensors to protect from overheat The input relay contactor in front of PFC turning off with the thermal fault signal Electrical and mechanical design requirements Safety and quality control during manufacturing
				Clogging of the cooling fluid circulating unit	Residue and dirt accumulation in the coolant and the cooling unit The properties of the coolant fluid is not adequate for the operating conditions Aging of the fluid Lack of filter maintenance and care	2	Temperature control disrupted Lead to excessive heating of the electronic active and passive components Increased power loss across components Damage to the other components and subsystems	2	4	Temperature sensors to protect from overheat The input relay contactor in front of PFC turning off with the thermal fault signal Electrical and mechanical design requirements Safety and quality control during manufacturing
				Poor performance of the thermal interface material between the power module and cold plate	Mechanical stress and strain due to thermal cycling Improper material selection during the design stage Degradation of material properties due to aging	2	Temperature control disrupted Lead to excessive heating of the electronic active and passive components Cause to increase in power losses Damage with the other components and subsystems	2	4	Temperature sensors to protect from overheating The input relay contactor in front of PFC turning off with the thermal fault signal Electrical and mechanical design requirements Safety and quality control during manufacturing
A.13.	Boost inductor	Multi-turn winding inductor made by Litz wire	Part of the PFC system for boosting rectified grid voltage to the desired output voltage	High voltage insulation breakdown	Over voltage due to problems in the grid such as surge, voltage sag, transient, and so on Mechanical deformation Improper manufacturing design Over temperature	1	Insulation breakdown between windings might cause electrical short circuit Significant damage such as fire with the other components and subsystems Electrical and thermal safety hazard Increased current and power losses Increase of conductive and differential emissions User safety hazard and energy exposure	4	4	Current, voltage, and temperature sensors Electrical and mechanical design requirements Safety and quality control during manufacturing
				Electrical open circuit	Over temperature and breakdown winding Mechanical failure Improper assembly and soldering during manufacturing Improper mechanical design	1	Damage to the functionality of the filter system, and other components and subsystems Electrical and thermal safety hazard Increased high current and power losses User safety hazard and energy exposure Damage functionality of PFC circuit	3	3	Voltage, current, and temperature sensors Electrical and mechanical design requirements Safety and quality control during manufacturing

				Electrical short circuit	Improper manufacturing and design for electrical or mechanical requirements High voltage breakdown of the wire insulation Improper isolation clearance between the wires	1	Damage to the functionality of the filter system, and other components and subsystems Dame PFC power module due to very high current demand Electrical and thermal safety hazard Increased high current and power losses User safety hazard and energy exposure	4	4	Voltage, current, and temperature sensors Electrical and mechanical design requirements Safety and quality control during manufacturing
				High temperature	High core losses due to improper design Degraded electrical property of the core material High conduction losses due to high current and/or conductivity degradation of wire Improper thermal design	1	High temperature might break the wire insulation and increase the possibility of short circuit between windings Damage to the functionality of the filter system, and other components and subsystems Electrical and thermal safety hazard Increased high current and power losses User safety hazard	4	4	Voltage, current, and temperature sensors Electrical and mechanical design requirements Safety and quality control during manufacturing
				Mechanical failure	Crash-induced mechanical failure Degradation due to external factors (e.g., temperature, humidity, water, air pressure) Aging of electrical and mechanical components Excessive vibration due to transportation and mounting Improper assembly and soldering during manufacturing	1	Mechanical damage Short circuit Damage PFC functionality and boosting function Electrical and thermal safety hazard Increased current and power losses User safety hazard	4	4	Voltage, current, and temperature sensors Electrical and mechanical design requirements Safety and quality control during manufacturing
A.14.	IGBT power module	Insulated gate bipolar transistor	PFC system switching power module	Power module short circuit (lower FET)	Excessive voltage and current stresses across the power module Gate driver output pulled high due to noise, failure, and so on Excessive heat dissipation Mechanical failure due to improper assembly or soldering during manufacturing Aging, water flooding, pressure, humidity, and so on Improper design during manufacturing	2	The input voltage is shorted through the inductor, resulting in high input currents to the switch and damage power module Inductor saturation due to high current High power losses in the inductor and switch power module High temperature in the PFC inductor and switch power module Damage in front of PFC components and subsystems Electrical and thermal safety hazard User safety hazard and energy exposure	4	8	Short circuit protection in gate driver High voltage protection in front of PFC The input relay contactor in front of PFC turning off with the fault signal Temperature sensors Electrical and mechanical design requirements Safety and quality control during manufacturing
				Power module short circuit (upper FET)	Excessive voltage and current stresses across the power module Gate driver output pulled high due to noise, failure, and so on Excessive heat dissipation Mechanical failure due to improper assembly or soldering during manufacturing Aging, water flooding, pressure, humidity, and so on Improper design during manufacturing	2	The output voltage across the capacitor will be shorted when the switch power module is conduction, resulting in high currents into the switch power module High power losses in the switch power module High temperature in the switch power module Damage in PFC and components and subsystems Electrical and thermal safety hazard User safety hazard and excessive energy exposure	4	8	DESAT protection in gate driver High voltage and current protection in front of PFC The input relay contactor in front of PFC turning off with the fault signal Temperature sensors Electrical and mechanical design requirements Safety and quality control during manufacturing
				Power module open circuit (Lower FET)	Excessive voltage and current stresses across the switch module Gate driver output pulled low due to noise, failure, and so on Excessive heat dissipation Mechanical failure due to improper assembly or soldering during manufacturing Aging, water flooding, pressure, humidity, and so on Improper design during manufacturing	2	PFC Inductor might be saturated High temperature in the inductor Electrical and thermal safety hazard User safety hazard and energy exposure	3	6	High voltage and current protection in front of PFC The input relay contactor in front of PFC turning off with the fault signal Temperature sensors Electrical and mechanical design requirements Safety and quality control during manufacturing
				Power module open circuit (Upper FET)	Excessive voltage and current stresses across the switch module Gate driver output pulled low due to noise, failure, and so on Excessive heat dissipation Mechanical failure due to improper assembly or soldering during manufacturing Aging factors, and so on Improper design during manufacturing	2	Open circuit to the output Zero voltage in the output The system controllability will be saturated threshing up the PWM control limits. This will cause high current in the lower FET and PFC inductor	3	6	High voltage and current protections The input relay contactor in front of PFC turning off with the fault signal Electrical and mechanical design requirements
				High temperature	Excessive voltage and current stresses across the switch module Mechanical failure due to improper assembly or soldering during manufacturing Aging, factors, and so on Improper design during manufacturing Degradation of thermal performance of the power module due to thermal and power cycling over time	1	High power losses in the inductor and switch power module Damage with the other components and subsystems Electrical and thermal safety hazard User safety hazard and excessive energy exposure	4	4	High voltage and current protection The input relay contactor in front of PFC turning off with the fault signal Temperature sensors Electrical and mechanical design requirements Safety and quality control during manufacturing Degradation monitoring of the module on a regular basis
A.15.	Gate driver	Provides an isolation from the microcontroller signal pulse to an output pulse at appropriate voltage levels capable of sourcing and sinking currents as required by the gate terminal of the power module switches	Controls turn on and turn off of the power switches in the power module for PFC	Output of gate driver constant high	Analog/digital circuitry failure Mechanical assembly failure PCB circuit failure Improper circuit design	1	The input voltage is shorted through the inductor, resulting in high input currents to the switch and damage power module Inductor saturation due to high current High power losses in the inductor and power module High temperature in the inductor and power module Damage in front of PFC components and subsystems Electrical and thermal safety hazard User safety hazard and energy exposure	4	4	Short circuit protection in gate driver High voltage protection in front of PFC The input relay contactor in front of PFC turning off with the fault signal Temperature sensors Electrical and mechanical design requirements Safety and quality control during manufacturing
				Output of gate driver constant low	Analog/digital circuitry failure Gate driver isolated power supply failure Mechanical assembly failure PCB circuit failure Improper circuit design	1	Inductor might be saturated High temperature in the inductor Electrical and thermal safety hazard User safety hazard	3	3	High voltage and current protection in front of PFC The input relay contactor in front of PFC turning off with the fault signal Temperature sensors Electrical and mechanical design requirements Safety and quality control during manufacturing

				Short circuit protection circuit failure	Analog/digital circuitry failure Mechanical assembly failure PCB circuit failure Faulty circuit design	2	No protection of the switches during short circuit Excessive currents during short circuit Damage the power module during short Inductor saturation due to high current High power losses in the inductor and switch power module High temperature in the inductor and switch power module Damage in front of PFC components and subsystems Electrical and thermal safety hazard User safety hazard and energy exposure	4	8	High voltage and current protection in front of PFC The input relay contactor in front of PFC turning off with the fault signal Temperature sensors Electrical and mechanical design requirements Safety and quality control during manufacturing
A.16	Capacitor	Film or electrolytic capacitor	PFC output capacitor for DC link voltage smoothing	Capacitor short circuit	Excessive voltage and current stresses High power losses and heat dissipation across the capacitor, which may translate in dielectric failure depending on capacitor property Aging of the capacitor Mechanical failure due to improper assembly or soldering during manufacturing Improper design during manufacturing	1	The output of rectifier will be shorted, resulting high current in the PFC Might damage the PFC power module High power losses in the PFC High temperature in the PFC Electrical and thermal safety hazard User safety hazard and energy exposure	4	4	High voltage and current protection in front of PFC The input relay contactor in front of PFC turning off with the fault signal Temperature sensors Electrical and mechanical design requirements Safety and quality control during manufacturing
				Capacitor open circuit	Excessive voltage and current stresses across the capacitor Excessive heat dissipation Mechanical failure due to improper assembly or soldering during manufacturing Aging factors, and so on Improper design during manufacturing	1	Ripple at the output of the PFC will appear at the input of WPT high-frequency inverter Might damage the functionality of the WPT system High power losses and temperature in the WPT system Damage to the other components and subsystems Electrical and thermal safety hazard User safety hazard and excessive energy exposure	2	2	High voltage and current protection in front of PFC The input relay contactor in front of PFC turning off with the fault signal Temperature sensors Electrical and mechanical design requirements Safety and quality control during manufacturing Adequate voltage derating during the design stage
				High temperature	Excessive voltage and current stresses across capacitor Mechanical failure due to improper assembly or soldering during manufacturing Aging, factors, and so on Improper design during manufacturing	1	High power losses in the PFC Damage to the other components and subsystems Electrical and thermal safety hazard User safety hazard and energy exposure	4	4	High voltage and current protection The input relay contactor in front of PFC turning off with the fault signal Temperature sensors Electrical and mechanical design requirements Safety and quality control during manufacturing
A.17.	Grid voltage sensor	Electronic analog to digital circuit	Measures the grid voltage for PFC controller and protection	Out of calibration	Aging, factors, and so on Water flooding, pressure, humidity, and so on Excessive heat dissipation due to inaccurate circuit design and component tolerance changes	1	Might damage the PFC Break the functionality of PFC High power losses in the PFC High temperature in the PFC Electrical safety hazard User safety hazard	3	3	Calibration is conducted or validated periodically MCU calibration reset in each cycle due to malfunction and so on High voltage protection sensors Temperature sensors Electrical and mechanical design requirements Safety and quality control during manufacturing
				Short circuit (not working properly)	Excessive voltage at the grid side due to sag, transient, and so on Analog/digital circuitry failure Water flooding, pressure, humidity, and so on Improper design during manufacturing PCB circuit design failure Mechanical failure due to improper assembly or soldering during manufacturing	1	Might damage the PFC Break the functionality of PFC High power losses in the PFC High temperature in the PFC Electrical safety hazard User safety hazard	4	4	High voltage protection sensors Temperature sensors Electrical and mechanical design requirements Safety and quality control during manufacturing
A.18.	Grid current sensor	Electronic analog to digital circuit	Measures the grid current for PFC controller and protection	Out of calibration	Aging, factors, and so on Water flooding, pressure, humidity, and so on Excessive heat dissipation due to inaccurate circuit design and component tolerance changes	1	Might damage the PFC Break the functionality of PFC High power losses in the PFC High temperature in the PFC Damage with the other components and subsystems Electrical safety hazard User safety hazard	3	3	Calibration is conducted or validated periodically MCU calibration reset in each cycle due to malfunction and so on High current protection sensors Temperature sensors Electrical and mechanical design requirements Safety and quality control during manufacturing
				Short circuit (not working properly)	Excessive current at the grid side due to inrush, transient, and so on Analog/digital circuitry failure Water flooding, pressure, humidity, and so on Improper design during manufacturing PCB circuit design failure Mechanical failure due to improper assembly or soldering during manufacturing	1	Might damage the PFC Break the functionality of PFC High power losses in the PFC High temperature in the PFC Damage to the other components and subsystems Electrical safety hazard User safety hazard	4	4	High current protection sensors Temperature sensors Electrical and mechanical design requirements Safety and quality control during manufacturing
A.19.	Temperature sensor	Electronic analog to digital circuit	Measures the temperature of certain components in PFC	Out of calibration	Aging, factors, and so on Water flooding, pressure, humidity, and so on Excessive heat dissipation due to inaccurate circuit design and component tolerance changes	1	Overheating of critical components in PFC Electrical safety hazard User safety hazard	3	3	Calibration is conducted or validated periodically MCU calibration reset in each cycle due to malfunction and so on High voltage and current protection sensors, Additional, redundant temperature are used sensors at different locations, Electrical and mechanical design requirements, Safety and quality control during manufacturing.
				Short circuit (not working properly)	Analog/digital circuitry or sensor failure Water flooding, pressure, humidity, and so on Improper soldering, placement, or error during manufacturing Mechanical failure due to improper assembly or soldering during manufacturing	1	Might damage with other components and subsystems Electrical safety hazard User safety hazard	4	4	High voltage and current protection sensors Additional multiple temperature sensors with the different locations Electrical and mechanical design requirements Safety and quality control during manufacturing

B. High-frequency inverter										
B.1.	Semiconductor power module (generally MOSFETs)	Silicon carbide MOSFETs	Converts the DC voltage to high- frequency square or quasi-square AC voltage	One switch in the module shorted	Excessive voltage, current and power stress across switch. Gate driver output pulled high Excessive heat dissipation, Mechanical failure due to improper assembly or soldering during manufacturing, Aging, water flooding, pressure, humidity, and so on, Improper design during manufacturing.	2	The DC voltage at inverter input is periodically shorted when the complementary switch turns ON resulting in high input currents, High power losses in the inductor and switch power module, High temperature in the PFC inductor and switch power, module, Electrical and thermal safety hazard, User safety hazard and energy exposure.	3	6	Short circuit protection in gate driver turns OFF the complementary switch
				Both switches in the module shorted	Excessive voltage, current and power stress across the module Gate driver output pulled high for both switches Excessive heat dissipation, Mechanical failure due to improper assembly or soldering during manufacturing, Aging, water flooding, pressure, humidity, and so on, Improper design during manufacturing.	2	The DC voltage at inverter input is permanently shorted resulting in high input currents DC link capacitor can be damaged due to high inrush current High temperature in the power module, Electrical and thermal safety hazard, User safety hazard and energy exposure.	3	6	The input relay- contactor turns OFF Current/voltage sensors communicates fault to upstream PFC or inverter microcontroller Short circuit protection in gate driver turns OFF the module entirely
				One module is open circuited	Excessive heat dissipation Mechanical failure Gate driver failure	1	No power flow to the GA or VA unit	3	3	Fault communicated by dedicated voltage and current sensors to the battery management system (BMS), gate-driver and upstream PFC The input relay contactor in front of inverter turning off with the fault signal
				Both modules are open circuited	Excessive heat dissipation Mechanical failure Gate driver failure	1	No power flow to GA coil or VA unit	3	3	Fault communicated by dedicated sensors and also from the BMS
				ZVS is lost between switching modules	Mistuning in the resonant tank Improper dead time Gate driver misccommunication	3	High temperature in the power module. Reduced lifetime of switching module	2	6	Temperature sensors communicate to microcontroller for protective action. System may need to be recalibrated
B.2.	Gate driver circuitry	Gate drivers receive signals from the FPGA/microcontroller and control the MOSFETs	Controls the turn-on and turn-off of the switches in the power modules of the inverter bridge on the GA side assembly	Gate driver fails and is pulled constant low	Excessive voltage, current, or power stress across gate drive circuitry Analog circuitry failure Mechanical failure due to improper assembly or soldering during manufacturing	2	Switches open circuited No power flow to GA cooil or VA unit	2	4	Fault detected and reported to FPGA/Microcontroller
				Gate driver fails and is pulled constant high	Excessive voltage, current, or power stress across gate drive circuitry Analog circuitry failure Failure of isolated auxilery power supply to gate drive circuitry Mechanical failure due to improper assembly or soldering during manufacturing	2	Switches are short circuited Mosfet switches damaged due to high input currents DC link capacitor damaged due to high inrush current High temperatures in power module	3	6	Fault detected and reported to FPGA/Microcontroller
				Short circuit protection circuit failure	Analog circuitry failure Mechanical/pcb failure	2	No protection of the switches during short circuit. Excessive currents during short circuit. May damage the MOSFET switches and the module	3	6	Input relay-contactor turns OFF Current/voltage sensors communicates fault to upsream PFC
B.3.	Cooling unit (heat sink and chiller)	Cold plate with a compressor pump and ethylene glycol storage tank (with Ethylene glycol and water mix 50-50%)	Dissipates heat to keep the junction temperature of the power modules under tolerable limits	Mechanical failure of cold plate and coolant circulating unit	Mechanical shock or crack Leakage or loose contact between the cold plate and the circulating unit	1	Temperature control disrupted. May lead to excessive heating of the MOSFET switches, increase in losses and damage of the switches	3	3	Temperature sensor communicates to microcontroller for protective action, gate driver turns OFF the MOSFETs
				Failure of the compressor pump	Electrical failure Mechanical failure	2	Temperature control disrupted. May lead to excessive heating of the MOSFET switches, increase in losses and damage of the switches	4	8	Temperature sensor communicates to microcontroller for protective action, gate driver turns OFF the MOSFETs
				Clogging of the cooling fluid circulating unit	Residue and dirt accumulation in the coolant and the cooling unit	1	Temperature control disrupted. May lead to excessive heating of the MOSFET switches, increase in losses and damage of the switches	4	4	Periodic maintenance Temperature sensor communicates to microcontroller for protective action, gate driver turns OFF the MOSFETs
				Failure of the thermal pad between the power module and cold plate	Mechanical stress and strain	1	Temperature control disrupted. Increased thermal stress on the MOSFET switches, increase in losses	3	3	Temperature sensor communicates to microcontroller for protective action, gate driver turns OFF the MOSFETs
B.4.	DC input capacitors or High-frequency decoupling capacitors	Film (metallized or polypropylene film) capacitor or PLZT ceramic capacitors	Stabalize DC voltage at input of inverter and supply switching frequency high frequency ripple currents	Capacitor failed resulting short circuit	Excessive voltage, current and power stress across the capacitor, which may translate in dielectric failure depending on capacitor property.	3	The DC voltage at inverter input is permanently shorted resulting in high input currents	3	9	Input relay-contactor turns OFF Current/voltage sensors communicates fault to upsream PFC
				Capacitor failed resulting open circuit	Excessive voltage, current and power stress across the capacitor, which may translate in dielectric failure depending on capacitor property. Mechanical failure	2	Switching harmonic ripple supplied from the input resulting in input voltage distortions. MOSFET switches might be subjected to higher voltage stress	2	4	Proper derating of the capacitor to avoid exceeding recommended operating range. PFC and inverter will trip the system if the current, voltage, and temperature ratings go out of operating range.
				Diminishing capacitance value	Excessive voltage stress over time Aging of the capacitor	4	Switching harmonic ripple supplied from the input resulting in input voltage distortions. MOSFET switches might be subjected to higher voltage stress	1	4	Proper derating of the capacitor to avoid exceeding recommended operating range. Lifetime estimation at the design stage to ensure the capacitor will survive expected lifetime. Condition monitoring scheme can be implemented for lifetime monitoring of the capacitors.

B.5.	Inverter enclosure	Epoxy or PSM enclosure which surrounds inverter when being embedded in concrete with the rest of the WPT	Protects the inverter from outside elemtents and also contributes to heat dissipation	Mechanical failure/breakdown	Aging, water flooding, pressure, humidity Extreme roadway/ambient temperatures	4	Cracking of epoxy leading to inverter exposed to elements and decreased lifetime of system MOSFET switches subjected to higher temperatures and increased mechanical stress	2	8	Temperature sensors communicate to microcontroller for protection action to decrease power capability of system Condition monitoring of component lifetimes Quality and durability test of the system under diverse operating conditions
C. Compensation networks											
C.1.	Compensation capacitors (GA)	Film (metallized or polypropylene film) capacitor	Part of the resonant network to achieve resonance at the desired frequency	Diminishing capacitance value	Excessive voltage stress over time, Aging of the capacitor, Improper design during manufacturing	4	Changes in resonant frequency resulting in lower efficiency of system	1	4	Proper derating of the capacitor to avoid exceeding recommended operating range. Lifetime estimation at the design stage to ensure the capacitor will survive expected lifetime. Condition monitoring scheme can be implemented for lifetime monitoring of the capacitors.
C.2.	Compensation capacitors (VA)	Film (metallized or polypropylene film) capacitor	Part of the resonant network to achieve resonance at the desired frequency	Diminishing capacitance value	Excessive voltage stress over time, Aging of the capacitor, Improper design during manufacturing	4	Changes in resonant frequency resulting in lower efficiency of system	1	4	Proper derating of the capacitor to avoid exceeding recommended operating range. Lifetime estimation at the design stage to ensure the capacitor will survive expected lifetime. Condition monitoring scheme can be implemented for lifetime monitoring of the capacitors.
C.1.1.	Compensation series capacitor in GA (referred as C_1 in Figure 2.1–2.4)			Capacitor failed short circuit	Excessive voltage, current and power stress across the capacitor, Over temperature, Aging of capacitor Water flooding, pressure, humidity, Improper design during manufacturing	2	Excessive current on GA side, which can damage the MOSFET switches	3	6	Voltage and current protection at the output of the inverter, The input relay contactor in front of inverter turning off with the fault signal, Fault communicated to the BMS and upstream PFC Electrical and mechanical design requirements, Safety and quality control during manufacturing
				Capacitor failed open circuit	Excessive voltage, current and power stress across the capacitor Mechanical failure Excessive heat dissipation, Aging factors, Water flooding, pressure, humidity, Improper design during manufacturing	1	Excessive current on GA side, which can damage the MOSFET switches	3	3	Voltage and current protection at the output of the inverter (especially for, LCC- series and LCC-LCC), The input relay contactor in front of inverter turning off with the fault signal, Fault communicated to the BMS and upstream PFC Electrical and mechanical design requirements, Safety and quality control during manufacturing
C.2.1	Compensation series capacitor in VA (referred as C_2 in Figure 2.1–2.3)			Capacitor failed short circuit	Excessive voltage, current and power stress across the capacitor, Over temperature, Aging of capacitor Water flooding, pressure, humidity, Improper design during manufacturing	2	Distorted input current	2	4	Voltage and current protection at the output of the inverter (especially, series- series), The input relay contactor in front of inverter turning off with the fault signal, Fault communicated to the BMS and upstream PFC Electrical and mechanical design requirements, Safety and quality control during manufacturing
							Reduced output power as resonance is lost	2	4	
				Capacitor failed open circuit	Excessive voltage, current and power stress across the capacitor Mechanical failure Excessive heat dissipation, Aging factors, Water flooding, pressure, humidity, Improper design during manufacturing	1	Distorted input current	2	2	Voltage and current protection at the output of the inverter (especially for, series- series), The input relay contactor in front of inverter turning off with the fault signal, Fault communicated to the BMS and upstream PFC Electrical and mechanical design requirements, Safety and quality control during manufacturing
							No power to output	2	2	
C.1.2.	Compensation parallel capacitor in GA (referred as C_{f1} in Figure 2.2–2.3)			Capacitor failed short circuit	Excessive voltage, current and power stress across the capacitor, Over temperature, Aging of capacitor, Water flooding, pressure, humidity, Improper design during manufacturing	2	Increased and distorted input current, which may damage the inverter MOSFETs, increased EMI in the inverter	2	4	Voltage and current protection at the output of the inverter, The input relay contactor in front of inverter turning off with the fault signal, Fault communicated to the BMS and upstream PFC Electrical and mechanical design requirements, Safety and quality control during manufacturing
							No coil current due to the short-circuit at the output of inverter, and subsequently no output power	2	4	
				Capacitor failed open circuit	Excessive voltage, current and power stress across the capacitor Mechanical failure Excessive heat dissipation, Aging factors, Water flooding, pressure, humidity, Improper design during manufacturing	1	Input current at the inverter and GA coil current is distorted	2	2	Voltage and current protection at the output of the inverter, The input relay contactor in front of inverter turning off with the fault signal, Fault communicated to the BMS and upstream PFC Electrical and mechanical design requirements, Safety and quality control during manufacturing
							Reduced output power, reduced and distorted coil current	2	2	
C.2.2	Compensation parallel capacitor in VA (referred as C_{f2} in Figure 2.3)			Capacitor failed short circuit	Excessive voltage, current and power stress across the capacitor Over temperature, Aging of capacitor, Water flooding, pressure, humidity, Improper design during manufacturing	2	Input inverter current is distorted	2	4	Voltage and current protection at the output of the inverter, The input relay contactor in front of inverter turning off with the fault signal,
							VA coil is shorted (rectifier input is shorted), excess voltage and current stress on the series VA compensation capacitor,	3	6	Voltage and current protection within the VA communicating to the vehicle
							No output power, distorted and increased input current	2	4	Fault communicated to the BMS and upstream PFC Electrical and mechanical design requirements, Safety and quality control during manufacturing

				Capacitor failed open circuit	Excessive voltage, current and power stress across the capacitor Mechanical failure Excessive heat dissipation, Aging factors, Water flooding, pressure, humidity, Improper design during manufacturing	1	Input current is distorted and output power is reduced	2	2	Voltage and current protection at the output of the inverter, The input relay contactor in front of inverter turning off with the fault signal, Fault communicated to the BMS and upstream PFC Electrical and mechanical design requirements, Safety and quality control during manufacturing
C.2.3	Compensation parallel capacitor in VA (referred as C_p in Figure 2.4)			Capacitor failed short circuit	Excessive voltage, current and power stress across the capacitor Over temperature, Aging of capacitor, Water flooding, pressure, humidity, Improper design during manufacturing	2	Input current increases, and may damage the inverter MOSFETs	3	6	Voltage and current protection at the output of the inverter, The input relay contactor in front of inverter turning off with the fault signal, Fault communicated to the BMS and upstream PFC Electrical and mechanical design requirements, Safety and quality control during manufacturing
							The VA coil is shorted (rectifier input) and subsequently no power transfer to the battery	2	4	
				Capacitor failed open circuit	Excessive voltage, current and power stress across the capacitor Mechanical failure Excessive heat dissipation, Aging factors, Water flooding, pressure, humidity, Improper design during manufacturing	1	Input current increases, the VA coil current increases, and the output power decreases	3	3	Voltage and current protection at the output of the inverter, The input relay contactor in front of inverter turning off with the fault signal, Fault communicated to the BMS and upstream PFC Electrical and mechanical design requirements, Safety and quality control during manufacturing
C.1.3	Capacitor enclosure	Epoxy or PSM enclosure which surrounds the GA capacitor bank when being embedded in concrete with the	Protects the capacitor bank from outside elemtents and also contributes to heat dissipation	Mechanical failure/breakdown	Aging, water flooding, pressure, humidity Extreme roadway/ambient temperatures	4	Cracking of epoxy leading to capacitors exposed to elements and decreased lifetime of system Capacitors subjected to higher temperatures and increased mechanical stress	2	8	Temperature sensors communicate to microcontroller for protection action to decrease power capability of system Condition monitoring of component lifetimes Quality and durability test of the system under diverse operating conditions
C.3.	Compensation Inductors (GA)	Inductors with ferrite core, and Litz wire for the winding	Part of the resonant network to achieve resonance at the desired frequency	Inductance value change	Water flooding, pressure, humidity Quality factor permanently decreased when embedded in epoxy or concrete Cracking of inductor ferrite due to mechanical shock or stress	3	Changes in resonant frequency resulting in lower efficiency of system	1	3	Lifetime estimation at the design stage to ensure the inductor will survive expected lifetime. Condition monitoring scheme can be implemented for lifetime monitoring of the inductor
C.3.1	Compensation series inductor in GA (referred as Lf1 in Figure 2.3)			Inductor failed open circuit	Mechanical shock or stress or assembly issues (both coil and core) Over temperature and breakdown winding, Mechanical failure, Improper assembly and soldering during manufacturing, Water flooding, pressure, humidity	1	No output power	2	2	Voltage, current, and temperature sensors, The input relay contactor in front of inverter turning off with the fault signal, Fault communicated to the BMS and upstream PFC Electrical and mechanical design requirements, Safety and quality control during manufacturing.
				Inductor failed short circuit	Excessive current stress causing inductor to saturate Insulation breakdown of coil Water flooding, pressure, humidity	1	Input current increases and is highly distorted	3	3	Voltage and current protection at the output of the inverter, The input relay contactor in front of inverter turning off with the fault signal
					Improper isolation clearance between the wires.	1	Distorted current and increased current stress across the GA parallel capacitor	3	3	Fault communicated to the BMS and upstream PFC Electrical and mechanical design requirements, Safety and quality control during manufacturing
C.3.2	Compensation series inductor in VA (referred as Lf2 in Figure 2.3)			Inductor failed open circuit	Mechanical shock or stress or assembly issues (both coil and core) Over temperature and breakdown winding, Mechanical failure, Improper assembly and soldering during manufacturing, Water flooding, pressure, humidity	1	No output power	2	2	Voltage and current protection at the output of the inverter, The input relay contactor in front of inverter turning off with the fault signal, Fault communicated to the BMS and upstream PFC Electrical and mechanical design requirements, Safety and quality control during manufacturing
							Increases voltage and current stresses across the compensation capacitor at GA and VA	3	3	
				Inductor failed short circuit	Excessive current stress causing inductor to saturate Insulation breakdown of coil Improper isolation clearance between the wires. Water flooding, pressure, humidity	1	Distorts input current at GA	3	3	Voltage and current protection at the output of the inverter, The input relay contactor in front of inverter turning off with the fault signal, Fault communicated to the BMS and upstream PFC Electrical and mechanical design requirements, Safety and quality control during manufacturing
							Distorted voltage and current across VA the parallel capacitor, which results in distorted currents through the rectifier	2	2	
							Reduced output power or no power based on the load condition	2	2	
C.3.3	Inductor enclosure	Epoxy or PSM enclosure which surrounds the GA inductor when being embedded in concrete with the	Protects the inductor bank from outside elemtents and also contributes to heat dissipation	Mechanical failure/breakdown	Aging, water flooding, pressure, humidity Extreme roadway/ambient temperatures	4	Cracking of epoxy leading to inductor exposed to elements and decreased lifetime of system Inductor subjected to higher temperatures and increased mechanical stress	2	8	Temperature sensors communicate to microcontroller for protection action to decrease power capability of system Condition monitoring of component lifetimes Quality and durability test of the system under diverse operating conditions
D. Wireless charging pads										
D.1.	Litz wire–based coil	Litz wire–based coil of the transmitter and receiver pads. Multiturn coil made with high- frequency Litz wire	Carries high-frequency AC current and generates AC magnetic field	Electrical open/short circuit failures	Insulation failure due to extremely high current and voltage in the coil	2	The voltage and current in the coil at high-power are significantly high.	5	10	Current and temperature sensor Safety and control requirements
					High loss in the coil or core.	3	Increased temperatures in and around the coil	2	6	Electrical and mechanical design requirements Quality and safety test for diverse operating conditions
				Mechanical failure	Heavy vehicle running over the coil Crash induced mechanical failure Over temperature due to high loss and fault in thermal management system	1	Increase in electrical resistivity and loss Exposed coil may cause electrical open or short circuit Electrical safety hazard User exposure to energized component of the charging pad	5	5	Parallel-wire based coil design. Strict electrical and mechanical design requirements considering bending limitation during manufacturing, installation and operation. Quality and safety test for diverse operating conditions Safety and control requirements

				High-voltage insulation failure	Faulty design/manufacturing Mechanical deformation of the charging pad Over voltage operation	1	Electrical open or short circuit Electrical and thermal safety hazard Significant damage in other components and subsystems	2	2	Electrical and mechanical design requirements Safety and quality control during manufacturing Current and temperature sensor Quality and safety test for diverse operating conditions
				Conductivity degredation	Mechanical degredation Over temperature Internal insulation failure in Litz wires due to high-temperature or high voltage	2	Increase in electrical resistivity Increase in loss, Over temperature	4	8	Electrical and mechanical design requirements Safety and quality control during manufacturing Current and temperature sensor Quality and safety test for diverse operating conditions
D.2.	Ferrite core	Ferrite core of the transmitter and receiver pads. Made with high-permeability magnetic material, such as ferrite. Ferrite is a highly brittle material	1. Guides the magnetic flux, 2. Increases the self and mutual inductances	High loss/High temperature	Significantly high hysteresis loss Fault in thermal management Improper/faulty thermal design when embedded	2	Degraded performance of the core Increased resistivity and insulation degradation of the coil Thermal runaway Drop in system efficiency Hazard for surrounding components	4	8	Temperature sensor in the core Well designed thermal management system Safety and quality test for diverse operating conditions
				Mechanical breakdown	Ferrite is extremely brittle Excessive vibration from the vehicle excessive pressure on the charging pad Improper mechanical design Damage from accident or heavy impact Aging, water flooding, pressure, humidity	4	Slightly reduced self and mutual inductances	1	4	Mechanical design requirements of the core as well as surrounding materials Safety and quality test for diverse operating conditions
D.3.	Backplate shield	Backplate sheilds are made with aluminum plate, and put behind the ferrite core	1. Gives mechanical support 2. Reduces the leakage magnetic field	Excessive loss in the shield	High eddy curent loss in shield Mechanical breakdon, deformation, or crack in coil, core or shield Increased current in the coils Increased misalignment between the charging pads	4	Excessive temperature and thermal hotspot Increased EMF emissions due to the reduced shield current	2	8	Current and temperature sensor Safety, quality, and control requirements Safety and quality test for diverse operating conditions
				Increased EMF emissions	Mechanical breakdown/bending of the sheild Degraded conductivity of the conductive shield Degraded permeability of the magnetic sheild	2	High EMF emission, potentially above the safety limits	5	10	Strict design requirement for low EMF emission Safety and quality test for diverse operation conditions
D.4.	EMF shield	EMF shield above the receiver pad. Made with large aluminum plate, put on the receiver pad	1. Reduces the leakage magnetic field 2. Protect the vehicle chassis form the magnetic field	Excessive loss in the shield	High eddy current loss in shield will be one of the most critical challenge for extremely fast WCS.	3	Excessive high temperature on the shield	4	12	Temperature sensor in the shield The misalignment between transmitter and receiver must be low
				Increased EMF emissions	Degradation of conductivity of the aluminum shield.	3	Exceeding the EMF emission above the ICNIPR limit, causing significant health and safety hazard. Damage of the EV sensors due to high EMF exposure	4	12	Monitoring the EMF emissions at the edge of the vehicle using EMF sensors.
		EMF shield below and around the transmitter pad. Made with aluminum plate, or high- permeability materials, such as ferrite, magment, and so on	Reduce the leakage magnetic field around the vehicle	Excessive loss in the shield	Mechanical deformation. The shield of the high power WCS causes high eddy-current and core loss. Any mechanical deformation of the aluminum or ferrite would increase the eddy loss in the aluminum and hysteresis loss in the ferrite.	2	Thermal hazard Exceeding the EMF emission above the ICNIPR limit, causing significant health and safety hazard. Damage of the EV sensors due to high EMF exposure	3	6	Temperature sensor in the shield Monitoring the EMF emissions at the edge of the vehicle using EMF sensors
				Increased EMF emissions	Degradation of conductivity of the aluminum shield Degradation of the effective permeability of the magnetic shield layer	2	Exceeding the EMF emission above the ICNIPR limit, causing significant health and safety hazard. Damage of the EV sensor due to high EMF exposure	3	6	Monitoring the EMF emissions at the edge of the vehicle using EMF sensors
D.5	Nonmagnetic coil enclosures	Nonmagnemtic enclosures are put around both transmitter and reciever pads	1. Protect the magnetic component of the charging pad 2. Provide mechanical support and required heat dissipation	Mechanical failure/breakdown	Over temperature Aging, water flooding, pressure, or humidity in embedded GA coil enclosure	1	Potential change in the Quality factor of the coil resulting in decreased efficiency Decreased lifetime of the overall system	2	2	Quality and durability test of the system under diverse operating conditions
				Pucture/Intrusion of foreign object	Crash-induced puncture Degredation of the road which opens up enclosure to the elements such as aging, water flooding, pressure, humidity	2	Decreased lifetime of the overall system Potential damage to ferrites and thus a decrease in efficiency, increase in temperature and decrease in total operating power	2	4	Quality and durabilty test oof the system under diverse operating conditions
E. Rectifier											
E.1.	Diode rectifier on VA	Silicon carbide diodes/fast recovery silicon diodes	Converts the high-frequency AC voltage to DC voltage	One diode in the module shorted	Excessive voltage, current and power stress across diode	2	Reduced output power and distorted inverter current with LCC-LCC tuning	3	6	Voltage and current protection at the output of the inverter, The input relay contactor in front of inverter turning off with the fault signal, Fault communicated to the BMS and upstream PFC
							Increases the VA coil current, which increases the output power (LCC-series)	3	6	Electrical and mechanical design requirements
							Other diodes are subjected to increased current stress (LCC-series)	3	6	
				Both diodes in the module shorted	Excessive voltage, current and power stress across the module	2	Output is shorted, excessive energy dissipation due to stored energy in the output capacitor. (LCC-series and LCC-LCC)	3	6	Voltage and current protection at the output of the inverter, The input relay contactor in front of inverter turning off with the fault signal, Fault communicated to the BMS and upstream PFC
							Inverter current increases, VA coil current increases, no output power, and increased current stress across other rectifier diodes (LCC-series)	3	6	Electrical and mechanical design requirements
							Distored inverter current, VA coil current reduces, and no output power (LCC-LCC)	2	4	

				One module is open circuited	Excessive heat dissipation Mechanical failure	1	Increases voltage stress across complementary diode (due to DC bias), no output power, DC bias across VA coil voltage, which increases the voltage stress, and the inverter current is distorted (LCC- series)	3	3	Voltage and current protection at the output of the inverter, The input relay contactor in front of inverter turning off with the fault signal, Fault communicated to the BMS and upstream PFC Electrical and mechanical design requirements
							Increases inverter current, increased voltage and current stress across VA coil, series capacitor, and parallel capacitor, no output power (LCC-LCC)	3	3	
				Both modules are open circuited	Excessive heat dissipation Mechanical failure	1	Increased distortions in inverter current, no output power (LCC-series)	2	2	Voltage and current protection at the output of the inverter, The input relay contactor in front of inverter turning off with the fault signal, Fault communicated to the BMS and upstream PFC Electrical and mechanical design requirements
							Increases inverter current, increased voltage and current stress across VA coil, series capacitor, and parallel capacitor, no output power (LCC-LCC)	3	3	
E.2.	Cooling unit (heat sink and chiller) for diode rectifier on VA	Cold plate with a compressor pump and ethylene glycol storage tank (with Ethylene glycol and water mix 50-50%)	Dissipates heat to keep the junction temperature of the diode modules under tolerable limits	Mechanical failure of cold plate and coolant circulating unit	Mechanical shock or crack Leakage or loose contact between the cold plate and the circulating unit	2	Temperature control disrupted. May lead to excessive heating of the diode rectifier, increase in losses and damage of the diodes	3	6	Temperature sensor communicates to microcontroller for protective action
				Failure of the compressor pump	Electrical failure Mechanical failure	2	Temperature control disrupted. May lead to excessive heating of the diode rectifier, increase in losses and damage of the diodes	4	8	Temperature sensor communicates to microcontroller for protective action
				Clogging of the cooling fluid circulating unit	Residue and dirt accumulation in the coolant and the cooling unit	1	Temperature control disrupted. May lead to excessive heating of the diode rectifier, increase in losses and damage of the diodes	4	4	Periodic maintenance Temperature sensor communicates to microcontroller for protective action
				Failure of the thermal pad between the diode module and cold plate	Mechanical stress and strain	1	Temperature control disrupted. Increased thermal stress on the diode rectifier, increase in losses	2	2	Temperature sensor communicates to microcontroller for protective action
E.3.	High-frequency decoupling capacitors for the rectifier on VA	Film or PLZT Ceramic Capacitors	Filtering switching frequency (or its higher order harmonics) ripple currents	Capacitor failed short circuit	Excessive voltage, current and power stress across the capacitor, which may translate in dielectric failure depending on capacitor property	3	Output is shorted	3	9	Fault communicated by dedicated sensors and also from the BMS
				Capacitor failed resulting open circuit	Excessive voltage, current and power stress across the capacitor, which may translate in dielectric failure depending on capacitor property. Mechanical failure	2	Switching harmonic ripple supplied from the input resulting in input voltage distortions	2	4	Proper derating of the capacitor to avoid exceeding recommended operating range. PFC and inverter will trip the system if the current, voltage, and temperature ratings go out of operating range. High voltage and current protection in front of the inverter
				Diminishing capacitance value	Excessive voltage stress over time Aging of the capacitor	4	Switching harmonic ripple supplied from the input resulting in input voltage distortions. MOSFET switches might be subjected to higher voltage stress	1	4	Proper derating of the capacitor to avoid exceeding recommended operating range. Lifetime estimation at the design stage to ensure the capacitor will survive expected lifetime. Condition monitoring scheme can be implemented for lifetime monitoring of the capacitors.
E.4.	Filter capacitor after rectifier (referenced as C_{out} in Figure 1.2)	Film capacitor	To filter high- frequency ripple current on the output DC bus	Capacitor open circuit	Mechanical failure	1	Ripple in output power goes to battery Vehicle battery lifetime reduction	1	1	Control action taken by BMS
				Capacitor short circuit	Excessive voltage, current and power stress across the capacitor, which may translate in dielectric failure depending on capacitor property Aging of the capacitor	2	Output is shorted	3	6	Fault communicated by dedicated sensors and also from the BMS
						3	Increased inverter current subsequently increasing the voltage and current stress across input inductor and parallel capacitor, VA coil current increases which results in excess current through VA recifier, no output power (LCC-series)	3	9	
							Reduced and distorted inverter current, reduced VA coil current, no output power (LCC-LCC)	2	6	
E.5.	Filter inductor (typically required for parallel compensation in secondary)	Ferrite core inductor with Litz wire winding	To filter high- frequency ripple in the voltage output from the rectifier in VA unit	Inductor short circuit	Excessive current stress causing inductor to saturate Insulation breakdown of coil	1	Distortions in Output current Vehicle battery lifetime reduction	2	2	Voltage and current protection Electrical and mechanical design requirements, Safety and quality control during manufacturing
				Inductor open circuit	Mechanical failure	1	No output power	2	2	Voltage and current protection Electrical and mechanical design requirements, Safety and quality control during manufacturing
F. WPT system control and communication subsystem										
F.1	Input voltage sensor	Isolated voltage sensor	Sense the input DC voltage	Sensor damage	Short circuit Aging Open circuit	1	Input voltage not communicated to microcontroller. Controller action is not as desired, output voltage or power might be different from the reference value	2	2	Microcontroller communicates fault Periodic calibration
F.2	Output voltage sensor	Isolated voltage sensor	Sense the output voltage	Sensor damage	Short circuit Aging Open circuit	1	Output voltage not communicated to microcontroller. Controller might saturate and MOSFETs operate at maximum pulse width for phase shift control. Input current increases. Output voltage is different from the reference value	3	3	Desat protection in gate driver triggers Other sensors, microcontroller and BMS communicates fault Periodic calibration
F.3	GA coil current sensor	Isolated current sensor	Sense the coil current series	Sensor damage	Short circuit Aging Open circuit	1	Coil current magnitude not communicated to microcontroller. Controller might saturate and MOSFETs operate at maximum pulse width for phase shift control. Input current increases. Output voltage is different from the reference value	3	3	Desat protection in gate driver triggers Other sensors, microcontroller and BMS communicates fault Periodic calibration

F.4	Output current sensor	Isolated current sensor	Sense the output current	Sensor damage	Short circuit Aging Open circuit	1	Output current magnitude not communicated to microcontroller Output power control (if being used) is affected	2	2	Microcontroller communicates fault Periodic calibration
F.5	GA side high-frequency inverter temperature sensor	Thermistor based temperature sensor	Sense the GA side MOSFETs' temperature	Sensor damage	Short circuit Aging Open circuit	1	Temperature monitoring is lost, which may result in increased junction temperature of MOSFETs' under certain operating condition Efficiency decreases	2	2	Microcontroller communicates fault Periodic calibration
F.6	VA side high-frequency rectifier temperature sensor	Thermistor based temperature sensor	Sense the VA side diode rectifier temperature	Sensor damage	Short circuit Aging Open circuit	1	Temperature monitoring is lost, which may result in increased junction temperature of diodes in the rectifier under certain operating condition Efficiency decreases	2	2	Microcontroller communicates fault Periodic calibration
F.7	Ambient and other passives temperature sensor	Thermistor based temperature sensor	Sense the ambient temperature and temperature of selective passives	Sensor damage	Short circuit Aging Open circuit	1	Thermal stress across passives increases Efficiency decreases	2	2	Microcontroller communicates fault Periodic calibration
F.8	Microcontroller unit	Off the shelf digital microcontroller	Controlling the overall WPT system	Sensing unit failure	Analog circuitry failure Microcontroller ADC unit failure	1	Signals imperative for the control and fault monitoring not communicated to microcontroller Controller saturates and MOSFETs operate at maximum pulse width for phase shift control. Input current increases. Output voltage/power is different from the reference value	3	3	Desat protection in gate driver triggers Periodic calibration
				PWM unit failure	Analog circuitry failure Microcontroller EPWM unit failure	1	PWM signals lost to MOSFETs leading to no output power Constant high PWM signal communicated to one or multiple MOSFETs leading to an increased input current or short circuit	3	3	Desat protection in gate driver triggers Periodic calibration
F.9	Wireless communication network	Off the shelf wireless communication ICs interfaced with LAN or serial port of the microcontroller	Communicating of sensed signals from VA side sensors to GA side microcontroller	Wireless communication network damage	Analog circuity failure Open circuit of wireless to microcontroller interface	1	Communication from VA side is lost or erroneous Output voltage feedback signal to microcontroller is interrupted. Controller saturates and MOSFETs operate at maximum pulse width for phase shift control. Input current increases. Output voltage/power is different from the reference value	2	2	Desat protection in gate driver triggers Microcontroller communicates fault Periodic calibration
F.10	Foreign Object detection coil/sensor	Potentially low power coil put on the transmitter pad	1. Detect small and large conductive and magnetic undesire objects near charging pad 2. Detect living object such as animals near the charging pads 3. Essential safety features to shut down the system to protect the system as well as fire and health hazard	Breakdown or damage	Mechanical breakdown or deformation in the transmitter pad due to over temperature, pressure, or an accident	1	Increased loss due to undetected foreign object Potential thermal hotspot and fire-hazard	2	2	Increased testing considereing widely diverse operating conditions and samples of foreign objects
				Electrical failure including short or open circuit	Over temperature, over presssure Mechanical failure, puncture, crash-induced breakdown	2	Increased loss due to undetected foreign object Potential thermal hotspot and fire-hazard	2	4	Adopting a self-test method to identify if there is any potential fault in the FOD system Shutting down the power transfer if there is any potential failure
				Failure to detect certain conductive/magnetic object with irregular shape	large diversity of size and shape of foreign objects, and limited testing against such diverse situations	1	Increased loss due to undetected foreign object Potential thermal hotspot and fire-hazard	4	4	Quality and durability test of the system under diverse operating conditions